https://doi.org/10.15388/vu.thesis.631
https://orcid.org/0009-0009-3401-9491

VILNIUS UNIVERSITY

Kotryna Čekuolytė

Potential Antimicrobial Mechanism of Silver Nanoparticles Synthesized by Thermophilic *Geobacillus* Genus Bacteria

DOCTORAL DISSERTATION

Natural Sciences,
Biology N 010

VILNIUS 2024

The dissertation was prepared between 2019 and 2023 in Vilnius University, Life Sciences Center, Institute of Biosciences.
The reaserch was supported by Research Council of Lithuania, PhD project No. KD-19142 ("Analysis of the *Geobacillus* sp. Synthetized Silver Nanoparticles Mechanisms of Action on the Biocontrol of Pathogenic Skin Microbiota").

Academic supervisor – Prof. Dr. Eglė Lastauskienė (Vilnius University, Natural Sciences, Biology – N 010).

This doctoral dissertation will be defended in a puclic meeting of the Dissertation Defence Panel:

Chairman – Assoc. Prof. Dr. Raimondas Šiukšta (Vilnius University, Natural Sciences, Biology – N 010).
Members:
Dr. Kaja Kasemets (National Institute of Chemical Physics and Biophysics, Estonia, Natural Sciences, Biology – N 010);
Prof. Dr. Nomeda Kuisienė (Vilnius University, Natural Sciences, Biology – N 010);
Dr. Rasa Petraitytė-Burneikienė (Vilnius University, Natural Sciences, Biochemistry – N 004);
Dr. Živilė Strazdaitė-Žielienė (Nature Research Centre, Natural Sciences, Biology – N 010).

The dissertation shall be defended at a public meeting of the Dissertation Defence Panel at 11:00 on the 4th July 2024 in Room R105 of the VU LSC (7 Saulėtekio ave., LT-10257, Vilnius, Lithuania).
Dissertation will be defended in English

https://doi.org/10.15388/vu.thesis.631
https://orcid.org/0009-0009-3401-9491

VILNIAUS UNIVERSITETAS

Kotryna Čekuolytė

Termofilinių *Geobacillus* genties bakterijų sintetinamų sidabro nanodalelių antimikrobinio poveikio mechanizmas

DAKTARO DISERTACIJA

Gamtos mokslai,
Biologija N 010

VILNIUS 2024

Disertacija rengta 2019 – 2023 metais Vilniaus universiteto Gyvybės mokslų centro Biomokslų institute.
Mokslinius tyrimus rėmė Lietuvos Mokslų Taryba, doktorantūros projektas Nr. KD-19142 („*Geobacillus* sp. bakterijų sintetinamų sidabro nanodalelių veikimo mechanizmo tyrimas ir jų panaudojimas žmogaus patogeninės odos mikrobiotos biokontrolei").

Mokslinė vadovė – prof. dr. Eglė Lastauskienė (Vilniaus universitetas, gamtos mokslai, biologija N 010).

Gynimo taryba:
Pirmininkas – doc. dr. Raimondas Šiukšta (Vilniaus universitetas, gamtos mokslai, biologija – N 010).
Nariai:
dr. Kaja Kasemets (Nacionalinis cheminės fizikos ir biofizikos institutas, Estija, gamtos mokslai, biologija – N 010);
prof. dr. Nomeda Kuisienė (Vilniaus universitetas, gamtos mokslai, biologija – N 010);
dr. Rasa Petraitytė-Burneikienė (Vilniaus universitetas, gamtos mokslai, biochemija – N 004);
dr. Živilė Strazdaitė-Žielienė (Gamtos tyrimų centras, gamtos mokslai, biologija – N 010).

Disertacijos gynimo laikas ir vieta: 11:00 val., 2024 liepos 4, R105 auditorija, Gyvybės mokslų centras, Saulėtekio al. 7., LT-10257, Vilnius, Lietuva
Disertacija bus ginama anglų kalba.

CONTENT

ABBREVIATIONS

ACD – accidental cell death
AgNP – silver nanoparticles
BSA – bovine serum albumin
DCF – 2',7'-dichlorofluorescein
DCFDA – 2',7'-dichlorodihydrofluorescein diacetate
DLS – dynamic light scattering
ER – endoplasmic reticulum
HBSS – phosphate buffer without Ca^{2+}/Mg^{2+}
IMDM – Iscove's Modified Dulbecco's Medium
IRE – irreversible electroporation
GSH – glutathione
Ker-CT – keratinocytes
LAA – linoleamide alkyne
LB – Luria-Bertani medium
LPS – lipopolysaccharide
MDA – malondialdehyde
MIC – minimum inhibitory concentration
MRSA – methicillin-resistant *Staphylococcus aureus*
MTT – 3-(4,5-Dimethylthiazol-2-yl)-2,5-diphenyltetrazolium bromide
NP – nanoparticles
PAMP – pathogen-associated molecular pattern
PBS – phosphate buffered saline
PCD – programmed cell death
PE – phosphatidylethanolamine
PEF – pulsed electric field
PI – propidium iodide
PRR – pattern recognition receptor
RCD – regulated cell death
ROS – reactive oxygen species
SEM – scanning electron microscopy
TBHP – *tert*-butyl hydroperoxide
TEM – transmission electron microscopy
VBNC – viable but non-culturable
YPD – yeast extract peptone dextrose medium

INTRODUCTION

Constantly increasing resistance of bacteria and yeasts to antimicrobial therapy necessitates the search for new means in the fight against bacterial and fungal infections. Patients with chronic conditions should receive priority care due to the aging population and the rising number of people suffering from immune-related disorders. Due to these reasons, the number of patients affected by skin diseases is increasing. The majority of microorganisms living on the skin are commensal. Although many skin-colonizing commensals are assumed to be harmless they can cause serious skin conditions in people with impaired immune systems [1]. Dysbiosis, or an imbalance in the skin microbiota, is often the cause of many harmful conditions [2].

As a result of dysbiosis, *Candida* infections are constantly increasing and provide serious difficulties for people with autoimmune or immune-related disorders [3]. Invasive candidiasis affects approximately 25,000 people in the USA annually [4]. In addition, people with immune-related disorders frequently spend a long time in the hospital care, and *Candida* yeasts can develop biofilms on surfaces, which can contaminate important medical equipment needed to treat patients [5]. While a lot of research effort has been put into *Candida albicans*, there is cause for concern due to the growing number of non-albicans cases of the illness. An urgent problem is the fluconazole and amphotericin B resistance in non-albicans *Candida* species [6,7].

Skin diseases caused by yeasts are not the only concern. Frequent and inappropriate use of antibiotics has enabled bacteria to develop antibiotic resistance mechanisms, especially in the hospital environment [8]. Infections caused by multidrug-resistant bacteria are difficult to treat with modern antibiotic therapy, leading to them being characterized by high morbidity and mortality [9]. All these reasons encourage the research for alternatives to the currently used drugs for the treatment of various skin infections.

The distinctive physical and chemical characteristics of silver nanoparticles (AgNP) are widely recognized, and they can be used in a variety of applications. AgNP have become increasingly important in antimicrobial therapy due to the increasing resistance of microorganisms to currently used antimicrobial chemicals. Physical and chemical techniques can be used to make AgNP, however, they are highly environmentally unfriendly and yield a lot of side compounds (such as sodium borohydride and *N*,*N*-dimethylformamide). Thus, to obtain AgNP, different technologies are needed [10]. There is a lot of knowledge about AgNP obtained by biological synthesis using plants, fungi, and mesophilic bacteria, but little is known about

AgNP obtained using thermophilic bacteria. Hence, this thesis describes the biological synthesis of AgNP induced by thermophilic *Geobacillus* spp. bacteria, their properties, and antimicrobial potential.

One of the main advantages of AgNP compared to currently used drugs is their complex antimicrobial effect. They affect various parts of the cell, such as the cell wall, membranes, proteins, DNA, and enzymes, thereby disrupting various cell functions. Also, they cause oxidative stress, which further enhances their antimicrobial effect [11]. Because they do not have a single target in cells, the chance of developing resistance to AgNP is not as high as, for example, to antibiotics. The antimicrobial mechanism of AgNP obtained in different techniques can be somewhat different, so it is important to determine how this antimicrobial substance affects cells [12]. To this end, this thesis outlines the determined effects of AgNP on membranes, ROS generation, and lipid peroxidation, and identifies whether caspase activation (programmed cell death) is enhanced after AgNP exposure.

However, even though AgNP are widely used in cosmetics, the use of AgNP to treat diseases raises concerns. Because they do not have one specific target in the cell, they can harm human cells as well mainly by causing oxidative stress. Therefore, there are worries that AgNP can damage human organs. The conducted studies show different results, so it can be said that this property may also depend on the method of obtaining AgNP, their size, shape, and other properties [13–15]. To this purpose, this thesis also determined the toxic effects on human keratinocyte cells and the migration of these cells after wounding and AgNP exposure.

The aim

To evaluate the capability of silver nanoparticles obtained by thermophilic *Geobacillus* spp. bacteria-induced synthesis for application in biocontrol of microorganisms related to the human skin diseases.

Tasks:

1. To optimize AgNP synthesis using thermophilic *Geobacillus* spp. bacteria;
2. To determine whether the prepared AgNP have antimicrobial properties against skin pathogenic microorganisms (*Staphylococcus aureus*, *Streptococcus pyogenes*, *Pseudomonas aeruginosa*, *Candida guilliermondii*);

3. To assess whether electroporation enhances the antimicrobial effect of these AgNP;
4. To determine the mechanism of death caused by AgNP in microorganisms;
5. To determine whether the prepared AgNP, with a concentration that affects microorganisms, have a cytotoxic effect on human keratinocyte cells.

Scientific novelty and importance

Even though silver nanoparticles were obtained using *Geobacillus* spp. bacteria before [16], there is little information about their antimicrobial properties and application in real use. This thesis describes AgNP obtained using thermophilic *Geobacillus* spp. bacteria-induced synthesis, a comprehensive analysis of obtained AgNP, and their antimicrobial potential.

Also, there is little information on the effects of AgNP on skin pathogens, especially *S. pyogenes* and *C. guilliermondii*, which are studied in this work. There is a lot of data in the literature on the mechanism of antimicrobial action of AgNP obtained by chemical, physical, and biological methods, but there is no data on the mechanism of action of AgNP obtained using thermophilic bacteria. This thesis describes potential mechanisms of antimicrobial activity against skin pathogenic bacteria and yeasts. So, this work expands the knowledge of antimicrobial properties of AgNP obtained using thermophilic *Geobacillus* spp. bacteria.

Since the use of AgNP in the treatment of diseases raises concerns, due to the concentrations used and the possible cytotoxic effect, in this thesis, for the first time, a combination of AgNP and electroporation was applied, enhancing the antimicrobial effect of this nanomaterial.

This work also evaluates for the first time the cytotoxic effect of AgNP obtained by the thermophilic *Geobacillus* spp. bacteria-induced synthesis on human keratinocyte cells. This allows us to assess whether these AgNP are safe to use in real life for a biocontrol of pathogenic skin microbiota.

Defending statements

1. Thermophilic *Geobacillus* spp. bacteria are suitable for the synthesis of silver nanoparticles.
2. AgNP obtained using *Geobacillus* spp. bacteria have antimicrobial properties against pathogenic microorganisms.
3. Electroporation enhances the antimicrobial effect of AgNP.

4. AgNP obtained using *Geobacillus* spp. bacteria affect membranes of microorganisms, increase generation of ROS, and cause programmed cell death in yeasts.
5. 5 μg/mL concentration of AgNP obtained using *Geobacillus* spp. bacteria do not have a cytotoxic effect on human keratinocyte cells.

1. LITERATURE REVIEW

1.1. Human skin: its environment and microbiota

The skin is the largest human organ, which is colonized by microorganisms such as bacteria, fungi, and viruses. The microorganisms making up the skin microbiota also provide a physical barrier to protect the human body from pathogens [17]. Since the skin is an external human organ on which natural skin microorganisms interact with both skin cells and pathogenic microorganisms, the skin and its microbiota are the first line of defence attributed to the human immune system. From the first days of human life, the skin microbiota develop the human innate immune system [18]. Different areas of the skin have different characteristics, so the skin microbiota is adapted to certain microenvironments of the skin, which further strengthens the competition with pathogenic microorganisms [19].

1.1.1. Human skin and its environment

The epidermis (the outer layer) and dermis are the two layers of the skin. Epidermis is composed of layers of differentiated keratinocytes [20]. As keratinocyte stem cells divide, new keratinocytes are presented in the basal layer. They are pushed up through the epidermal layers, differentiating gradually until they reach the *stratum corneum*. It is made up of dead, flattened, keratin-rich cells. This layer prevents the body from drying out and keeps external substances, for example pathogenic viruses and bacteria, from entering the body. Keratinocytes regularly peel away from the surface of the skin to be replaced by new cells from the base layer [21]. The skin's ability to constantly create new cells and develop responses that protect against microorganism-caused infections is an important trait. This type of innate immunity is thought to be an extra and especially significant component influencing the balance of microorganisms in the human skin. Immune responses in the skin are mediated by Langerhans cells in the epidermis, as well as dendritic cells, macrophages, mast cells, T and B, plasma cells, and natural killer cells in the dermis [18]. Most cell types are permanently present in the skin, such as keratinocytes, sebocytes, and mast cells, producing antimicrobial peptides such as β-defensins, human cathelicidin LL-37, and antimicrobial enzymes such as lysozyme or RNase 7 [18,22,23].

Different parts of the body create different microenvironments based on ultraviolet light exposure, pH, temperature, humidity, fat content, and

topography (i.e., smooth skin or wrinkles). Skin areas can be classified as oily (face, forehead, top of the head, chest, and upper back), moist (elbows, armpits, dorsum of knees, groin, and feet), and dry (forearms, palms, legs, and lower back). Sweat and sebaceous glands, as well as hair follicles, determine the microenvironment of these areas. Sweat glands, which are vital for thermoregulation, predominate in moist parts of the skin. Sweat also lowers the skin's pH, making it difficult for some microorganisms to grow and colonize the skin [19]. Furthermore, perspiration contains antimicrobial compounds that impede skin colonization, such as antimicrobial peptides and free fatty acids [24]. Sebaceous glands around hair follicles secrete sebum, which forms a hydrophobic layer that lubricates the skin and acts as an antimicrobial shield for the skin and hair [2].

1.1.2. Skin microbiota

The way of birth influences the first colonization of the cutaneous microbiota in newborns. New-borns, who were born naturally, acquire those bacteria that colonize the mother's vaginal mucosa, whereas children born by Caesarean section obtain skin-associated microorganisms [25]. The long-term impact of such differences in the skin is unknown, but studies show that the increasing number of cases of atopic dermatitis in the Western world is not associated with any mode of delivery [26].

The formation of the skin's microbiota continues during the teenage years, when the sebaceous glands and skin are stimulated to produce more oil due to rising hormone levels. As a result, more lipophilic microorganisms, such as *Cutibacterium* spp. and *Corynebacterium* spp. bacteria, as well as *Malassezia* spp. fungi emerge on the skin during puberty. *Bacillota* (*Streptococcacea* spp.), *Bacteroidota*, and *Pseudomonadota* (betaproteobacteria and gammaproteobacteria) bacteria and more fungal species (*Aspergillus*, *Epicoccum*, and *Phoma* genera) predominate on children's skin before puberty [27,28]. It is unclear if new strains of microorganisms are acquired throughout puberty or whether the predominance of previous strains changes due to the changes in the skin environment. One of the hypotheses is that such a switch occurs due to the use of various hygiene and cosmetic products [29]. Such changes in microbiota with age are intriguing because many skin infections are age-related. Eczema, for example, is the most common among infants whereas acne and follicular diseases are more common in teenagers [30].

The physiology of the skin area influences the composition of the microbial community. Bacteria are the most abundant component of the skin microbiota, and regardless of skin type, the majority of bacteria belong to four phyla: *Actinomycetota* (*Corynebacterium*, *Cutibacterium*, *Micrococcus*, *Brevibacterium*), *Bacillota* (*Staphylococcus*, *Streptococcus*) and *Pseudomonadota*, and *Bacteroidota* [31]. Depending on the physicochemical conditions of the skin is populated by mesophilic, acidophilic, osmotolerant, xerophilic, and facultatively anaerobic microorganisms. However, depending on the specific location of the skin, other types of microorganisms can become skin commensals [32]. For a long time, it was thought that skin microorganisms colonized only the epidermis and the sebaceous and sweat glands, but research demonstrates that the deeper layers of the skin are not sterile either, which is especially important from the immunological point of view [33].

Figure 1.1. depicts the diversity of microorganisms found in different areas of the skin [34]. Lipophilic bacteria *Cutibacterium* (formerly known as *Propionibacterium*) dominate oily skin areas, whereas *Staphylococcus* and *Corynebacterium* species dominate moist skin areas such as elbows and feet [31,35]. β-*Proteobacteria* and *Flavobacteriales* predominate in dry skin areas [31]. In contrast to bacteria, the fungal community's composition was consistent across the torso, regardless of skin physiology. This area of the skin of the body is dominated by fungi of the genus *Malassezia*. Contrary to the case of the torso area, the feet are colonized by a wider range of fungal species: *Malassezia* spp., *Aspergillus* spp., *Cryptococcus* spp., *Rhodotorula* spp., *Epicoccum* spp., and others [36]. Bacteria colonize the most diverse parts of the skin, while fungi colonize less, even considering the fact that their diversity is greatest in the feet [27]. Interestingly, the microbiota of women is more diversified than that of men [37]. The composition of the microbiota is also affected by the host's diet, climate, UV radiation, profession of the host, antibiotic use, stress, and other factors, but there has been a lack of research to determine how these factors affect the composition of the microbiota [38].

Although the microbiota is classified as commensals, it has several types of relationships - mutualism, parasitism, and commensalism. Inhibiting the growth of harmful bacteria is one way the skin microbiota contributes to host immunity. The presence of commensal bacteria on the skin causes indirect competition for nutrients and space with the pathogenic microorganisms [39].

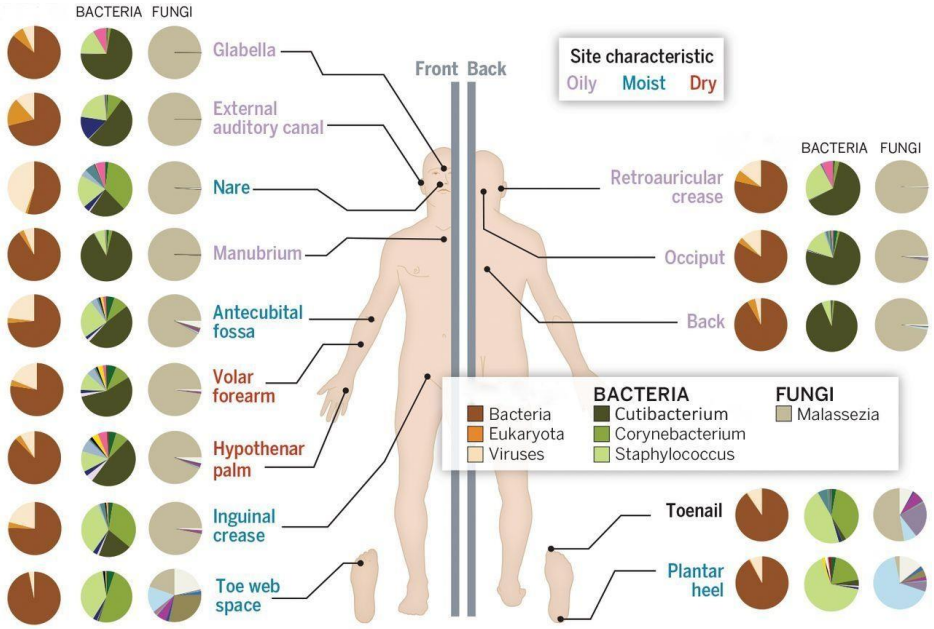

Fig. 1.1. Human skin microbiota in different parts of human body. Colours indicate different microenvironments on the skin: pink - sebaceous, blue - moist, red - dry. Relative abundance of bacteria, fungi, and viruses are shown in pie charts. The most commonly identified taxa of bacteria and fungi are indicated in the legend, and less commonly found taxa are marked with other colours to depict their proportion [34].

To survive, the inhabitants of the skin microbiota have adapted to utilize the food sources found in sweat, sebum secreted by the skin, and stratum corneum of the skin [40]. The facultative anaerobe *Cutibacterium acnes*, for example, can survive in anoxic sebaceous glands by employing proteases to acquire the amino acid arginine from skin proteins and lipases to degrade triglycerides in skin sebum [41,42].

Staphylococcus spp. also uses a variety of tactics to thrive on the skin's surface. These bacteria are halotolerant and can utilize urea in sweat as a nitrogen source. *Staphylococcus* spp. can produce adhesins, which facilitate adhesion to the skin surface, and proteases, which allow the uptake of nutrients from the stratum corneum, to aid in colonization [40]. To summarize, skin inhabitants are a heterogeneous group of microorganisms that must adapt to survive on the skin.

Because auxotrophic species of the *Malassezia* and *Corynebacterium* genera cannot produce lipids, they have evolved to rely on skin lipids. Members of the bacteria genus *Corynebacterium* make acids by breaking

down lipids, which they use to coat the surface of their cells. *Malassezia* spp. cells' genomes contain more lipases and fewer carbohydrate-degrading enzyme genes than other sequenced genomes of fungi due to the low carbohydrate but high lipid content of the skin. Such distinctions may explain why *Malassezia* species dominate the adult skin microbiota [40,43].

1.2. Pathogenic skin microbiota

Many skin-colonizing commensals are thought to be generally harmless, but in immunocompromised patients, they can cause significant skin diseases. Under certain conditions, typically beneficial microorganisms can become pathogens and cause severe skin infections [1,44]. The imbalance of the skin microbiota, also known as dysbiosis, is frequently the root cause of such disorders [2].

1.2.1. Pathogenic skin bacteria

Staphylococcus aureus are gram-positive, cocci-shaped bacteria that are commonly found on the skin and upper respiratory tract and are present in 30% of the human population [45]. Infections are usually caused by penetration through the skin or mucous membranes [46]. *S. aureus* can cause a wide range of diseases and infections of varying complexity. Impetigo, cellulitis, scalded skin syndrome, folliculitis, furuncle, and abscess are all caused by these bacteria. They also cause a variety of potentially fatal infections, including pneumonia, osteomyelitis, meningitis, toxic shock syndrome, endocarditis, and septicemia [47]. *S. aureus*, in comparison to other bacterial pathogens, possesses a diverse set of virulence factors that allow it to easily colonize the host [48]. Despite the diseases and infections, it causes, *S. aureus* is also highly resistant to antibiotics and is capable of forming biofilms. Infections caused by antibiotic-resistant strains of *S. aureus* have reached epidemic levels worldwide [9]. It is worth noting that *S. aureus* is the most common cause of nosocomial infections and the leading cause of death in hospitalized patients. The bacteria's ability to preserve genes responsible for resistance to various antibiotics and commonly used staphylococcal medications has a substantial influence on the high morbidity and mortality of diseases caused by this bacterium [49].

Streptococcus pyogenes (group A *Streptococcus* (GAS)) is a gram-positive, cocci-form bacteria of the *Bacillota* phylum that infects the skin and mucous membranes. *S. pyogenes* has well-developed and complex virulence

mechanisms that allow it to avoid detection by the human immune system once within a healthy person's body. *S. pyogenes* is mostly commonly associated with purulent infections such as pharyngitis, impetigo, and pyoderma [50]. Even for simple primary infections, antibiotic treatment is required to avoid the development of more serious secondary disorders such as rheumatic heart disease or glomerulonephritis [51]. In individuals with chronic diseases or weakened immune systems, *S. pyogenes* can cause considerably more severe and potentially fatal diseases, including necrotizing fasciitis and streptococcal toxic shock [52]. Penicillin resistant *S. pyogenes* in pharyngitis-tonsillitis is registered in 35% of cases [53]. Although β-lactam antibiotic therapy is frequently ineffective, the exact resistance genes of *S. pyogenes* to this class of antibiotics have not yet been identified [54]. One of the factors responsible for this resistance is thought to be mutations in the penicillin-binding protein PBP2x [55]. *In vitro, S. pyogenes* remained relatively sensitive to a wide range of antimicrobial agents [56].

Pseudomonas aeruginosa is a gram-negative, rod-shaped bacterium of the *Pseudomonadota* phylum. *P. aeruginosa* is an opportunistic pathogen found in the skin microflora of humans. It typically causes severe, chronic infections, particularly in individuals with weakened immune systems. *P. aeruginosa* biofilms are thought to be involved in 90% of chronic wound infections [57]. Infections caused by this bacterium have a high mortality rate because simple antimicrobial medicines such as antibiotics are often ineffective due to the bacteria's antibiotic resistance [58]. As the frequency of *P. aeruginosa*-caused acute infections increases, it is critically important to explore alternatives to traditional antibiotics [59].

1.2.2. *Candida*'s pathogenicity

Some *Candida* species can cause infection by growing inside human tissue or blood, in addition to existing commensally on the skin or mucous membranes [60,61]. Even though *Candida* can establish a generally advantageous relationship with its host, the use of antibiotics, disruption of host epithelial barriers (for instance, as a result of the use of catheters), or immune system suppression can cause *Candida* invasion and development of pathogenic state [62]. With a death rate of 10–72%, *Candida* is currently the fourth most common cause of hospital-acquired infections, particularly in immunocompromised patients [3,63]. Different tactics are used by *Candida* species to increase their capacity to infiltrate and cause diseases. Changes in

their shape, the development of biofilms, surface adhesion, and the secretion of hydrolytic enzymes are all examples of their virulence factors [5].

The most significant virulence trait of *Candida* species is their capacity to switch reversibly between yeast, pseudohyphal, and true hyphal morphologies (**Fig. 1.2.**) [64,65]. The most common default shape is that of yeast cells, which are typically round or oval and have unicellular morphology. On the other side, pseudohyphal cells exhibit multicellular, extended elliptic forms. These forms have a septa junction, which is a constriction between the mother and bud cells that is visible repeatedly along the entire pseudohyphae length. This connection is easily broken by mechanical agitation. Hyphae are multicellular, and tubular, and may create structures resembling roots. Without any neck construction in the mother cell, hyphae develop from an ungerminated yeast cell [66,67]. Mycelial flexibility is crucial during an infection since hyphal filaments are what invade the host and harm the outer epithelial layers [68]. Additionally, the switch to hyphae may help the fungus avoid the phagocytosis of the macrophage and cause more damage to its host [69].

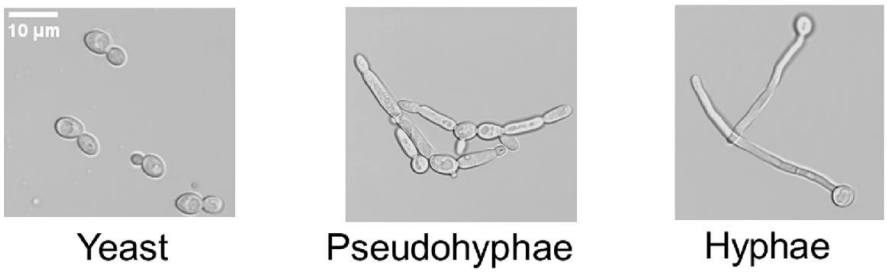

Fig. 1.2. Different cell forms of *Candida albicans* [65].

Hyphae may also integrate into developed biofilm formations. These biofilms may develop on tissues (such as the surface of a wound) as well as biomaterials (such as prosthetic heart valves) [5,70]. Patients suffer substantial clinical impact as a result of the increased morbidity and mortality risk caused by *Candida* biofilms' greater resistance to antifungal medications [71].

Temperature, CO_2, pH, serum, quorum sensing molecules, the availability of nutrients, and hypoxia are only a few of the variables that control morphogenesis [64]. The ability of *Candida* yeasts to adapt to various pH conditions is well recognized. For instance, at 37 °C, pH values close to neutral promote filamentation, but when pH values fall below 6 pH, this process is greatly inhibited. Yeast is the dominant form when the pH is 4 [72].

Production of adhesins, such as those in the agglutinin-like sequence (ALS) family, is another important virulence factor [73,74]. For instance, during the lag phase, agglutinin-like sequence 1 protein (Als1p) is expressed in hyphae and in planktonic *Candida* cells [75]. Additionally, it was discovered that Als1p is expressed in artificial biofilms and mouse infection models [76,77]. On the other hand, agglutinin-like sequence 5 protein (Als5p) may cause human macrophages to enter the tolerant M2 state. Als5p expression led to commensalism interactions between *Candida* yeasts and their host in the *Caenorhabditis elegans* model [78,79].

Extracellular enzymes are a significant subset of virulence factors that are essential for penetration and tissue adherence [80]. In addition to cytokines, antibodies, and complements, proteases can break down host cell proteins like keratin, mucin, and collagen [81]. By hydrolysing the ester linkages in glycerophospholipids, phospholipases cause the disintegration of cell membranes [82]. By inducing the breakdown of red blood cells and aiding the acquisition of iron, which is essential for the growth and spread of *Candida* infections, hemolysins dramatically increase the virulence of *Candida* [83]. Involved in ester hydrolysis and lipid digestion, esterases and lipases support nutrient uptake and host cell adherence [84,85].

Candida guilliermondii is an uncommon opportunistic yeast that causes candidiasis, specifically onychomycosis (commonly known as nail fungus), and is known for its resistance to antifungal medicines such as fluconazole, flucytosine, and amphotericin B [7,86,87]. *C. guilliermondii* caused as much as 43% of all *Candida* infections in the USA study, and as many as 1.2% of all candidiasis cases in China led *C. guilliermondii* to cause bloodstream infections, which frequently result in mortality [88,89].

C. guilliermondii illness is most common in cancer patients, accounting for 69% of the incidence of candidiasis cases. In addition, candidiasis developed in 16.7% of patients who were given central venous catheters. The global human mortality rate is approximately 17%. Weakened immunity is another risk factor that can lead to disease symptoms caused by *C. guilliermondii*, and morbidity is more common in children. Other disorders that provoke candidemia include liver disease, which caused 41.7% of candidemia cases in hospitals, renal failure (27.8%), and diabetes mellitus (22.2%) [90]. Depending on the geographic region, the incidence of candidemia caused by *C. guilliermondii* ranges from 0.5 to 4% [91]. Despite its low prevalence, *C. guilliermondii* has been demonstrated to be more resistant to antifungal medications than other *Candida* species. Interestingly, the organism is extensively spread in nature and is regularly isolated from soil,

plants, insects, seawater, and processed food, as well as being a component of the saprophytic human microbiota on the skin and mucosal surfaces. Yeast is most often identified in hospital departments of haematology and dermatology. *C. guilliermondii* yeast is also commonly cultured as a possible human pathogen from blood, skin, nail, soft tissue, and less commonly urine and genital tract samples [92].

1.2.3. Interaction of skin microbiota with pathogens

Host factors and interactions between microorganisms maintain the composition, stability, and functions of the microbial community. Microorganisms can act either competitively to eliminate one another or synergistically for mutual benefit. Interactions between microbiota members shape the microbial community on the skin and prevent pathogenic microorganisms from colonizing [2]. This phenomenon is known as colonization resistance [93]. *S. aureus* is one of the main objects of colonization resistance research on the skin. *S. aureus* colonizes one-third of the population's nasal passages, and its presence is associated with an increased risk of infection [94].

Because *S. aureus* bacteria frequently exhibit antibiotic resistance and vaccine development has shown minimal success, alternative elimination strategies, especially those involving commensal microorganisms, are under active investigation [95,96]. *Staphylococcus epidermidis* strains that secrete serine protease glutamyl endopeptidase (Esp) were the first to be recognized as suppressing the formation of *S. aureus* biofilms on the skin (**Fig. 1.3.**) [97]. These proteases degrade proteins from *S. aureus* that are required for biofilm formation and adherence to the host epithelium [98]. When protease activity was paired with β-defensin's antibacterial activity, the resulting bactericidal activity was adequate to eliminate *S. aureus* in biofilms [99].

Staphylococcus lugdunensis is another skin microorganism that regulates *S. aureus* growth (**Fig. 1.3.**). This bacterium inhibits the growth of *S. aureus* by producing the antibiotic lugdunin. *S. aureus* has not developed resistance to lugdunin or evaded breakdown by serine proteases, according to studies. This lack of resistance contrasts sharply with the microorganism's resistance to standard antibiotics and suggests that substances naturally generated by microbiota and the skin may be an even more efficient means of suppressing the growth of opportunistic pathogens [100].

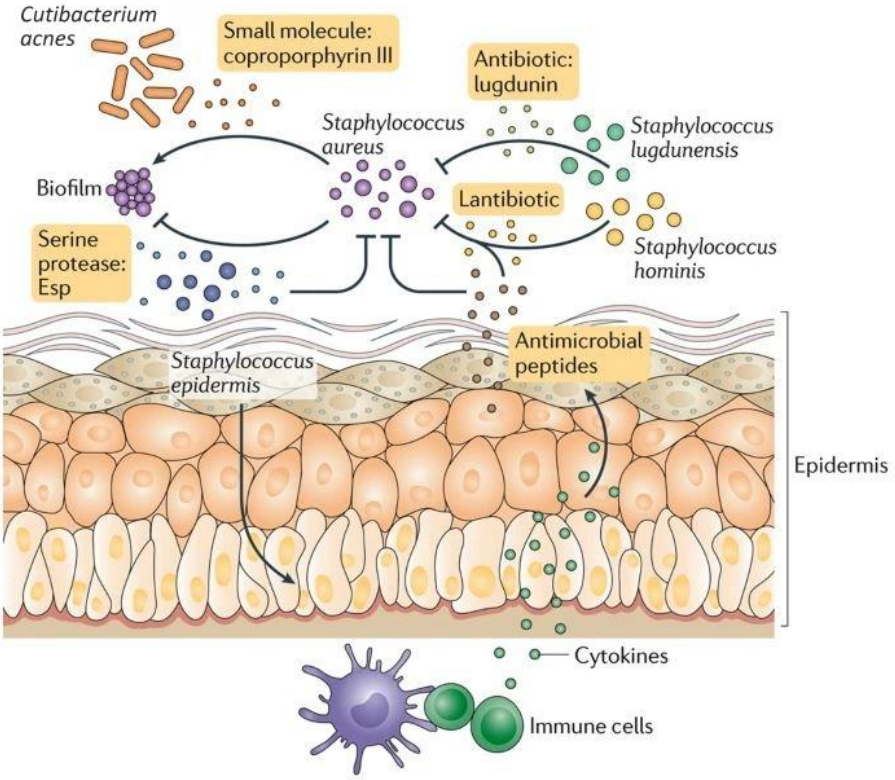

Fig. 1.3. *Staphylococcus aureus* interactions with skin commensals [2].

Coagulase-negative *Staphylococcus* spp., *S. epidermidis*, and *Staphylococcus hominis* produce lantibiotics that act synergistically with the human antimicrobial peptide cathelicidin LL-37 and inhibit the growth of *S. aureus* (**Fig. 1.3.**). Patients with atopic dermatitis who are frequently colonized with *S. aureus* have a lower prevalence of lantibiotic-producing strains. Topical therapy with strains secreting these antimicrobial substances reduced *S. aureus* colonization in atopic dermatitis patients, making it an alternative probiotic treatment strategy [101].

S. epidermidis secretes a variety of molecules that influence the growth of pathogenic microorganisms. PSM (phenol-soluble modulins) have a strong interaction with microbial lipid membranes (**Fig. 1.3.**). These compounds generated from *S. epidermidis* selectively kill the skin pathogens *S. pyogenes* and *S. aureus*, cooperate with host antimicrobial peptides (AMP) to improve bacterial elimination, and can be incorporated into neutrophil traps (innate host response) [102].

Not all skin microorganisms inhibit the growth of *S. aureus*. In contrast, depending on the quantity, growth phase, and pH, some species of the genus

Cutibacterium have been observed to promote *S. aureus* aggregation and biofilm formation [103]. The elimination of pathogenic microorganisms is not the only strategy for infection protection. *S. aureus* converted from a virulent to a commensal form *in vitro* when combined with *Corynebacterium striatum*. This shift in *S. aureus* behaviour opens the door to a therapeutic option that does not involve eliminating the pathogen but rather changing its behaviour [104].

1.3. Resistance of microorganisms to traditional antimicrobial therapy

There is a chance that resistance or tolerance will develop from a drug's initial, therapeutic use. Many medications used to treat bacterial, fungal, or viral infections fall under this category. The worst impacts in terms of morbidity and mortality are brought on by bacteria. The search for preventive and therapeutic methods began with the discovery of these infectious agents at the end of the 19th century, but effective therapy didn't emerge until the discovery of antibiotics. One of the most significant moments in human history, the discovery of antibiotics, changed medicine and saved countless lives. Unfortunately, the development of bacterial strains that are resistant to these medications has coincided with their consumption [105].

Antibiotic resistance mechanisms can be separated into five major categories: preventing the antibiotic from entering the cell, altering the antibiotic's target, turning the drug inactive, actively removing the antibiotic from the cell using efflux pumps, and protecting the target site by bacterial proteins [106]. Gram-positive and gram-negative cells employ marginally different antibiotic inactivation methods as a result of structural variations in their cell envelopes [107]. Gram-positive cells are less likely to restrict antibiotic entrance into the cell because they lack the lipopolysaccharide (LPS) layer and outer membrane and do not use some efflux mechanisms, whereas gram-negative cells can use all five of the mechanisms mentioned above [108].

Yeast resistance to antifungal drugs is also developing. Due to *Candida* yeasts' extensive repertoire of virulence factors, the importance of antifungal medications in combating *Candida* infections remains important. These infections can be treated with antifungal drugs from well-known classes such as polyenes, flucytosines, azoles, and echinocandins [109]. However, when *Candida* species develop resistance to antifungal treatments, these traditional therapies cannot be regarded as the safest and most efficient methods of therapy [5].

C. albicans is the species most responsible for systematic fungal infections caused by *Candida* yeasts. However, a recent study reveals an increase in non-albicans *Candida* species such as *C. krusei*, *C. glabrata*, *C. tropicalis*, *C. famata*, *C. parapsilosis*, and *C. guilliermondii*. These species have been reported often, especially in immunocompromised patients. Their prevalence, as well as resistance to antifungal medications, is increasing faster than that of *C. albicans* [110] . For example, *C. guilliermondii*, which has been described predominantly as a cause of candidemia in cancer patients, has a lower sensitivity to echinocandins and azoles [111]. It is worth noting that the minimum inhibitory concentration (MIC) of flucytosine was shown to be lower against *C. albicans* than against *C. guilliermondii* [112].

1.4. Methods of metal nanoparticles synthesis

To synthesize NP, **'**bottom-up' and 'top-down' strategies can be used. Using physical principles in processes such as ball milling, laser ablation, electrical arc-discharge, or vapour condensation techniques, is known as a 'top-down' approach. These methods enable the production of NP ranging from 1 to 100 nm in size. The 'bottom-up' approach, on the other hand, mainly consists of the synthesis of complicated structures from molecular building components [113].

1.4.1. Chemical methods of obtaining silver nanoparticles

Chemical reduction with organic and inorganic reducing agents is one of the most frequent methods of synthesis of AgNP. To reduce Ag^+ in aqueous and non-aqueous solutions, reducing agents such as sodium citrate, ascorbate, sodium borohydride ($NaBH_4$), hydrogen, Tolen's reagents, *N*,*N*-dimethylformamide (DMF), and others are used. These reductants reduce Ag^+ to elemental silver (Ag^0), which agglomerates into oligomeric clusters. These clusters then combine to generate colloidal AgNP [114]. It is critical to use protective agents during the manufacturing of metal nanoparticles to stabilize them and prevent them from being adsorbed or attached to the surface of the nanoparticles, hence preventing agglomeration [115]. Surfactants such as thiols, amines, acids, or alcohols stabilize the growth of particles and prevent them from sedimentation, agglomeration, or loss of surface characteristics [10].

Polymer compounds such as polyvinyl alcohol, polyethylene glycol, and others are efficient AgNP stabilizers. Kim et al. reported the synthesis of

spherical AgNP of controlled size using polyols and a modified precursor injection approach to produce very uniform-sized particles. The injection frequency and reaction temperature are critical elements in the precursor injection approach for producing AgNP with uniform shape and size. 17 ± 2 nm size AgNP were obtained by 2.5 mL/s injections at 100 °C. Injecting the precursor solution into the hot solution is an efficient technique to induce rapid nucleation in a short period of time, resulting in the creation of small AgNP with a narrower size distribution [116].

1.4.2. Physical methods of obtaining silver nanoparticles

Physical methods of obtaining AgNP are superior to chemical approaches since no solvents are required, and the obtained AgNP have the same characteristics. The two most common physical methods of obtaining AgNP are evaporation condensation and laser ablation.

The evaporation condensation method is based on the principle of silver evaporation and rapid condensation of the generated vapours. Silver is vaporized in an atmospheric pressure tube furnace heated to 1300–1400 °C [117]. The use of an atmospheric pressure tube furnace to produce AgNP has drawbacks because it takes up a lot of space, consumes a lot of energy, and raises the ambient temperature. It also takes a long time to reach thermal stability. A typical tube furnace consumes more than a dozen kilowatts of energy and takes several tens of minutes to reach the stable required temperature [118,119].

Laser ablation of bulk metal stocks in solution can also be used to obtain AgNP [120]. Many parameters influence ablation effectiveness and the characteristics of the resultant NP, including laser wavelength, laser pulse duration, laser scattering, ablation duration, and the presence of surfactants in the liquid medium [121]. One of the most significant advantages of the laser ablation approach over other AgNP production methods is that no chemical reagents are employed in the solutions. As a result, this approach yields pure and uncontaminated metal colloids [122]. By using the laser ablation method, 800 nm long band and femtosecond pulses, spherical AgNP with a diameter of 20–50 nm were obtained. The efficiency of production and size of the resultant NP were compared to those created using nanosecond laser pulses. The results reveal that whereas femtosecond pulses have a lower production efficiency than nanosecond pulses, they produce more uniformly sized NP. Furthermore, with femtosecond pulses, laser ablation efficiency was significantly lower in water than in the air [123].

Even though these methods prevent the use of chemicals that may be harmful to people and the environment, agglomeration still happens due to a lack of capping agents and stabilizers. Furthermore, external energy is required to put these methods into practice [113,124].

1.4.3. Biological synthesis of metal nanoparticles

The chemical and physical methods for producing AgNP pollute the environment and/or are expensive. As a result, it is critical to create innovative methods that do not necessitate costly equipment and are environmentally friendly: these methods do not use or produce harmful by-products or high temperatures. NP can be produced by both prokaryotic and eukaryotic cells (fungi, algae, and plants) [125].

Biological synthesis can be applied to the synthesis of extremely stable and well-characterized NP after evaluating the type of organism, hereditary and genetic characteristics of the organism, optimal conditions for cell growth and enzyme activity, optimal reaction conditions, and selecting the appropriate state of the biocatalyst. Some parameters, including substrate and biomass concentrations, pH, light, temperature, buffer strength, electron donor (e.g. glucose or fructose), stirring speed, and reaction time, can be changed to influence the size and shape of AgNP [10]. **Figure 1.4.** depicts a generalized scheme for the synthesis of AgNP in biological systems.

AgNP can be produced extracellularly or intracellularly, depending on how NP are disseminated. The extracellular strategy is better than the intracellular approach because it simplifies the process of recovering AgNP [126]. Because of the diverse organic components and the capabilities of the organisms used in the production of AgNP, AgNP produced using different systems are unique. Enzymes (e.g. nitrate reductase), exopolysaccharides, and peptides are examples of organic compounds found in organisms that can be employed as reducing agents [127–129].

The most studied and best recognized by various scientific groups mechanism of the AgNP synthesis using bacteria is the presence of the enzyme nitrate reductase. This enzyme converts nitrate to nitrite. During this process, the electron is transferred to the Ag^+ and thus silver is reduced from Ag^+ to Ag^0 [130]. One of the first bacteria in which this mechanism was demonstrated is *Bacillus licheniformis*. These bacteria have NADPH-dependent and -independent enzymes in their membranes, including nitrate reductase, which can convert Ag^+ to Ag^0 [131]. This mechanism was confirmed using purified *F. oxysporum* nitrate reductase mixed with $AgNO_3$ and NADPH. A

characteristic change in the colour of the synthesis of AgNP was determined [132].

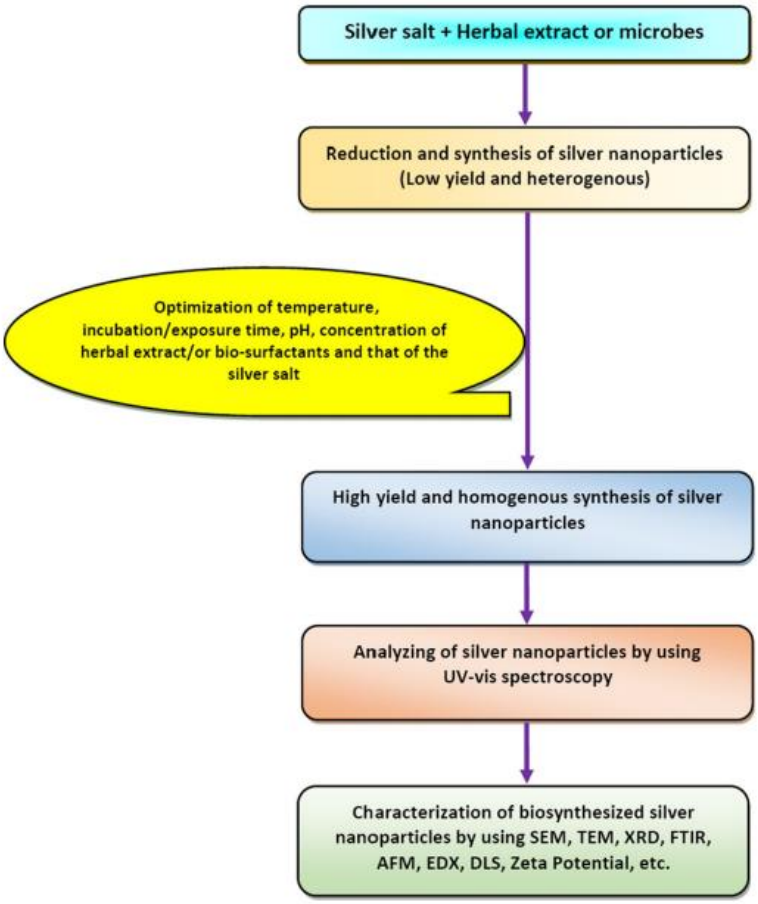

Fig. 1.4. Synthesis scheme of silver nanoparticles in biological systems [133].

Various bacteria can be adapted for the synthesis of nanomaterials. Because of their resistance to high concentrations of metal ions, thermophilic bacteria of the species *Geobacillus stearothermophilus* were used to induce the biological synthesis of AgNP. Using *G. stearothermophilus* secretomes and 1 mM $AgNO_3$, spherical AgNP with diameters of 5–35 nm were obtained [16]. Ghasemi et al. also used secretomes of *G. stearothermophilus* bacteria for the synthesis of AgNP. The AgNP obtained were spherical with a diameter of 15–50 nm [134]. The precise mechanism of AgNP formation in *G. stearothermophilus* bacteria is unknown, although it is thought that the proteins secreted into the medium by these bacteria play an important role in the reduction of Ag^+ and AgNP formation [16].

Although bacteria have been used for the production of AgNP for almost 20 years, new potential bacterial species capable of synthesizing this nanomaterial are still being sought. For example, *Lactobacillus acidophilus* cell-free supernatant was exposed to 0.1 M $AgNO_3$, which resulted in the production of AgNP. The obtained AgNP were spherical with sizes ranging from 10 to 20 nm (the average size of aggregates was 46 nm). Moreover, it was shown that these AgNP are thermal-stable [135]. The cell-free supernatant of *Pseudoduganella eburnea* was also used to produce AgNP. The size range of obtained AgNP was 8 to 24 nm, and their shape is spherical [136].

Fungi can also be employed for the synthesis of AgNP. Extracellular biosynthesis employing the mould *Fusarium oxysporum* can produce AgNP with diameters ranging from 5 to 50 nm. Even months after the reaction, the resulting AgNP do not flocculate. Because mould proteins stabilize the obtained nanomaterial, it exhibits long-term stability in solution. The form of the AgNP obtained varies; most are spherical, although triangular-shaped particles are also obtained [137].

Different fungi that can be applied to the synthesis are still being studied. For example, Yassin et al. used cell-free crude filtrate of *Penicillium verrucosum* to produce irregular morphology AgNP with an average size of 10 nm [138]. Cell-free filtrates of *Aspergillus brunneoviolaceusfor* can also be used for the biosynthesis of AgNP. The addition of 10 mM of $AgNO_3$ to the cell-free filtrate of this fungi resulted in spherical AgNP with the particle size distribution ranging between 0.72 and 15.21 nm [139].

Because plant-based AgNP synthesis is relatively cost-effective, it has the potential to become an environmentally friendly and valuable alternative to large-scale production of AgNP [140]. *Camelia sinensis* (green tea) extract is employed in the biosynthesis of AgNP as a reducing and stabilizing agent [141]. Caffeine and theophylline, two phenolic acid-type biomolecules found in *C. sinensis* extract, are responsible for the formation and stabilization of AgNP. AgNP has also been produced using black tea leaf extract. The resulting AgNP were stable and appeared in a variety of shapes including spheres, trapezoids, prisms, and rods [142].

New technologies are still being developed that allow the use of plant leaf extrats for the synthesis of AgNP. Vinodhini et al. for the biosynthesis of AgNP used *Allium fistulosum* (Welsh onion), *Tabernaemontana divaricata* (pinwheel flower) and *Basella alba* (Malabar spinach) leaf extracts. The obtained AgNP had rod-like shapes with dimensions of 40 nm, 55 nm and 57 nm respectively [143]. The leaf extract of *Alhagi graecorum* with

0.02 mmol/mL concentration of $AgNO_3$ produced spherical AgNP with a size range of 22–36 nm [144].

1.5. Mechanism of antimicrobial properties of silver nanoparticles

As demonstrated by experiments, AgNP have antimicrobial capabilities that can be used to fight a range of microorganisms, including bacteria, fungi, and also enveloped viruses [145]. AgNP have a complicated, multifaceted, and varied action. Efficient prevention of microbial growth and cell death is made possible by such a mechanism of action [11]. Antimicrobial action mechanisms of AgNP are depicted in **Fig. 1.5.** [146].

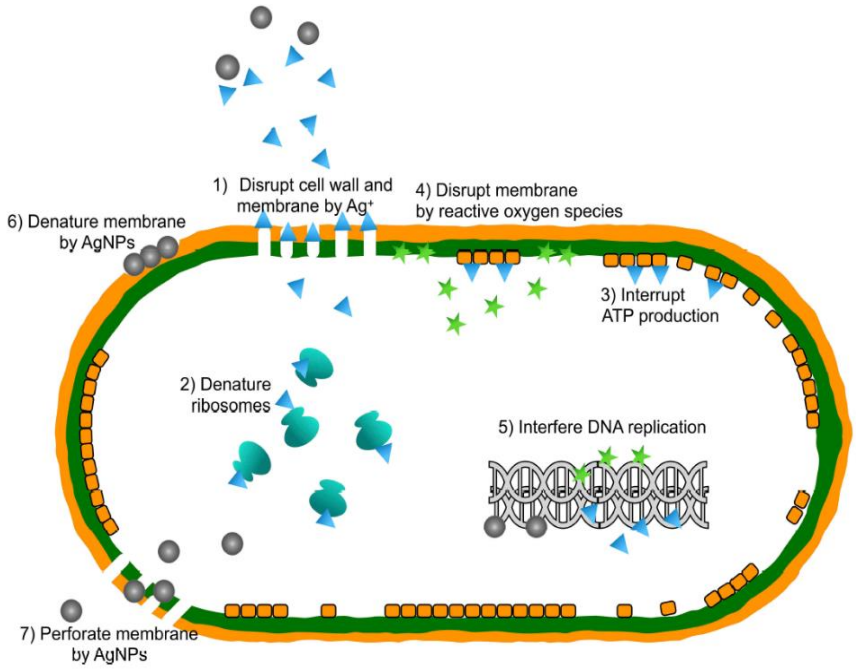

Fig. 1.5. Complex antimicrobial effect of AgNP. 1) Disruption of the cell wall and cytoplasmic membrane: Ag^+ released by AgNP adhere to or passes through the cell wall and cytoplasmic membrane. 2) Denaturation of ribosomes: Ag^+ denature ribosomes and inhibits protein synthesis. 3) Impairment of ATP synthesis: ATP production ceases as Ag^+ deactivates the respiratory enzyme in the cytoplasmic membrane. 4) Membrane disruption by ROS produced by a disrupted electron chain. 5) Interference with DNA replication: Ag^+ and ROS bind to DNA and prevent its replication and cell proliferation. 6) Accumulation of AgNP in the cell membrane: AgNP accumulate in the pits of the cell membrane and cause its denaturation. 7) Membrane perforation: AgNP directly move through the cytoplasmic membrane, which can release organelles from the cell [146].

Surface area to volume ratio and crystallographic surface structures are the primary factors that affect AgNP antimicrobial effectiveness [147]. MSSA (methicillin-susceptible *S. aureus*) and MRSA (methicillin-resistant *S. aureus*) studies have demonstrated that 5–10 nm AgNP have outstanding bacteriostatic and bactericidal properties [148]. AgNP with varied shapes but similar dimensions and surface areas behave differently in terms of bactericidal activity. AgNP in the form of the triangular pyramid has stronger antibacterial properties than spheres or rods. This difference in activity is possible due to the surface chemistry of the NP [149].

Because of the released silver cations (Ag^+), AgNP exhibit high antimicrobial activity [150,151]. By interacting with the functional groups of the microorganism's proteins, Ag^+ can make the proteins inactive. For instance, by binding to the thiol groups of membrane proteins, Ag^+ forms stable bonds and thus deactivates membrane proteins [151,152]. Both AgNP and Ag^+ are capable of altering the spatial structure of proteins; as a result, when the proteins in the cell undergo such structural alteration, the microorganism loses its capacity to carry out essential functions and dies [153]. Due to its small size and positive charge, Ag^+ easily attach to biomolecules after entering the cell [154]. Ag^+ capacity to damage cell envelopes, destabilize membranes, inhibit cellular respiration, generate reactive oxygen species (ROS), and react with intracellular proteins are all indications of its antimicrobial activity [155].

One of the key elements affecting the permeability of the cell membrane is the oxidative stress carried on by the free oxygen radicals generated by AgNP. Cell death or growth suppression may result from such a membrane imbalance [156]. Hydroxyl (-OH), superoxide (O_2^-), hydrogen peroxide (H_2O_2), and singlet oxygen ($^1O_2$) are among the ROS generated by AgNP. Studies have shown that whereas -OH and $^1O_2$ result in the death of the microorganism, O_2^- and H_2O_2 cause relatively mild stress responses that can be neutralized by endogenous antioxidants like superoxide dismutase and catalase [157,158]. The generation and elimination of ROS in a cell are usually in a constant balance, but when this equilibrium is disturbed, the cell experiences oxidative stress, which damages certain components of the cell, most commonly the cell membrane [159].

Lipid peroxidation is one of the processes resulting from intracellular ROS. When oxygen free radicals take electrons from cell membranes, it results in lipid peroxidation, which breaks down lipids and damages the cell membrane. The metabolites that are produced as a result (lipid peroxides) are likewise reactive and further harm the cell. Resistance to oxidative stress is significantly influenced by the lipid content of microorganism membranes.

Cells whose membrane phospholipids contain more saturated fatty acids are more resistant than those whose membrane phospholipids contain higher amounts of polyunsaturated fatty acids [160].

1.6. Which have a greater antimicrobial effect: silver nanoparticles or Ag^+?

According to recent studies, AgNP have superior antimicrobial qualities than Ag^+. Some research teams claim that whilst AgNP cause cell lysis, Ag^+ induce cells to enter a viable but non-culturable cell (VBNC) state [161,162]. However, the effects caused by AgNP may vary depending on the method by which they are obtained, their concentration, and the cells of the affected organism. Konig et al. study showed that nanosilver induced VBNC in *P. aeruginosa* cells rather than lysis [163].

AgNP can be engineered with diverse characteristics (such as surface coatings), allowing Ag^+ to be released at a desired rate and location, even though AgNP do not naturally have a large direct specific toxicity to microorganisms. In addition, AgNP can serve as a tool to deliver Ag^+ more efficiently as they are less sensitive to natural ligands that reduce bioavailability to the bacterial cytoplasm and membrane, whose proton motive force would lower the local pH (as low as pH 3) and increase Ag^+ separation. Ag^+ are released from AgNP when they oxidize, which is a slow process [164–166].

The most significant AgNP bioavailability processes include NP aggregation, which results in the formation of larger particles. AgNP become less mobile, tend to precipitate, and are consequently less accessible to organisms if they increase in size as a result of aggregation processes [167,168]. Since AgNP only act in the presence of oxygen, anaerobic conditions will prevent bioavailability to living organisms [164,169]. AgNP bioavailability has been demonstrated to be decreased by both organic and inorganic sulphur compounds, particularly cysteine (Ag-cysteine complex). AgNP's surface charge and shape both affect its bioavailability [170].

Because the cell's surface is negatively charged, the more positive the zeta potential of AgNP, the more bioavailable they are [171]. However, research has revealed that AgNP with low zeta potential also possess antimicrobial qualities. It is believed that in this instance AgNP may bind to the cationic moieties of the cell surface or the interaction is non-specific [172].

1.7. Studies on the antimicrobial effect of silver nanoparticles

Excellent antimicrobial properties are displayed by AgNP against a variety of microorganisms. AgNP size, shape, coating, and morphology all affect their properties, which in turn depend on the technique of preparation, solvent type, concentration, reducing agent strength, and temperature [12]. AgNP age is an important factor in their toxicity as well. It was noticed that 6 months aged AgNP in an aqueous solution are more toxic due to Ag^+ ions released into the solution [173]. Additionally, NP produced by biosynthesis are more toxic than NP obtained by other methods. Microorganisms' critical functions are inhibited by AgNP when they slowly envelop and enter their cells [133].

After 1 h of exposure to AgNP, SEM micrographs of the exposed *Salmonella enterica Typhimurium* revealed multiple obvious signs of cell envelope destruction, such as deep pits and sticky membranes (**Fig. 1.6.B**). After being exposed to AgNP for 2 h, the damaged bacterial cells were fractured and distorted, and there were numerous destroyed cells (**Fig. 1.6.C**). There were morphological alterations in the rods, including severe modifications in the cell wall with the creation of holes and invaginations, and the cells were shrunken and wrinkled. The characteristic bacillus shape was seen in transmission electron micrographs of unaffected bacterial cells, whereas *S. Typhimurium* treated with AgNP for 30 min had characteristic cell wall rupture and condensed cytoplasm. The *S. Typhimurium* outer membrane was covered in AgNP. A 24 h AgNP exposure revealed fully lysed cells with AgNP inside and adhered to the cell membrane. A possible effect of AgNP-bacteria interaction could be a change in the structural integrity of physicochemical changes in the cell wall, which could then change the cells' osmoregulation and cause the release of intracellular material, which ultimately causes death [174,175].

Other studies' TEM analysis demonstrated that unaffected *S. aureus* cells maintained their normal morphology. *S. aureus* exposed to AgNP, on the other hand, were severely harmed and degraded. TEM analysis revealed that AgNP aggregated and localized on the cell wall, cell membrane, and cytoplasm. The cell wall and cytoplasmic membrane were separated from each other. A bacterial membrane with such a morphology negatively affects cell permeability, so bacterial cells cannot regulate the process of transport through the plasma membrane and ultimately cause cell death. Many cells were severely damaged, and their cell walls detached, indicating a clear biocidal effect [176].

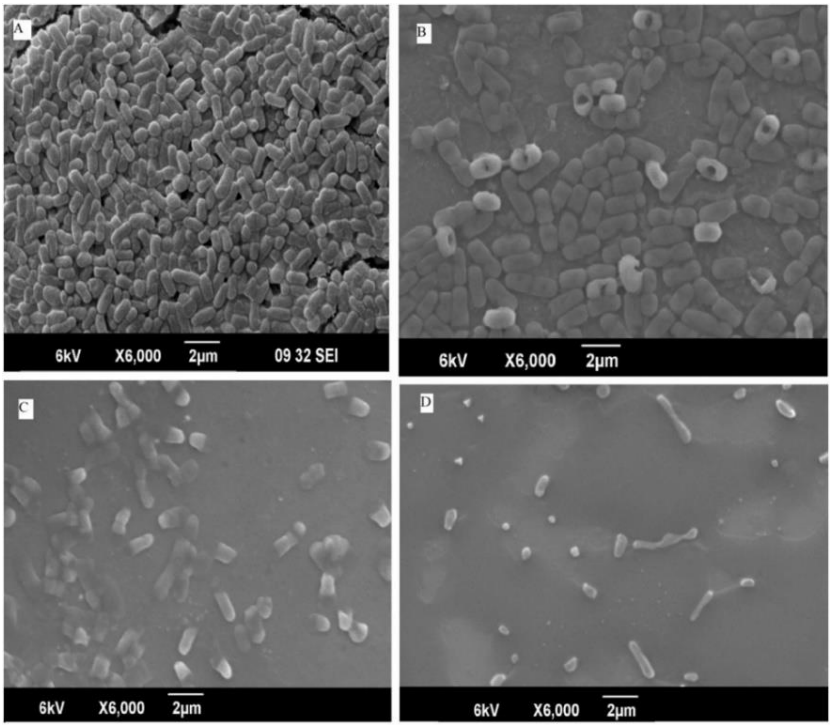

Fig. 1.6. SEM micrographs of *S. Typhimurium* cells affected with AgNP. **A** - unaffected cells; **B** - cells after 1 h; **C** - cells after 2 h; **D** - cells after 4 h of exposure [174].

Mirzajani et al. analysed the mechanisms underlying the impacts of AgNP on *S. aureus* bacterial cell walls. This included investigating both glycan and peptide moieties as well as the general fate of the bacteria. Therefore, their circular dichroism spectra were taken to assess the impact of AgNP on bacterial peptidoglycan in the cell wall, specifically on its peptide portion (**Fig. 1.7.**). AgNP can modify the secondary structures of peptidoglycan, as evidenced by differences between the samples' pre- and post-exposure of 30 min and 3 h. The investigation showed that AgNP have an impact on the hydrogen bonds and the α-helix, i.e., peptide secondary structure. Within 30 min of AgNP exposure, such a considerable effect becomes apparent. In addition, the research demonstrated that AgNP modify the peptidoglycan's general structure [177].

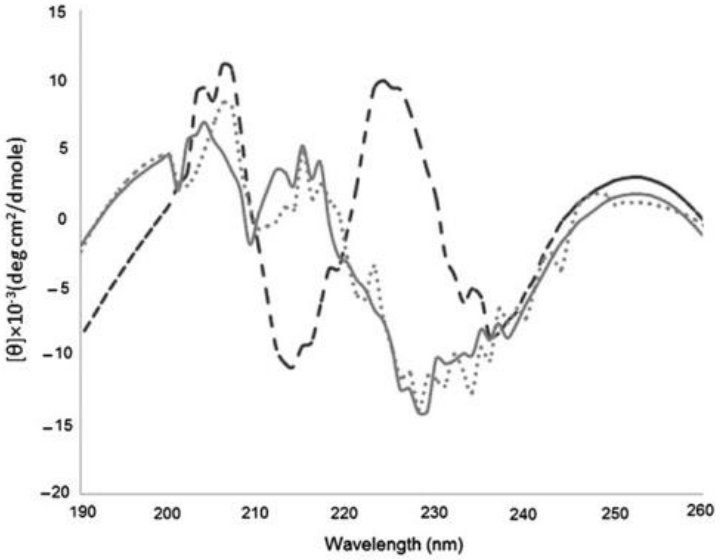

Fig. 1.7. Circular dichroism spectra of peptidoglycan (– –), peptidoglycan treated with AgNP after 30 min (·····) and 3 hours (—) [177].

Ansari et al. investigated how LPS and the phospholipids in bacterial cell membranes were affected by AgNP. Phospholipid phosphatidylethanolamine (PE) and proteins are the primary biomolecules that can interact with NP in *E. coli* cells. In addition to serving as adhesins, they are essential for preserving cells' normal physiological activity. Since the toxicity of NP is linked to their ability to attach to bacteria, probable causes of NP toxicity to microorganisms include harm to the structure of surface biomolecules and modifications to their physical and chemical characteristics. The main biological surface that NP interact with is the cell membrane. In their work, interactions between AgNP membrane biomolecules were studied using *E. coli* as a model and their membrane molecules (LPS and PE). Because they make up a significant portion of the outer membrane of *E. coli* cells, these biomolecules were given priority [178]. LPS is an amphiphilic molecule made up of a hydrophilic O-antigen and a lipid A region that is connected to the outer membrane of gram-negative bacteria. A core oligosaccharide that often includes phosphate and carboxylic acid groups lies between the lipid A region and the O-antigen chain [179]. The results of the investigation indicated that the O-antigen was probably what caused AgNP to interact with the LPS molecule. In the case of phospholipids, specifically PE, it was discovered that some of the $-PO_2$ groups in the phosphodiester were converted to two terminal

groups of phosphoryl (-PO_3) after the addition of AgNP. The phosphodiester bond was broken by AgNP [178].

The damage to cell membranes could be linked to the leakage of proteins. According to Soo-Hwan et al., AgNP make *S. aureus* and *E. coli* cell membranes more permeable, which enhances protein efflux. Protein efflux from cells exposed to AgNP considerably increases after 6 h after treatment, however, the amount of protein leakage from cells in the control group remained constant, demonstrating that AgNP can increase membrane permeability. Notably, more protein leaked through the membranes of *E. coli* than those of *S. aureus*, suggesting that gram-positive *S. aureus* was less susceptible to antibacterial agents than gram-negative *E. coli*. This difference may be explained by the thickness of the peptidoglycan layer on *S. aureus*, which serves the crucial role of shielding against antibacterial substances such as antibiotics, toxins, chemicals, and degrading enzymes [180].

The potential method of action by AgNP can be deduced from the accumulation of envelope protein precursors in cells exposed to AgNP. It has been proven that the translocation of envelope protein precursors across the inner (cytoplasmic) membrane and their subsequent conversion to mature forms (i.e., cleavage of the N-terminal signal sequences) depend on transmembrane electromechanical potential, or membrane potential [181]. It is well known that substances that reduce membrane potential might lead to an accumulation of envelope protein precursors in the cytoplasm [182]. Additionally, ATP is needed for the transfer of precursors of the envelope protein [183]. It was hypothesized that the putative membrane-destabilizing and energy-scavenging capabilities of AgNP may have contributed to the accumulation of these protein precursors in cells exposed to AgNP [150].

AgNP have antimicrobial qualities that extend beyond just bacteria. Thombre et al. evaluated AgNP impact on haloarchaea. Malondialdehyde (MDA) measurements were used to identify lipid peroxidation that AgNP-induced damage causes in haloarchaea (**Fig. 1.8.**). AgNP-exposed haloarchaea cells showed an increase in MDA levels after 24 h exposure. Archaeal lipids are characterized by isoprenoid side chains connected to the *sn*-glyrecol-1-phosphate moiety by an ether bond. MDA is a common indicator of lipid peroxidation even though archaeal lipids are distinct from bacterial and eukaryotic lipids. Lipid peroxidation is caused by cellular stress and is associated with the production of membrane-mediated ROS that cause DNA damage. More harmful degradation products, including MDA, are produced because of free radicals and ROS-induced lipid peroxidation. It was also investigated how much protein leaked from membranes damaged by AgNP.

It was shown that haloarchael samples treated with AgNP had considerably more protein leakage than the control group after 24 h [184].

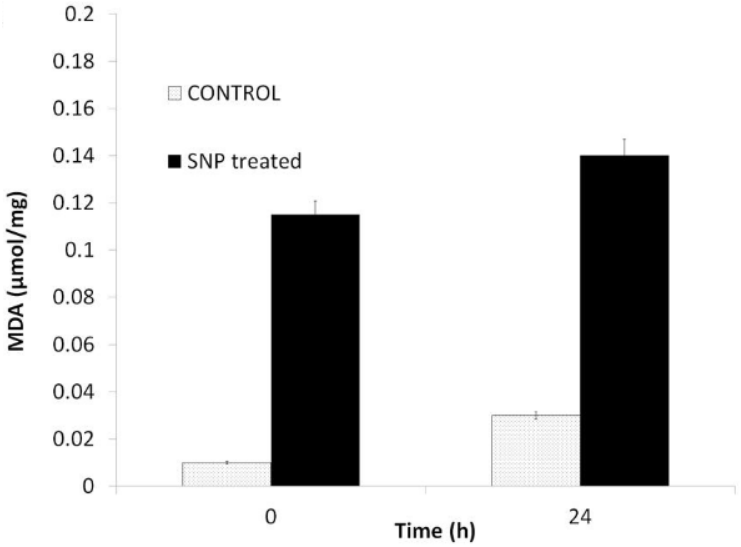

Fig. 1.8. Effect of lipid peroxidation as detected by MDA content in haloarchaea *Haloarcula argentinensis*. SNP - silver nanoparticle [184].

Also, eukaryotic microorganisms are affected by AgNP (**Fig. 1.9.**). One of the antifungal mechanisms is the inhibition of β-glucan synthase, which is primarily in charge of building the yeast cell walls. The wall's mechanical resistance is thus decreased [185]. A different investigation found that AgNP damage the membranes of *Candida* yeasts, prevent them from budding, and ultimately cause cell death [186]. AgNP also affects the amount of fatty acids, which are essential for the morphological shift to hyphae [187]. Additionally, it was noted that AgNP made using green synthesis exhibit effectiveness against *Candida* species biofilms both *in vitro* and *in vivo*. AgNP significantly slow down the biosynthesis of exopolysaccharide and the conversion from yeast form to hyphae in *C. albicans* [188]. Furthermore, AgNP inhibit cell growth, prevent the synthesis of enzymes, and may not only affect the cells found in the biofilm but also penetrate and damage the extracellular matrix [189].

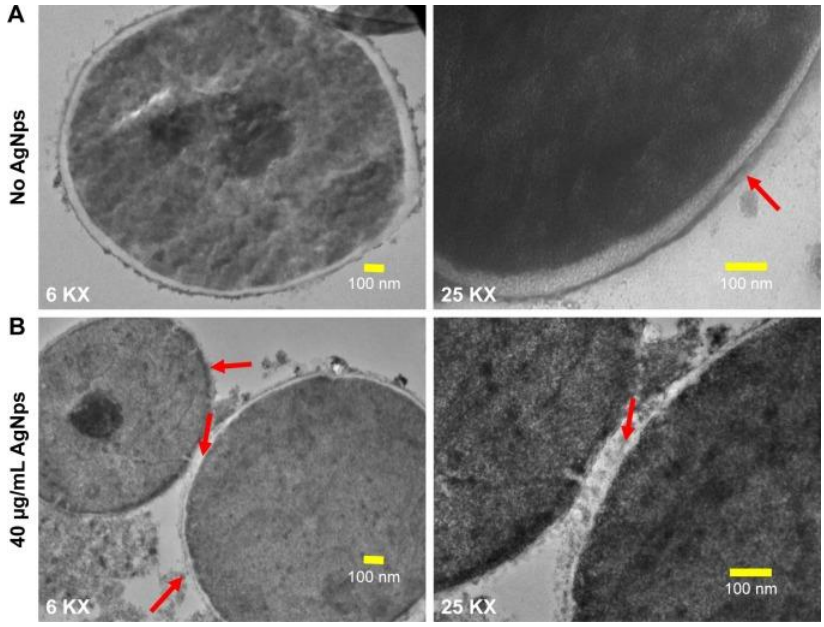

Fig. 1.9. TEM images of *Candida* cells grown without (**A**) and with (**B**) AgNP. Untreated cells revealed well-maintained ultrastructural characteristics, including a distinctive cell wall and cytoplasmic membrane, while cells treated with AgNP showed disruption to the cytoplasmic membrane and cell wall's structural integrity [187].

When Ag^+ adhere to prokaryotic organisms' cell membranes, they also interfere with the electron transport chain. The generated ROS also harms the mitochondrial membrane, breaks DNA, and results in cell death in eukaryotic microorganisms like *Candida*. Additionally, the signalling transduction pathway, which is important for the control of several cellular activities, may be impacted [156].

1.8. Sources of ROS generation in yeast cells

ROS naturally develop in yeast cells as a result of exposure to the environment and side reactions of normal aerobic metabolism. The primary source of ROS is oxidative phosphorylation, a respiratory process that occurs in mitochondria [190]. Protein complexes in the electron transport chain transfer electron to the final electron acceptor, molecular oxygen, where it is reduced to water, in order to create ATP. The complete reduction of molecular oxygen to water is slow, so the intermediates of reduction, ROS, may be generated. Additionally, the endoplasmic reticulum (ER) may also be a source

of ROS given that oxygen is used as the ultimate electron acceptor during oxidative protein folding [191].

The oxidative deamination of amino acids by D-amino acid oxidases when D-amino acids are used as a carbon source and the β-oxidative degradation of fatty acids in peroxisomes are two additional metabolic processes that, depending on the growth conditions, can also result in the production of ROS in yeast cells [192,193]. In addition, yeast may be exposed to xenobiotics, carcinogens, UV and ionizing radiation, as well as ROS produced by neutrophils and macrophages during immune defence mechanisms [194].

1.9. Commonly used model compounds for ROS generation

Hydroperoxides. As a bioproduct of aerobic respiration and in response to interactions with biological and environmental elements, the hydrogen peroxide (H_2O_2) molecule is formed. By causing oxidative stress, it can damage cells, but it also serves as a crucial signalling molecule in a variety of biological functions [195]. H_2O_2 must be removed from cells to prevent Fenton and Haber-Weiss reactions (**Fig. 1.10.**), which lead to the formation of the highly reactive hydroxyl ($-OH^{\cdot}$) radical. Organic hydroperoxide ($C_9H_{12}O_9$) is another potential source of ROS since it produces highly reactive free radicals like alkoxy radicals, which have exceptionally high mutagenic toxic potential [196]. At low concentrations, the lipid hydroperoxide linoleic acid hydroperoxide (LoaOOH) is more toxic to yeast cells than H_2O_2 [197].

Superoxide anion. When an oxygen molecule acquires one electron, O_2^{-} is produced. It is the primary ROS by-product of the mitochondrial electron transport chain runoff. Although the superoxide anion itself is not highly reactive, it can serve as a precursor to other ROS by producing H_2O_2 during dismutation and hydroxyl radicals in metal-catalysed reactions, both of which are extremely reactive. Menadione and paraquat, redox-recycling drugs that transfer electrons to molecular oxygen, can produce superoxide anions in yeast cells [198,199].

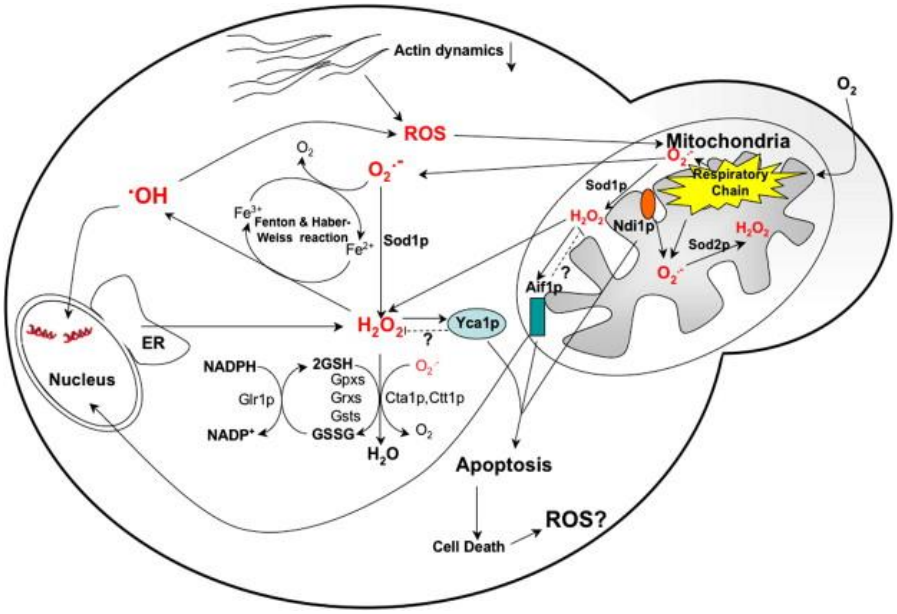

Fig. 1.10. Potential sources of ROS important to yeast apoptosis (in red). Fenton and Haber-Weiss reactions are responsible for the production of highly reactive hydroxyl radical [200].

Thiol-reactive compounds. Oxidative stress is frequently produced using substances that react with thiols. These include substances that directly oxidize thiol groups as well as those that indirectly produce oxidative stress by accumulating and depleting thiol groups. One such substrate for glutathione transferases is 1-chloro-2,4-dinitrobenzene (CDNB) [201]. Although it does not oxidize thiol groups in yeast, it causes oxidative stress by depleting cellular glutathione (GSH), which contributes to the formation of endogenous ROS [202]. Diamide is a thiol-specific oxidant that is membrane-permeable and promotes the production of disulphides [203]. Because it quickly triggers GSH oxidation, which causes the redox balance to shift to the oxidized GSH form, it is employed to generate oxidative stress in yeast cells [204].

Heavy metal stress. Cellular ROS production can be significantly impacted by the presence of free redox-active metals like iron or copper [205]. For instance, through the Fenton reaction reduced Fe^{2+} can produce extremely reactive hydroxyl radicals (**Fig. 1.10**.). Superoxide anion can reduce oxidized Fe^{3+}, which also triggers the Haber-Weiss reaction and generates a hydroxyl radical. Since proteins can also be a source of free iron, it is crucial for the cell that the amounts of free metal ions are managed, for instance by incorporation into [4Fe-4S] clusters in proteins [205,206].

Another metal, cadmium, is a highly toxic metal and a well-characterized human carcinogen. It can also lead to oxidative stress [207]. It can enter the cell through the same transport systems as the necessary metals. GSH depletion and attachment to sulfhydryl groups are its primary toxic mechanisms once within the cell [208]. Additionally, it can also replace iron, zinc, and copper in various cytoplasmic and membrane proteins, increasing the levels of unbound free copper, zinc, and iron ions, that through the Fenton reaction, cause oxidative stress [209,210].

1.10. Cellular responses to ROS

In response to ROS, yeast cells change the expression of genes encoding enzymes responsible for antioxidant defence mechanisms as well as genes that encode proteins responsible for repairment and detoxifying the cellular damage that results.

Redox homeostasis and oxidative stress. To keep redox balance within the cell, cells must react to oxidative stress by controlling their thiol systems. Thiol groups are key mediators in oxidative signalling [211].

Accessible thiol groups in proteins and low molecular weight molecules have highly dynamic compositions that change depending on the environment and growth conditions. Protein-protein interactions are a common component of signalling pathways, and oxidative factors can influence these interactions. The oxidation of cysteine residues in proteins serves as the foundation for most ROS-specific regulatory mechanisms. This is a result of the high reactivity of cysteine residues and the ease with which cysteine residues and some sulphur derivatives (such as disulphides, sulfenic acid, sulfinic acid, and sulfonic acid) can change their oxidation state. Although cysteine residues react slowly with ROS, their ionization status, which relies on the nearby protein environment, can make them more reactive. H_2O_2 stress in yeast cells induces protein-specific oxidations instead of non-specific oxidation of protein –SH groups [212].

All organisms have intricate regulatory systems that help them maintain redox homeostasis, most notably the GSH/glutaredoxin and thioredoxin systems. These systems are all thermodynamically linked since they each rely on NADPH as a source of reducing equivalents [213].

Translation regulation of gene expression. Global protein synthesis suppression is a typical response to stressful conditions. For cells to survive under stressful circumstances, particular mRNAs must be differentially controlled during translation [214,215]. While gene expression is being

reprogrammed in response to developing stress, inhibition of protein synthesis under oxidative stress can prevent continued gene expression under error-prone conditions and modify existing mRNAs and proteins. Yeast cells respond to hydrogen peroxide stress by reversibly and rapidly suppressing protein synthesis, which inhibits translation by more than 60% within 15 min [216–218]. The inhibition is quantity-dependent and mostly regulated by Gcn2 (general control nonderepressible 2) protein kinase, which phosphorylates the α-subunit of translation initiation factor 2 (eIF2). Phosphorylation changes the form of eIF2 from a substrate to a competitive inhibitor, eIF2B, which reduces eIF2 activity and inhibits translation initiation [218].

As Gcn2 can be activated after exposure to organic hydroperoxides like cumene hydroperoxide, thiol oxidants (e.g., diamine), and heavy metals (e.g., cadmium), phosphorylation of eIF2 is a generic response to ROS. Conditions of oxidative stress cause Gcn2 to become active due to the presence of uncharged tRNAs. ROS can affect the transport and storage of amino acids. Additionally, the oxidation of proteins and nucleic acids necessary for tRNA aminoacylation can result in an accumulation of uncharged tRNAs and the activation of Gcn2 [219].

Several genes whose translation is repressed under H_2O_2 oxidative stress are actively transcribed. Increased gene transcription compared to weak translation provides a source of mRNA that can be rapidly translated once the cell has removed the resulting stress [218].

Since protein synthesis is similarly severely suppressed in *gcn2* mutants, oxidative stress also controls translation through Gcn2-independent pathways [218]. One such mechanism could be the phosphorylation of the elongation factor eEF2 by protein kinase Rck2, which affectes ribosome elongation during stress [220].

Metabolic remodelling is a rapid and regulated response to oxidative stress. It is widely known that yeast cells change their gene expression in response to oxidative stress, including the transcription and translation of genes encoding antioxidants and other stress-protective components. However, the stress response also depends heavily on metabolic changes. While changes in gene expression occur more slowly (in a matter of minutes), metabolic changes in yeast cells can be observed within seconds [221,222]. Rearranging carbohydrate metabolisms is one of the main metabolic adjustments that occur to keep the redox balance in the cell under oxidative conditions. A conservative response to oxidative stress is switching from glycolysis to the pentose phosphate pathway associated with NADPH production [223].

The pentose phosphate pathway is the source of cellular reducing power, in the form of NADPH. NADPH is particularly important in the presence of oxidants because it provides the reducing potential for most antioxidants and redox-regulating enzymes such as the GSH/glutaredoxin and thioredoxin systems. Glucose-6-phosphate dehydrogenase (G6PDH) and 6-phosphogluconate dehydrogenase (6PGDH) catalyse the first two steps of the pentose phosphate pathway and are the main sources of NADPH. G6PDH catalyses the key NADPH-producing step and is important in protecting against oxidative stress [217,224].

1.11. The impact of NP on ROS production and antimicrobial effect

At lower doses AgNP exhibit little toxicity towards human cells. For instance, it was shown that biogenic AgNP have no cytotoxic action on peripheral blood mononuclear cells even at a dosage that was 5 times the minimum inhibitory concentration (MIC) for *Candida albicans* (about 5 μg/mL). However, when the dosage is increased further, cell death ensues [225]. Therefore, it's crucial to reduce AgNP concentrations.

Synergistic effects may be produced to boost the antimicrobial effectiveness of lower concentrations of AgNP [226]. It has been shown that AgNP and fluconazole have synergistic effects on *C. albicans*, increasing the production of intrinsic ROS. Fluconazole had high MIC (128 μg/mL) in both used *C. albicans* strains, according to the study. MIC for AgNP was 32 μg/mL. The MICs for fluconazole for *C. albicans*, however, drastically dropped to 0.5 μg/mL and 1 μg/mL when combined with AgNP. Additionally, it was noted that the MIC for AgNP was significantly lowered to 0.5 μg/mL [227].

It has been noted that AgNP-caused generation of ROS has antifungal effects. When compared to the control group in the study, the fluconazole-treated *C. albicans* had less ROS induction. AgNP significantly increased ROS levels, while the fluconazole and AgNP combination group produced the most ROS. Also, the increased fluconazole accumulation worsens the production of ROS, showing that fluconazole and AgNP work together to promote ROS production at 0.5 μg/mL [227].

ROS can also be produced via physically applied means. Yusupov et al. showed that ROS are generated in the presence of an electric field [228]. According to Wang et al., ROS can develop in bacteria as a result of extracellular electron interference [229]. A higher voltage current may carry more electrons, which produces more ROS and has a stronger antibacterial effect [230].

Based on a study using the fungus *A. fumigatus*, ROS can harm the unsaturated fatty acids contained in the membranes of pathogenic moulds. The results showed that the antifungal medications terbinafine and itraconazole dramatically exacerbated lipid peroxidation [231].

Another study used DCFH-DA and MDA staining to measure ROS production and lipid peroxidation following treatment with zinc oxide NP (SaZnO NP) from *Syzygium aromaticum* flower bud extract. The SaZnO NP-treated samples showed more ROS production compared to the control. The findings showed a connection between the dose of SaZnO NP and the build-up of ROS. In line with the results of the ROS investigation, SaZnO NP also has a significant impact on lipid peroxidation, and MDA accumulation closely associated with SaZnO NP dose [232].

1.12. Electroporation and its application

High-voltage electrical pulses can temporarily increase membrane permeability to various compounds. Electroporation is the process used to increase membrane conductivity. When electroporation is reversible, it is used to transfer genes and deliver drugs to cells more effectively, but electroporation can also cause cell death [233,234]. Irreversible electroporation (often with more electric pulses and amplitude of electric pulses) (IRE), which causes cells death, has been successfully employed as a new technique for the ablation of soft tissues like tumours or arrhythmogenic heart tissue [235,236]. Although different electrical pulse characteristics and conditions may have an impact on the causes of cell death, these mechanisms are still not fully understood [236].

Electroporation has been used in medicine for at least 40 years [237]. It is applied to DNA delivery to cells (gene electrotherapy), DNA vaccination, tumour reduction, and more [238]. In rat models, the application of IRE has been shown to completely repair skin wounds without leaving any scars. Although this method of treatment causes cell death, the extracellular matrix of the skin is preserved. Half a year after this treatment, the epidermis, sebaceous glands, hair follicles, and other parts of the skin tissue have completely reformed in the entire affected area. Such results also indicate that the extracellular matrix is crucial for skin cell migration, signaling, and differentiation, suggesting that IRE is an excellent tool for scar-free tissue regeneration [238].

Partial IRE (pIRE) can also be applied to the reduction of burn scars. It was found that 5 therapy sessions every 20 days reduced the scar area by about

60% compared to pIRE-unaffected scars. This pIRE model led to a linear regression model that predicts scar size 6 months after third-degree burn in rat models [239].

It is well known that the electric pulses affect the water molecules trapped in the hydrophilic region of the phospholipid bilayer and that this influence causes the water molecules to direct their dipoles in the direction of the electric field. Because of the hydrogen bonds between neighbouring molecules, clusters are being formed. The clusters expand and penetrate the hydrophobic area of the membrane, leaving a hydrophilic hole (**Fig. 1.11.**). When lipids interact with water, their polar groups rotate in the direction of water molecules, stabilizing the pore. If electroporation is reversible, the procedure above repeats as the pore closes in reverse order [240]. Biological membranes' electrical conductivity and permeability can be rapidly boosted by exposing them to an electric field. The formation of pores is made possible by such a shift in the charge of the cell membrane, but because the membrane is fluid-like, the pores can shut on their own. If the exposure to the electric field was not too strong or not too long, electroporation can be reversed. After exposure to the electric field, the stable pores that form have various lifetimes that can range from a few milliseconds to several minutes [241].

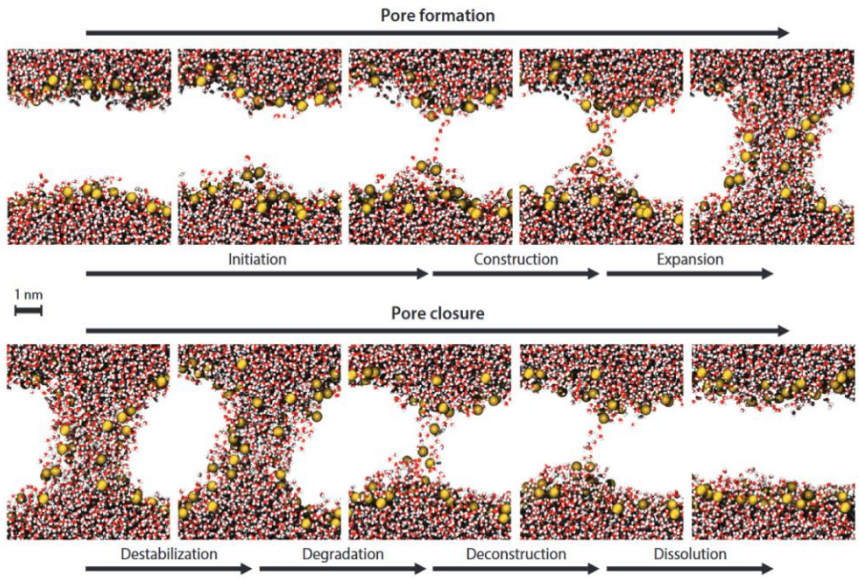

Fig. 1.11. The life cycle of an electrically produced pore in a lipid bilayer. Pore generation and closure steps are displayed in the order in which they occur, disregarding any deviations from their regular timing. The beginning of the electric field starts formation, and its end starts closure. Just the water molecules and phosphorus atoms are shown for simplicity [242].

Damage to the plasma membrane causes an open pore, which allows calcium ions (Ca^{2+}) from the external environment to enter the cell [243]. Several cell signalling pathways (e.g., activation of caspases) associated with the cell stress may be activated as a result [244,245]. Due to the activation of Ca^{2+}-ATPases and the suppression of ATP synthesis in mitochondria, a high Ca^{2+} influx depletes ATP and is linked to cell death [243,246].

Electric stimuli result in the production of ROS and oxidative lipid damage, which are associated with a longer time for the cell membrane to seal after the pulse [247,248]. This could result in more permeability after the pulse. In the cell, particularly in the mitochondria, a pulsed electric field may cause the creation of ROS. Depending on the type of the cell and the features of the pulse, these ROS can harm molecules, cause oxidative stress, and result in various types of cellular death [243,249,250].

1.13. The classification of yeast cell death

Cell death is a process that regulates homeostasis and biochemical changes in healthy cells. For a long time, yeast cell death was classified based on macroscopic morphological changes in the cells [251]. Such morphotypes, along with the mechanisms by which dead cells and their fragments are removed, are used to classify cell death in three distinct groups: type I cell death of apoptosis, characterized by chromatin condensation (pyknosis), cytoplasmic shrinkage, plasma membrane contraction, and nuclear fragmentation (karyorrhexis), resulting in the formation of apoptotic bodies, which are efficiently absorbed by neighbouring cells with phagocytic activity; type II cell death or autophagy, manifested by cytoplasmic vacuolization and culminating in phagocytic uptake and degradation in lysosomes; and type III cell death or necrosis, lacking distinctive features of type I or type II cell death and resulting in the destruction of dying cells in the absence of phagocytic and lysosomal involvement [252,253]. Currently, the classification of yeast cell death considers not only morphological changes but also enzymatic and functional aspects [254]. The possible ways of death of yeast cells are shown in **Figure 1.12.**

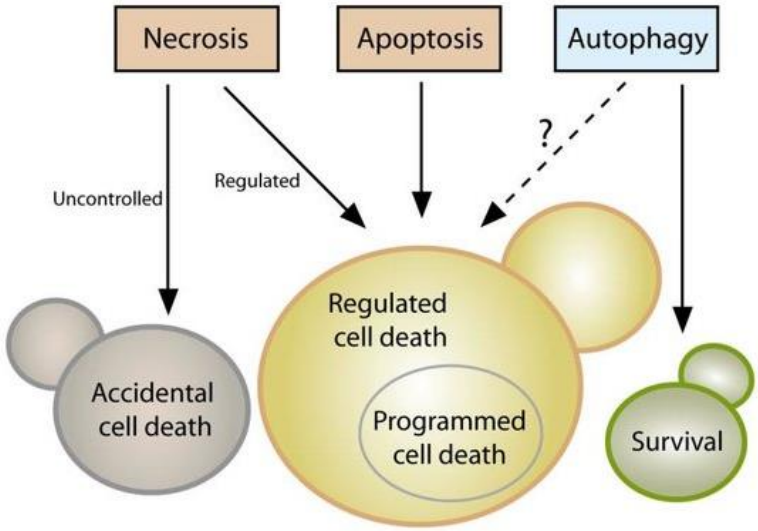

Fig. 1.12. Types of yeast cell death. Yeast cells can die after exposure to harsh environmental conditions by accidental cell death (APC) or after the failure to cope with moderate stress via regulated cell death (RCD). The potential role of autophagy as a cell death pathway in yeast remains elusive [254].

Yeast cells can die when exposed to very harsh microenvironmental conditions, either by accidental cell death (ACD) or by failing to respond to mild stress through regulated cell death (RCD). While spontaneous cell death always manifests as a necrotic morphotype (disintegration of cell structure, rupture of the plasma membrane), regulated cell death can have a variety of morphologies and can occur through multiple signaling pathways, including regulated necrosis or apoptosis. Programmed cell death (PCD), which occurs in strictly physiological scenarios (such as development), is a specific type of RCD. Although apoptosis is the most common form of PCD, there are other (non-apoptotic) types of biologically relevant cell death. It is yet unclear how autophagy may contribute to yeast cell death. For the above reasons, an understanding of the biochemical and genetic aspects of cell death is essential to assess the mode of cell death [254,255].

1.13.1. Yeast cell apoptosis

Apoptosis in yeast cells was first identified in yeast with a *CDC48* gene mutation ($cdc^{48S565G}$). The product of this gene is AAA-ATPase, which is involved in cell division, ER protein degradation (ERAD) functions, and

vesicular transport [256]. Like mammalian cells, apoptotic yeast cells have apoptosis-specific markers, the most important of which are: activated metacaspases, changes in phosphatidylserine localization, chromatin condensation, and ongoing DNA fragmentation (**Fig. 1.13.**). In nature, this process occurs in order to remove old, unhealthy cells from the population, thus reducing the consumption of nutrients and ensuring their availability to healthy, young yeast cells [257].

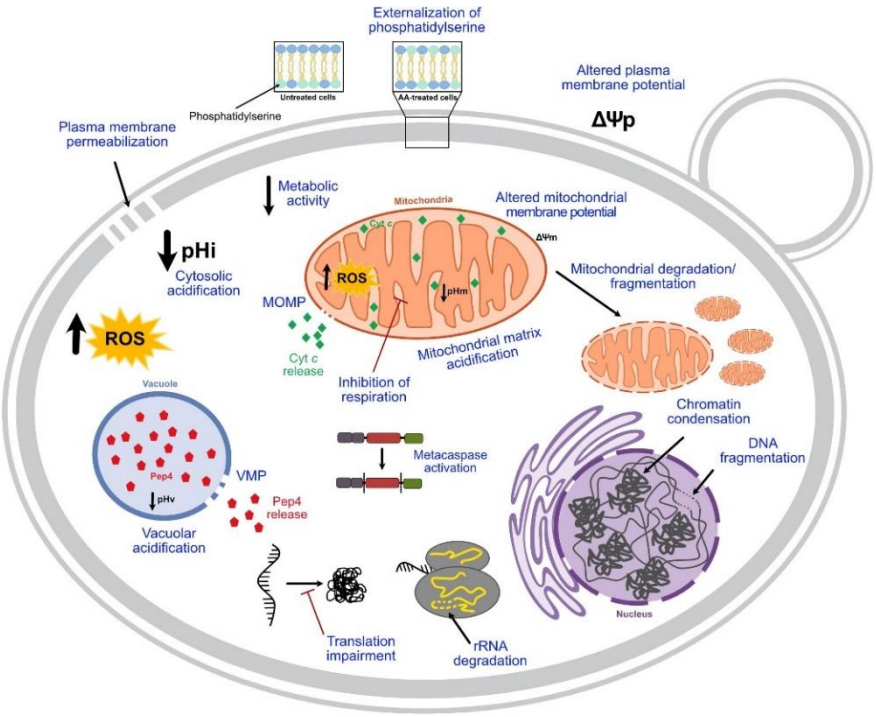

Fig. 1.13. Apoptosis markers in yeast cells. When yeast cells are exposed to harmful substances, such as acetic acid, a programmed death response, written in blue, can be triggered [258].

In yeast cells, apoptosis can be induced by both intrinsic and extrinsic factors, such as acetic acid, dysfunction of cellular processes, H_2O_2 (**Fig. 1.13.**), and many others [259,260]. For example, when yeast cells are exposed to acetic acid, depending on the concentration, various markers characteristic of apoptosis are determined, as shown in **Fig. 1.13.** In addition to the activation of caspases, chromatin condensation and changes in phosphatidylserine localization occur, as well as rRNA degradation, inhibition of the translation process, permeability of vacuoles and membranes, and changes in mitochondria [258]. Although yeast lacks *Bax* and *Bcl* genes,

several orthologs of key mammalian apoptosis genes such as *AIF1*, *NUC1*, *YCA1*, and *NMA111* have been identified in yeast, which confirms the presence of a basal apoptotic machinery in this microorganism [261].

1.13.2. Yeast cell autophagy

Autophagy is a tightly regulated conservative process required for the degradation and recycling of cytoplasmic components, translocating various molecules and organelles to the vacuole or lysosomes. Autophagy helps maintain the balance between the synthesis, degradation, and recycling of cellular products and plays an important role in ensuring proper cell growth, development, and maintenance of homeostasis. A morphological indication of autophagy is the formation of autophagosomes, vesicles surrounded by a double membrane, in which cytoplasmic components are randomly (non-selective autophagy) or selectively (selective autophagy) segregated. Selective autophagy ensures cell survival by removing protein aggregates and recycling structures and components of mitochondria (mitophagy), peroxisomes (pexophagy), lipids (lipophagy), and ER (ER-phagy), which can be potential triggers of apoptosis [255]. Upon fusion with the vacuole, the cell's components are broken down into simpler molecules, which are then released back into the cytoplasm for reuse. Autophagy in yeast cells occurs continuously at a basal level and is regulated by nutritional changes and starvation. Regulation of the process determined the size and number of autophagosomes under normal and inducing conditions. Studies in yeast have identified more than 30 autophagy-related proteins, most of which are conserved in higher eukaryotes. In the presence of sufficient nutrients, most autophagy-related genes are repressed at the transcriptional level, either through inhibition of activators or activation of autophagy inhibitors [262,263]. In some organisms, autophagy-mediated a specific type of RCD, which is described as autophagic cell death [264]. In yeast, the relationship between autophagy and cell death is still not much researched, and some studies suggest that autophagy can accelerate cell death in *Saccharomyces cerevisiae* following apoptosis regulator BAX expression and starvation [265]. It was also observed that changes in the morphology of vacuoles and fragmentation of mitochondria occur in yeast cells, which may be associated with autophagic cell death [263].

1.13.3. Yeast cell necrosis

In dying yeast, characteristics of typical necrosis may result from a primary or secondary necrotic process. Although secondary necrosis is often a consequence of apoptosis, the primary necrotic phenotype (which occurs without any previous apoptotic features) can result from two cell death pathways: ACD and RCD [261]. Indeed, primary yeast necrosis may not only be a consequence of severe damage (non-regulated necrosis) but may occur as a genetically regulated process (regulated necrosis) [266]. In both cases, this type of cell death exhibits distinct morphological and biochemical characteristics that define them as necrotic [254]. In contrast to apoptosis, necrotic cells are characterised by plasma membrane damage that leads to the leakage of cell contents into the environment [255]. As previously described, low concentrations of H_2O_2, acetic acid, and heavy metals are known inducers of apoptosis. Higher concentrations of these substances can cause spontaneous necrosis, due to increased damage to cellular components [259,260,267]. In yeast, regulated necrosis is positively affected by aging, low pH, and mitochondria, and inhibited by spermidine, endonuclease G, vacuolar, and peroxisomal functions [268]. Homologs of known mammalian necrosis mediators have been found in the *S. cerevisiae* genome, but the altruistic significance of necrotic cell death in yeast is still unknown [255]. Liponecrosis is an additional model of RCD cell death in yeast cells exposed to exogenous palmitoleic acid. Cells that undergo liponecrosis do not show signs of apoptosis or necrosis and, as in autophagy, non-selective degradation of cell organelles occurs. This suggests that there are several alternative ways of yeast cell death [269].

2. MATERIALS AND METHODS

2.1. Reagents and kits

The reagents and kits used in the work are presented in **Table 2.1.**

Table 2.1. Reagents and kits used.

Reagents and kits	Manufacturer
Acetic Acid, $CaCl_2$, Ethanol, Formaldehyde, Meat Extract, Na_2HPO_4, NaCl, Triton X-100, $ZnSO_4$, Poli-L-lysine, Crystal violet	MERCK, Germany
Bovine Serum Albumin, Ethidium bromide	Sigma Aldrich, Germany
Click-iT® Lipid Peroxidation Detection with Linoleamide Alkyne (LAA) Kit	Thermo Fisher Scientific, USA
D(+)-Glucose Monohydrate, D-Sorbitol, Yeast Extract, Peptone, $AgNO_3$, Agar	ROTH, Germany
DCFDA/H_2DCFDA-Cellular ROS Assay Kit (ab113851), Apoptosis DNA Ladder Assay Kit (ab66090)	Abcam, UK
KH_2PO_4, KCl	BDH, Germany
Propidium iodide, Gluteraldehyde	SIGMA, Germany
CaspACE^{TM} FITC-VAD-FMK In situ Marker Kit (QIA90)	Calbiochem, USA
Agarose	SIGMA, USA
Isopropanol	REACHIM, Russia

2.2. Sources of microorganisms and keratinocytes

The *Geobacillus* spp. strains used in the biological synthesis of AgNP were strains 18, 25, 95, and 612. These strains were isolated in the Department of Microbiology and Biotechnology, Institute of Biosciences (former Faculty of Natural Sciences), Life Sciences Center, Vilnius University (Lithuania), from an oil well in Lithuania. These strains were identified as *Geobacillus stearothermophilus* (unpublished for strains 25 and 612). Identification of

Geobacillus sp. strain 18 was published in [270]. The *Geobacillus* sp. strain 95 was deposited in the DSMZ culture collection under the number DSM 104629 [271].

The antimicrobial effect of the obtained AgNP was studied against pathogenic skin bacteria *Staphylococcus aureus* (ATCC29213), *Streptococcus pyogenes* (ATCC12384), and *Pseudomonas aeruginosa* (ATCC27853), and yeasts *Candida guilliermondii*, which was isolated from the skin of an atopic dermatitis patient [272], and *Saccharomyces cerevisiae* (BY4742). These strains were obtained from the collection of the Laboratory of Eukaryotic Molecular Microbiology, Institute of Biosciences, Life Sciences Center, Vilnius University (Lithuania).

The human keratinocyte cell (Ker-CT) line was obtained from the collection of the Department of Biological Models of the Institute of Biochemistry, Life Sciences Center, Vilnius University (Lithuania). Ker-CT cells are cultured for *in vitro* experiments using deep-frozen cryoampules with cells.

2.3. Cultivation media for microorganisms, solutions, buffers, and other tools used in the work

Geobacillus spp. cultivation medium:

- peptone 1%
- meat extract 0.5%
- NaCl 0.5%

After autoclaving (30 min at 121 °C), a final concentration of 2.3 mM $CaCl_2$ and 0.91 μM $ZnSO_4$ are added.

Yeast extract peptone dextrose (YPD) medium:

- glucose 2%
- peptone 2%
- yeast extract 1%

Sterilized by autoclaving (15 min at 112 °C).

Luria-Bertani (LB) medium:

- peptone 1%
- yeast extract 0.5%
- NaCl 0.5%

Sterilized by autoclaving (30 min at 121 °C).

2% agar is added in all cases to prepare agar plates.

1 M sorbitol solution (1 L):
182.18 g of D-sorbitol is dissolved in 800 mL of deionized water. After dissolving, water is added to bring the final volume to 1 L. Sterilized by autoclaving (15 min at 112 °C).

1 × PBS buffer (1 L):

- 8 g NaCl
- 200 mg KCl
- 1.44 g Na_2HPO_4
- 240 mg KH_2PO_4

First, the salts are dissolved in 800 mL of deionized water. pH of the resulting solution adjusted with 1 M HCl to pH 7.4. Water is added to bring the final volume to 1 L. Sterilized by autoclaving (30 min at 121 °C).

10% Bovine serum albumin (BSA) (1 L):
100 g of BSA powder is dissolved in 800 mL of deionized water. After dissolving, water is added to bring the final volume to 1 L.

1 × TAE: 50 × TAE buffer is diluted 50 times with distilled water.

Polylysine slides:
A drop of 0.1% Poly-L-lysine solution is dried on microscope slides overnight at room temperature or for 1 h at 55 °C.

2.4. Methods

2.4.1. Extracellular synthesis of silver nanoparticles

The *Geobacillus* strains were grown aerobically in liquid 100 mL *Geobacillus* sp. cultivation medium in 250 mL Erlenmeyer flasks. The cultures were grown in an orbital shaker (Esco, Singapore, Singapore) at 55 °C with aeration at 180 rpm. After 48 h of incubation, cells were separated by centrifugation at 16,000× *g* for 10 min. Cell-free supernatants were used as material for AgNP synthesis. The supernatants of the targeted strains were treated with $AgNO_3$ solution at final concentrations of 2 mM. The whole mixtures were incubated in a shaking incubator for 48 h at 55 °C and 200 rpm. The supernatants without $AgNO_3$ and sterile bacterial growth medium

supplemented with 2 mM $AgNO_3$ were used as controls. After 48 h of incubation, the mixtures were centrifuged at 3000× *g* for 10 min to remove media components. The mixtures were centrifuged at 16,000× *g* for 15 min to collect AgNP. To remove unconverted silver ions, the obtained pellets were washed three times with 70% ethanol and three times with deionized water by centrifugation at 16,000× *g* for 15 min.

2.4.2. Characterization of silver nanoparticles

The formation of the AgNP was monitored using an ultraviolet-visible (UV–Vis) spectral analysis. The spectra of cell-free supernatants treated with 2 mM $AgNO_3$ were measured at 300–600 nm using a UV–Vis spectrophotometer (Ultrospec 5300 pro, Amersham Biosciences Corp., Piscataway, NJ, USA). The size, distribution, and morphology of the nanoparticles were further analysed via scanning electron microscopy (SEM) (Tescan Vega 3, Brno – Kohoutovice, Czech Republic). Samples for SEM were prepared by drop-coating the AgNP solution onto an aluminium grid. Before transferring samples to the microscope, they were dried at 55 °C. The zeta potential values of AgNP were measured using a Malvern Zetasizer Nano ZS (Malvern Panalytical, Malvern, UK) and recalculated applying the Smoluchowski model. The AgNP particle size distribution was evaluated using the dynamic light scattering (DLS) method (ZetaSizer Nano ZS (Malvern Panalytical, Malvern, UK) equipped with a 4 Mw He-Ne laser emitting at a wavelength of 633 nm). Measurements were performed at 25 °C and an angle of 173°. These parameters were determined using AgNP at a concentration of 1 mg/mL in deionized water. To determine changes in size distribution and zeta potential values in microorganism nutrient media (YPD and LB) and 1 M sorbitol solution, the obtained AgNP were kept in these media for 12 h (the AgNP were rinsed with deionized water before measurements).

2.4.3. 'Spot test' to determine the minimum inhibitory concentrations (MICs) of AgNP against skin pathogenic bacteria and yeast

The 'Spot test' to determine AgNP MIC was adapted according to Kasemets et al. [273]. The microorganism culture is grown aerobically in 5 mL liquid LB (*S. aureus*, *S. pyogenes*, *P. aeruginosa*) or YPD (*C. guilliermondii*) medium until it reaches OD_{600} = 1 at 37 °C or 30 °C temperature respectively. 1 mL of the grown culture of microorganisms is

washed three times by centrifugation and resuspension in 1 M sorbitol solution. 100 µL of the prepared microorganism culture suspension is dispensed into a 96-well plate. Next, 100 µL of different concentrations (**Table 2.2.**) of *Geobacillus* spp. strains 18, 25, 95, and 612 AgNP solution are added. 100 µL of prepared microorganism suspension with 100 µL of 1 M sorbitol is used as a control. The plate is incubated at 35 °C (for bacteria) or 30 °C (for yeast) for 24 h. After the incubation, 5 µL from each well is transferred onto agar LB (for bacteria) or YPD (for yeast) plates. Results are evaluated after 24 h (for bacteria) or after 48 h (for yeast).

Table 2.2. The concentrations (µg/mL) of *Geobacillus* spp. strains 18, 25, 95, and 612 AgNP used for the 'Spot test' to determine MIC against skin pathogens.

Geobacillus spp. strain / Microorganism	18	25	95	612
S. aureus	50; 25; 12.5; 6.25; 3.12; 1.56		100; 50; 25; 12.5; 6.25; 3.12	25; 12.5; 6.25; 3.12; 1.56; 0.78
S. pyogenes	50; 25; 12.5; 6.25; 3.12; 1.56		25; 12.5; 6.25; 3.12; 1.56; 0.78	
P. aeruginosa	50; 25; 12.5; 6.25; 3.12; 1.56	25; 12.5; 6.25; 3.12; 1.56; 0.78		
C. guilliermondii	15; 12.5; 10; 7.5; 5			10; 7.5; 5; 2; 1

2.4.4. Electroporation of skin pathogens

Tested bacteria and yeast are grown in 5 mL liquid LB or YPD medium in 25 mL test tubes. The cultures are grown in an orbital shaker at 37 °C or 30 °C temperature respectively until the cultures reached the exponential growth phase. The cultures are then prepared for electroporation: washed three times with deionized water and three times with 1 M sorbitol solution. The cells are diluted with 1 M sorbitol solution to make the cell concentration in suspension 1.5×10^4 CFU/mL. 80 µL of the cell suspension is then transferred to a cuvette for electroporation. The cells are exposed to a single 100 µs electric field pulse (PEF) with amplitude ranging from 2.5 to 15 kV/cm with a step of 2.5 kV/cm. As control untreated cells are used. After the electroporation, the cell suspension is transferred to agar LB or YPD (according to the type of the microorganism) plates and incubated for 24 h at

35 °C (in the case of bacteria) or 48 h at 30 °C (in the case of yeast). Results are evaluated by counting CFU.

In the case of *P. aeruginosa* biofilms, the grown biofilms were washed three times with deionized water and three times with 1 M sorbitol. 60 μL of the grown biofilms were transferred to cuvettes for electroporation. The conditions of electroporation were: eight 100 μs impulses at 15, 20, and 25 kV/cm PEF. As a control, 60 μL of disintegrated biofilms unaffected by electroporation was used. After the electroporation, suspensions were transferred on LB agar plates and incubated at 30 °C for 72 h. Colony-forming units were counted for the survival assay. At least three independent replicates were performed for each unique experiment.

2.4.5. Effects of silver nanoparticles and electroporation on skin pathogens

Tested bacteria and yeast are prepared for electroporation as mentioned in Section 2.4.4. A solution of *Geobacillus* spp. strains 18, 25, 95, and 612 AgNP are added to the *C. guilliermondii* cell suspension to a final concentration of 1 μg/mL (18, 25, and 95) and 0.5 μg/mL (612) to a total volume of 80 μL. A solution of *Geobacillus* sp. 612 AgNP is added to the final concentrations of 2.5 μg/mL for *S. aureus*, 1 μg/mL for *S. pyogenes*, and 2 μg/mL for *P. aeruginosa*. The prepared cells and AgNP mixture are transferred to a cuvette for electroporation. The cells are exposed to a single 100 μs electric field pulse with PEF amplitude ranging from 2.5 to 15 kV/cm with a step of 2.5 kV/cm. As controls untreated cells and cells exposed only to AgNP are used. 10 min after the electroporation, the cell suspension is transferred on agar LB or YPD (according to the type of the microorganism) plates and incubated for 24 h at 35 °C (in the case of bacteria) or 48 h at 30 °C (in the case of yeast). Results are evaluated by counting CFU.

2.4.6. SEM visualization of effects of silver nanoparticles and electroporation on *Candida guilliermondii*

Cells were prepared for electroporation and electroporation was performed as described in Section 2.4.4. Cells were affected by electroporation with and without *Geobacillus* sp. 25 AgNP (5 μg/mL). Electroporation parameters - single 100 μs pulse, 10 kV/cm PEF, control - PEF or AgNP unaffected cells. Next, cells were prepared for SEM. Cells were washed by repeated centrifugation and resuspension three times in 1 × PBS

buffer. Cells were fixed with 3% glutaraldehyde for 2 h at 4 °C. After fixation, cells were washed again by centrifugation and resuspension three times in 1 × PBS buffer. Cells were fixed with 3% glutaraldehyde for 24–48 h at 4 °C. After fixation, cells were washed by centrifugation and resuspension three times in 1 × PBS buffer. Subsequently, water was removed from the cells by exposing them to different concentrations of ethanol: 50, 70, 80, and twice 95%. Between ethanol concentration changes, the cells were kept in ethanol of the corresponding concentration for 10 min at room temperature, and the cells were centrifuged when the ethanol concentration was changed. After that, cells were affected in the same manner three times with 99.8% ethanol (cells were kept in ethanol for 15 min). The prepared cell suspension was transferred onto a gold-coated silicon disc and maintained until the ethanol was completely evaporated. Subsequently, SEM (microscope Tescan Vega 3, Czech Republic) was performed.

2.4.7. Determination of ROS formation in yeast cells after exposure to silver nanoparticles and in combination with electroporation

To test the formation of ROS in the yeast cells exposed to AgNP, cell cultures of *C. guilliermondii* are cultivated aerobically in liquid YPD media at 30 °C up until the exponential phase (12–14 h). Cells are washed twice with deionized water and twice with a 1 M sorbitol solution by centrifugation and then suspended in 1 M sorbitol. The cells are treated with AgNP MICs and incubated at 30 °C for 15 min. Untreated cells are used as negative control and cells treated with 50 μM of *tert*-butyl hydroperoxide (TBHP) for 4 h are used as a positive control. Next, cells are prepared for ROS formation analysis by using a modified DCFDA/H_2DCDFA-Cellular ROS Assay Kit (ab113851) protocol. A diluted DCFDA solution to the final concentration of 10 μM is added for staining the cells. Then cells are incubated for 2 h at 30 °C in the dark. Afterward, cells are washed once with 1 × Buffer (provided in the kit). Fluorescence microscopy is performed in VU LSC Bioscience Institute with a Nikon Eclipse 80i microscope (Nikon, Japan) (FITC filter is used). ImageJ is employed for the quantitative evaluation of fluorescent cells.

To study ROS generation by electroporation, the cells are prepared for electroporation as described in Section 2.5.5. Untreated cells (negative control) are transferred on YPD agar plates, while affected cells are prepared for staining by washing them once with 1 × Buffer (provided in the kit). After suspending the cells in the buffer, samples were treated with DCFDA and positive controls - with TBHP, as described above. For qualitative and

quantitative evaluation of fluorescent cells intensity, the ImageJ program is applied.

2.4.8. Determination of ROS formation after exposure to silver nanoparticles by flow cytometry

Cell cultures are cultivated aerobically in liquid YPD media at 30 °C (for yeasts) and in liquid LB media at 37 °C (for bacteria) up until the exponential phase. Cells are washed twice with a 1 M sorbitol solution by centrifugation and then suspended in 1 M sorbitol. Next, cells are prepared for ROS formation analysis by using a modified DCFDA/H_2DCDFA-Cellular ROS Assay Kit (ab113851) protocol. Samples are diluted to 1×10^4 CFU/mL. Cells are washed and suspended in 1 × Buffer (provided in the kit) before staining, and after staining with 10 μM DCFDA, incubated at 30 °C for 2 h. After that cells are treated with AgNP MICs and incubated at 30 °C for 15 min (for *C. guilliermondii*) or 1 h (for bacteria and *S. cerevisiae*). Untreated yeast cells are used as a negative control. Afterward, cells are washed with 1 × Buffer (provided in the kit) two times. Then the samples are analysed in VU LSC Biochemistry Institute with a BD "FACSort" flow cytometer (for *C. guilliermondii*) and in VU LSC Biotechnology Institute BD FACSymphony™ A1 flow cytometer (BD Biosciences, San Jose, CA, USA) (for bacteria and *S. cerevisiae*) (excitation wavelength 488 nm, emission wavelength 535 nm). A sample of 20,000 cells is analysed. Flowing Software 2.5.1 is employed for the analysis.

2.4.9. Determination of lipid peroxidation in yeast cells after exposure to silver nanoparticles and in combination with electroporation

Cell cultures of *C. guilliermondii* are cultivated aerobically in liquid YPD media at 30 °C up until the exponential phase (12–14 h). Cells are washed twice with deionized water and twice with a 1 M sorbitol solution by centrifugation and then suspended in 1 M sorbitol. To study lipid peroxidation by electroporation, cells are prepared for electroporation as described in Section 2.4.5. Untreated cells (negative control) are transferred on YPD agar plates, while affected cells are prepared for staining by washing them once with 1 × PBS buffer and suspended in it. In the case of determination of the effect of AgNP alone, the cells are treated with MICs of AgNP in 1 × PBS buffer. For positive controls Cumene hydroperoxide is added to the final concentration of 100 μM and for negative control untreated cells are used.

Then cells are prepared for lipid peroxidation analysis by using the modified Click-iT® Lipid Peroxidation Detection with Linoleamide Alkyne (LAA) Kit protocol. First, the final concentration of 50 μM Click-iT® LAA solution is administered to the cells, and they are incubated for 2 h at room temperature. The cells are washed with 1 × PBS buffer three times to eliminate excess Click-iT® LAA before adding 3.7% formaldehyde in 1 × PBS and incubated at room temperature for 15 min. Later, 1 × PBS buffer is used to wash the cells three times. Next, Triton X-100 is diluted to 0.5% in 1 × PBS buffer and added to the cells before incubating for 10 min at room temperature. The cells are then blocked by adding 1% of BSA in 1 × PBS buffer and incubated for 30 min at room temperature. Afterward, the cells are washed twice with 1 × PBS buffer to remove BSA entirely. Click-iT® reaction cocktail is prepared for a total volume of 100 μL: 86 μL 1 × Click-iT® reaction buffer, 4 μL $CuSO_4$, 0.24 μL Alexa Fluor® 488 azide, 10 μL 1 × Click-iT® buffer additive. The cells are incubated at room temperature for 30 min in the dark. The cells are washed twice with 1% BSA in 1 × PBS buffer and twice with 1 × PBS buffer. Fluorescence microscopy is performed with a Nikon Eclipse 80i microscope (FITC filter is used). ImageJ is employed for the quantitative evaluation of fluorescent cells.

2.4.10. Evaluation of cell membrane permeability changes

Changes in microorganism cell membrane permeability were determined by staining the cells with propidium iodide (PI). After the exposure of *Geobacillus* spp. strains 25 and 612 AgNP cells for 30 min. are washed in 1 × PBS buffer and centrifuged at 2000 rpm for 5 min. Cells are resuspended in 1 mL of 1 × PBS buffer and 1 μL of PI (1 mg/mL) is added. The cells are incubated with the dye for 10 min at room temperature. After incubation, cells are washed with 1 × PBS buffer and fixed with 10% buffered formaldehyde for 30 min, centrifuged, and resuspended in 1 × PBS buffer. In the cases of *C. guilliermondii*, *S. aureus*, and *S. pyogenes*, fluorescence was measured at VU LSC Institute of Biotechnology with a BD FACSymphony™ A1 flow cytometer (excitation wavelength 488 nm, emission wavelength 535 nm). A sample of 20,000 cells is analysed. Flowing Software 2.5.1 is employed for the analysis. In the cases of *S. cerevisiae* and *P. aeruginosa*, a drop of the sample is transferred onto a slide covered with Poly-L-lysine, covered with a coverslip. Samples were analysed with an Olympus IX83 Inverted Light Microscope (Olympus, Japan).

2.4.11. Preparation of *Pseudomonas aeruginosa* biofilms and their cultivation

P. aeruginosa cells were grown (24 h at 30 °C) on an agarized LB medium. One colony was inoculated into a 5 mL sterile liquid LB medium in a test tube. Then 100 μL of OT_{600}=1 bacterial suspension was transferred to fresh test tubes with 5 mL sterile liquid LB medium. The test tubes were incubated stationary at a temperature of 30 °C. Biofilms were grown for seven days until visible biofilm was formed.

Test tubes were divided into three groups:

1. Research group: for further experiments;
2. Control I: grown control biofilms were stained with crystal violet for evaluation of cell distribution and biofilm structure;
3. Control II: grown biofilms were washed and disintegrated for optical density measurement and seeding on nutrient media.

2.4.12. Evaluation of the effect of silver nanoparticles on *Pseudomonas aeruginosa* biofilms

The grown biofilms were exposed to a solution of *Geobacillus* sp. 25 AgNP with a concentration of 10 μg/mL for 0, 2, 4, 6, and 24 h. Then the biofilms were seeded on an agarized LB medium. Biofilms without AgNP incubated only in 1 M sorbitol solution were considered as a control.

2.4.13. Evaluation of the effect of silver nanoparticles and electroporation on *Pseudomonas aeruginosa* biofilms

In the case of *P. aeruginosa* biofilms, the grown biofilms were prepared for electroporation as mentioned in Section 2.4.4. The prepared biofilms were mixed with 5 μg/mL of *Geobacillus* sp. 25 AgNP immediately before electroporation (total volume of 60 μL). The prepared mixtures of biofilms and AgNP were transferred to a cuvette for electroporation. The conditions of electroporation were: eight 100 μs impulses at 15, 20, and 25 kV/cm PEF. A 60 μL suspension of biofilms was used as a control. After electroporation, cells were transferred to LB agar plates and incubated at 30 °C for 72 h.

2.4.14. Detection of active caspases

Active caspases in yeast cells are detected using the CaspACE™ FITC-VAD-FMK In Situ Marker kit. After induction of apoptosis with *Geobacillus* spp. 25 and 612 AgNP, cells are washed three times with 1 × PBS buffer and centrifuged at 2000 rpm for 5 min. After washing, the yeast cells are suspended in 1 mL of 1 × PBS buffer, and 300 μL of the cell suspension is transferred to a new tube. After that, 1 μL of FITC-VAD-FMK was added and incubated in the dark for 30 min (for *S. cerevisiae*) or 1 h (for *C. guilliermondii*) at 30 °C. After incubation, cells are washed three times in 1 × PBS buffer. Cells are suspended in 100 μL 1 × PBS buffer and fixed with 10% buffered formaldehyde for 30 min at room temperature. After fixation, cells were washed three times. For fluorescence microscopy, cells are suspended in 100 μL 1 × PBS buffer. A drop of the sample is transferred onto a slide covered with poly-L-lysine, covered with a coverslip. Samples are analysed with VU LSC Bioscience Institute "Nikon eclipse 80*i*" fluorescence microscope, using a FITC filter. For flow cytometry, cells are suspended in 100 μL of 1 × PBS buffer. A sample of 20,000 cells is analysed. BD FACSymphony™ A1 flow cytometer was used for flow cytometry experiments (excitation wavelength 488 nm, FITC emission wavelength 535 nm). Flowing Software 2.5.1 is employed for the analysis.

2.4.15. Evaluation of DNA fragmentation in yeast cells after exposure to silver nanoparticles

Assessment of DNA fragmentation is performed using the "Apoptosis DNA Ladder Assay" kit. Two replicates of each experiment were performed according to the provided protocol. Samples were fractionated in a 1.2% agarose gel (stained with 0.5 μg/mL ethidium bromide). Electrophoresis was carried out under conditions of 5 V/cm for 1.5 h. After electrophoresis, the gel was visualized with a UV transilluminator and photographed.

2.4.16. Keratinocyte cell preparation and cultivation

According to the standard protocol, Ker-CT cells were thawed and grown in a special medium for Ker-CT with additives in 25 cm^2 vials. The medium for Ker-CT should reach room temperature and normal pH (7.0–7.6) before experiments to avoid excessive alkalinity of the medium during cell recovery and growth, so it is kept for at least 5 min in a 37 ºC incubator or a water bath.

After thawing the cryoampule at 37 ºC, the cell suspension is transferred to a sterile vial filled with 5 mL of Ker-CT growth medium. Ker-CT cell culture is incubated in a thermostat at 37 ºC (5% CO_2, 95% humidity). After the cells have been attached, usually after 6–12 h, the medium is replaced with fresh. Changing the old medium with a fresh one is done every 2–3 days.

After evaluating the cell monolayer and population increase with an inverted microscope, cells are plated after reaching 70–80% confluency. First, the monolayer is washed - the medium is poured off and 2–3 mL of phosphate buffer without Ca^{2+}/Mg^{2+} (HBSS) is poured onto the cells, then the HBSS with the rest of the medium is poured off and the same action is repeated. Next, adherent cells are lifted from the surface - the monolayer is dispersed in 1–2 mL of trypsin, which is gently distributed over the surface of the vial and poured off. This step is repeated by adding 1–2 mL of trypsin and placing the vial in a 37 ºC thermostat to incubate for 5–9 min. Cell monolayer dissociation is assessed with an inverted microscope - 90% of cells must be detached. To neutralize trypsin 4–6 mL of IMDM medium supplemented with 10% fetal calf serum and an antibiotic are poured onto the cells with trypsin. The entire mixture was transferred to a sterile 10 mL tube and centrifuged at 300 *g* for 7 min at room temperature. 5–6 mL of Ker-CT medium is poured into the vial from which the cells were lifted. After centrifugation, the supernatant is poured off and 2–4 mL of fresh Ker-CT medium is added. The sample is well suspended and divided into new sterile vials in equal proportions. Another 4–5 mL of Ker-CT medium is added to each new vial with cells. Cells are further grown in a thermostat (37 ºC, 5% CO_2, 95% humidity). Passage is repeated after 24–48 h until the required number of cells is obtained for the experiments.

2.4.17. Crystal violet staining of keratinocyte cells

Ker-CT cells were harvested, counted, and seeded at a density of 5.5 x 10^4 cells/mL in a 96-well plate and then incubated for 24 h. Then cells were treated with AgNP at concentrations of 5 µg/mL, 10 µg/mL, and 15 µg/mL for 24 h. Cells were placed on ice washed 2 times with cold PBS and fixed for 10 minutes with ice-cold 100% methanol. Then cell monolayer was covered with 0.5% crystal violet solution in 25% methanol and incubated for 10 minutes. After removal, the crystal violet cells were washed with water several times. Stained cells were allowed to dry at room temperature overnight. The next day cells were captured (at 4x magnification) under white light using an Olympus IX51 microscope.

2.4.18. Evaluation of cytotoxicity of silver nanoparticles by MTT method

Ker-CT cells are washed, and adherent cells are detached from the surface by the same method as described in Section 2.4.16. When the cells are centrifuged and the supernatant is poured off, the number of cells in 1 mL of the suspension is estimated using a light microscope with a Neubauer chamber. The counted cells are diluted to the concentration of $1.4–1.7 \times 10^5$ cells/mL. The resulting cell suspension is divided into 200 µL portions in a 96-well plate. The plate is incubated in a thermostat (37 ºC, 5% CO_2, 95% humidity) for 24 h.

After incubation, after assessing the adherence of the cells in the wells (monolayer formation) with the help of an inverted microscope (confluence should reach 70–80%), prepared mixtures of different concentrations of *Geobacillus* sp. strain 612 AgNP (5, 10, 15, 20, and 25 µg/mL) and Ker-CT medium in 200 µL each, were added to the wells with cells. Three replicate wells are used for each concentration. The plate is incubated in a thermostat (37 ºC, 5% CO_2, 95% humidity) for 24 h.

After the incubation, the cytotoxicity of *Geobacillus* sp. 612 AgNP is assessed using the 3-(4,5-Dimethylthiazol-2-yl)-2,5-diphenyltetrazolium bromide (MTT) method. A ready-made MTT dye at a concentration of 5 mg/mL is used (MTT dye is mixed with PBS buffer), which is warmed to room temperature in a 37 ºC water bath for several min before use. Very carefully from the corners of the wells (so as not to damage the monolayer of adherent Ker-CT), the mixtures of *Geobacillus* sp. strain 612 AgNP and media are aspirated and washed with PBS. 200 µL of PBS is carefully poured into the wells on the cells and immediately aspirated. This process is repeated twice. The 50 µL of MTT solution is added and incubation is carried out for 1 h in a 37 ºC thermostat (5% CO_2, 95% humidity). After incubation, the MTT solution is aspirated from the wells. The resulting blue compound is eluted from the cells with 50 µL of 96 % ethyl alcohol. Also, 50 µL of ethyl alcohol is added to several empty wells, which are used as a background for analysing the results. The spectrophotometer measured the OD_{570} in the selected area of the plate (the relevant number of wells is selected; there must also be some empty wells (background)). The obtained results are analysed.

2.4.19. Study of the influence of silver nanoparticles on the proliferative activity of keratinocytes

After the Ker-CT cells reached 70–80% confluency, the cells were exposed to *Geobacillus* sp. strain 612 AgNP for 24, 48, and 72 h. Using the light microscope and Neubauer chamber, the cells are counted to estimate the number of cells in 1 mL of cell suspension. The counted cells are diluted to the concentration of 7×10^4–1.1×10^5 cells/mL. The obtained cell suspension is poured into a 96-well plate at 200 µL per well. Plates with cells are incubated in a 37 ºC thermostat (5% CO_2, 95% humidity) for 24 h. When the cells reach 70% confluency, the initial medium is replaced with fresh Ker-CT medium supplemented with different concentrations (5, 10, 15, 20, and 25 µg/mL) of *Geobacillus* sp. strain 612 AgNP, and subsequently incubated for 24, 48, or 72 h. After the incubation time, the cytotoxicity of *Geobacillus* sp. strain 612 AgNP is evaluated using the MTT method (see Section 2.4.18).

2.4.20. Wound healing assay

Ker-CT cells were seeded into 12-well plates in Ibidi inserts (Ibidi GmbH, Gräfelfing, Germany) at a density of 3×10^5 cells/mL to obtain a confluent cell layer. 110 µL of cell suspension was added directly inside each insert well. After seeding, cells were grown for 24 h until they reached confluence. After incubation, inserts were gently removed with sterile tweezers to create a cell-free area (pseudo-"wound") of approximately 500 µm in diameter. Then cells were washed once with PBS to remove cell debris and non-attached cells. Prepared *Geobacillus* sp. 612 AgNP at different concentrations (5 µg/mL, 10 µg/mL, 15 µg/mL) were mixed with fresh Ker-CT medium and loaded onto wells containing cells that have pseudo-“wound” areas. At different time intervals, fields of the pseudo-“wound” area horizontally were visualized under a white light using microscope (Olympus IX51) at 4x magnification. Images at 0 h were captured to record the initial area of the wounds, and the recovery of the wounded monolayers was evaluated at 2 h, 6 h, 24 h, and 48 h. For negative and positive control, we used unaffected Ker-CT cells (0 µg/mL AgNP) and 4 µg/mL concentration of lipopolysaccharides (LPS) respectively. All measurements of different treatments were performed analysing three different fields of pseudo-"wound" view area.

To quantify the characteristics of the cell migration and percentage of cell-covered area at each time, images were analysed using an image

processing software (ImageJ) and Macro language (IJM) as described [274]. The cell covered area (µm²) and average wound width (µm) are given as the mean of three different areas of the wound. For wound closure % the equation (1) was used and for wound healing rate equation (2).

$$(1)\ \text{Wound closure}\ (\%) = \frac{A_{t=0} - A_{t=\Delta h}}{A_{t=0}} \cdot 100$$

$A_{t=0}$ = area of the wound measured immediately after making a wound
$A_{t=\Delta h}$ = area of the wound measured h hours after making a wound

$$(2)\ \text{Wound healing rate}\ (\mu m^2/h) = \frac{A_{t=0} - A_{t=\Delta h}}{t_{\Delta h}}$$

$A_{t=0}$ = area of the wound measured immediately after making a wound
$A_{t=\Delta h}$ = area of the wound measured h hours after making a wound
$t_{\Delta h}$ = number of hours of treatment

3. RESULTS

3.1. Extracellular biosynthesis of the obtained silver nanoparticles and their characterization

Four *Geobacillus* spp. strains (18, 25, 95, and 612) have been selected for AgNP production. The studies revealed that the supernatants of *Geobacillus* spp. strains 18, 25, 95, and 612 successfully promoted the extracellular synthesis of AgNP. The supernatants' colour changed from light brown to dark brown after being exposed to a 2 mM aqueous $AgNO_3$ solution for 48 hours at 55 °C. The reduction of Ag^+ and the formation of AgNP were both suggested by this change. One of the most common methods for determining AgNP structural characteristics is UV–Vis spectroscopy which was used in order to examine the produced AgNP [134]. After 48 hours of exposure to 2 mM $AgNO_3$, samples containing *Geobacillus* spp. cell-free supernatants were examined using UV–Vis spectroscopy in the range of 300–600 nm (**Fig. 3.1.**). The distinctive AgNP absorbance peak at 410–425 nm was visible in all four tested samples. In the bacterial growth medium treated with 2 mM $AgNO_3$ (control sample), a colour change from light brown to greenish brown was noticed, but no precipitation of aggregates was noted.

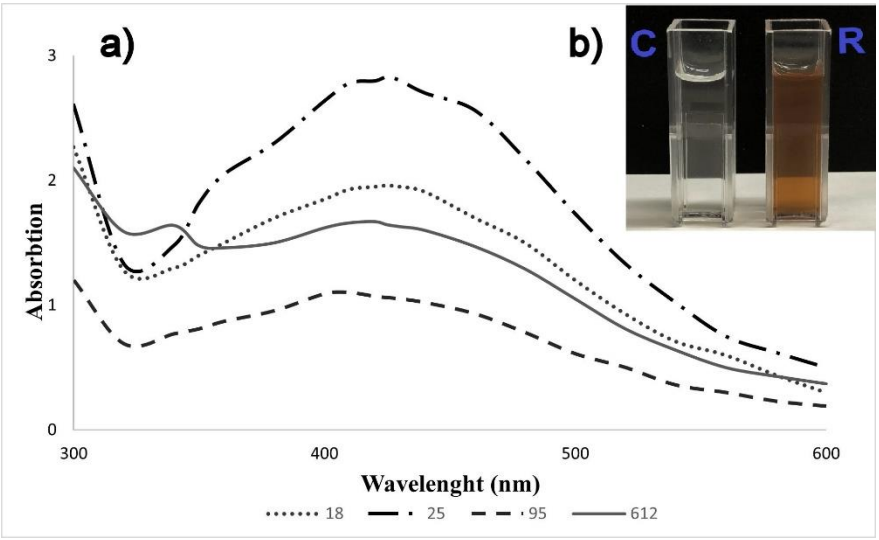

Fig. 3.1. UV–Visible spectra of AgNP produced by the *Geobacillus* spp. 18, 25, 95, and 612 supernatants treated with 2 mM $AgNO_3$ after 48 h incubation at 55 °C. Numbers refer to the respective *Geobacillus* spp. strain (**a**), and the colour change caused by a reaction employing the supernatant of the *Geobacillus* sp. strain 612 (**b**). R – reaction mix; C – control.

The AgNP were additionally analysed using SEM (**Fig. 3.2.**), which demonstrated that the produced particles are spherical. Additionally, it was observed that agglomeration took place as the AgNP dried, creating different nanostructures (**Fig. 3.2.**).

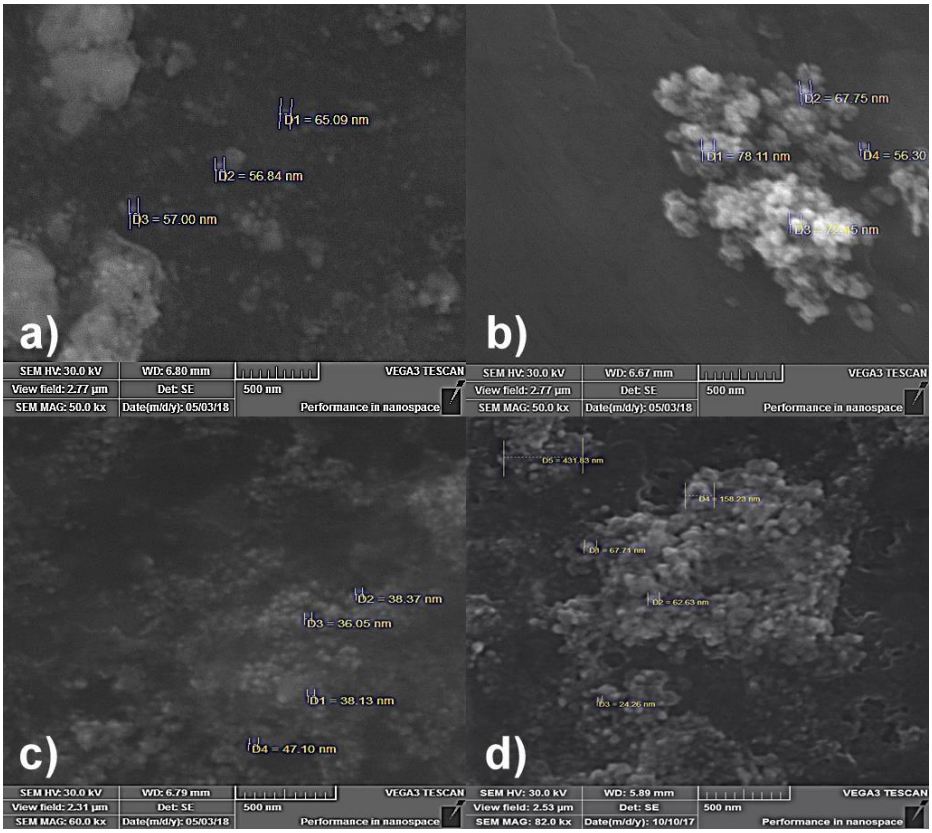

Fig. 3.2. SEM analysis of acquired AgNP. **a** - *Geobacillus sp.* 18; **b** – *Geobacillus* sp. 25; **c** – *Geobacillus* sp. 95; **d** – *Geobacillus* sp. 612.

Additional zeta potential measurements at 25 °C using the Smoluchowski model were carried out to explain particle aggregation in dispersions. **Table 3.1.** is a summary of the results. The finding revealed that the zeta potentials of each AgNP obtained by four different *Geobacillus* spp. strains were negative and ranged between −25 and −31 mV in an aqueous environment. The absolute zeta potential value of NP in the aqueous dispersion must be greater than 30 mV (either $\xi > +30$ mV or $\xi < -30$ mV) in order for them to be stable [275]. Since the AgNP produced by *Geobacillus* spp. strains with the lowest negative zeta potential value of -31.28 ± 0.47 mV have the fewest aggregates - roughly 1% of all particles in the aqueous dispersion of

Geobacillus sp. strain 25 - the zeta potential data are in good agreement with the theory. The surface charge was less pronounced and the electrostatic repulsion forces between the particles were insufficient to effectively maintain stability for particles produced by other *Geobacillus* spp. strains. In these situations, DLS measurements revealed a larger portion of aggregated particles in the dispersions.

Table 3.1. Values of the zeta potential (mV) of AgNP obtained using supernatants of four different *Geobacillus* spp. strains.

Geobacillus spp. strain / Solution	18	25	95	612
Water	−26.60 ± 0.24	−31.28 ± 0.47	−25.70 ± 0.51	−27.43 ± 0.27
1M sorbitol	−27.98 ± 0.33	−30.03 ± 0.05	−28.70 ± 0.28	−30.13 ± 0.28
LB medium	−28.07 ± 0.19	−36.17 ± 0.46	−30.43 ± 0.59	−28.77 ± 0.28
YPD medium	−28.73 ± 0.47	−30.93 ± 0.21	−32.40 ± 0.28	−28.37 ± 0.14

DLS analysis was used to determine the size and size distribution of the obtained AgNP. For AgNP produced by four different *Geobacillus* spp. strains, 100 separate measurements were made. The findings reveal that the bulk of the particles in the aqueous dispersion (82% of *Geobacillus* sp. strain 18; 99% of strain 25; 75% of strain 95; and 88% of strain 612) had a diameter of less than 100 nm. However, some aggregates were found, and the particle size distribution is rather wide (**Fig. 3.3a**). Since AgNP are added to nutrient media and sorbitol solution when studying the antimicrobial effect of *Geobacillus* spp. AgNP, the sizes of these AgNP were also determined in the used media (1 M sorbitol solution, LB, and YPD nutrient media). The results show that after incubation of AgNP in these media, more aggregates are formed than in aqueous environment, the least number of them are in 1 M sorbitol (**Fig. 3.3b**), more aggregates formed in LB medium (**Fig. 3.3c**), and the most in YPD medium (**Fig. 3.3d**). These differences can be explained by the fact that the media is rich in nutrients (sugars, peptides, salts, etc.) that can lead to the aggregation of individual particles.

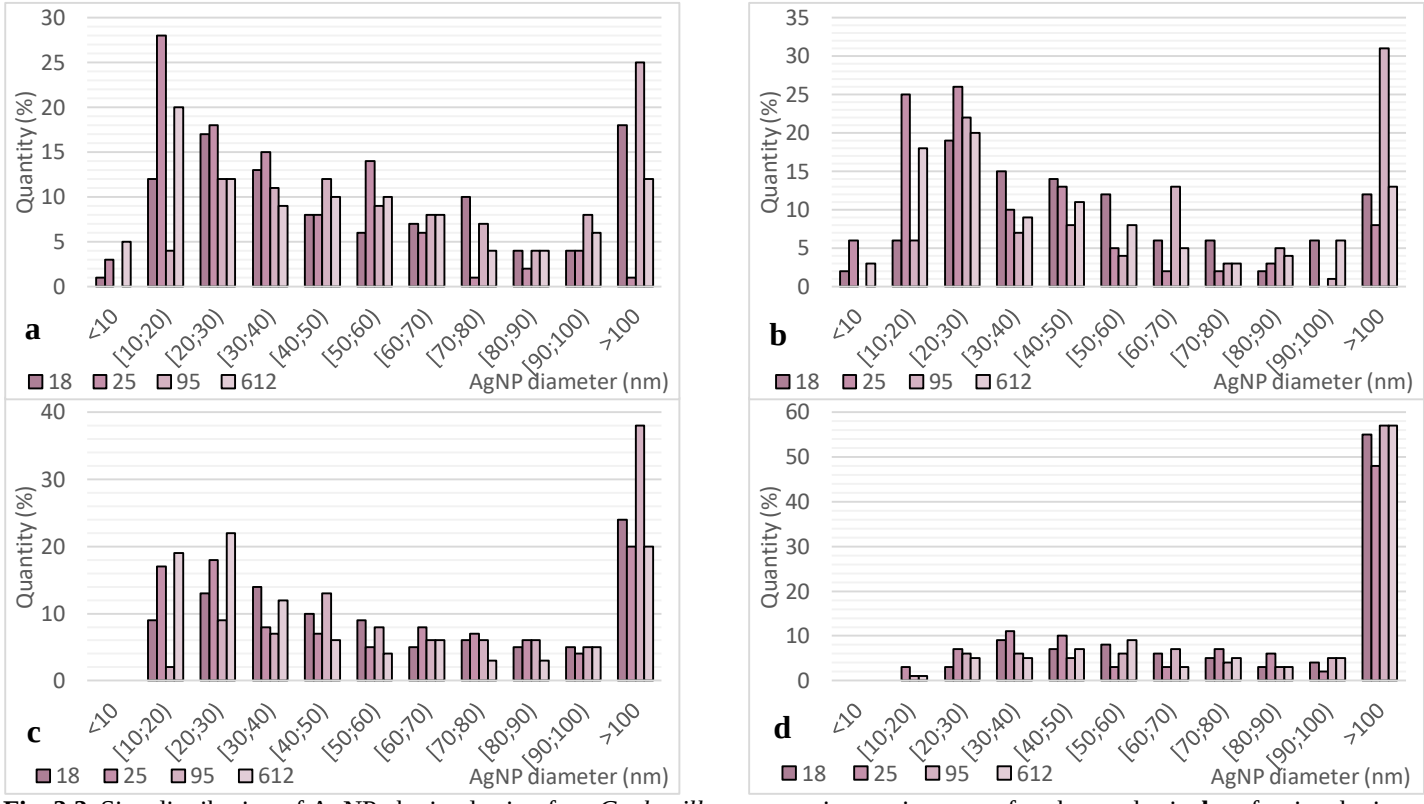

Fig. 3.3. Size distribution of AgNP obtained using four *Geobacillus* spp. strains. **a** - in water after the synthesis; **b** - after incubation in 1 M sorbitol solution; **c** - after incubation in LB medium; **d** - after incubation in YPD medium. Number refers to the respective *Geobacillus* spp. strain numbers.

Zeta potential values of *Geobacillus* spp. AgNP obtained after their incubation (12 h) in 1 M sorbitol solution and LB and YPD nutrient media were also determined (**Table 3.1.**). In all cases, it can be seen that the zeta potential values of *Geobacillus* spp. AgNP have changed, but the obtained values show that AgNP are quite stable in these media. Changes in these values are possible due to the presence of sugars, salts, peptides, and other additives in solutions, especially nutrient media, which change the bioavailability and activity of these AgNP.

3.2. Determination of MIC against skin pathogens using the 'Spot test'

Kasemets et al. [273] proposed the 'Spot test' for determining the MICs of AgNP against microorganisms. This method was adapted to determine MIC against skin pathogens (bacteria *S. aureus*, *S. pyogenes*, *P. aeruginosa*, and yeast *C. guilliermondii*) in this work. The MICs are determined visually, and they are judged to have been reached when colonies of the microorganism being tested are no longer visible on the agarized medium. The experiment was repeated at least three times for each microorganism and different *Geobacillus* spp. AgNP.

C. guilliermondii MICs were 10 μg/mL following treatment with *Geobacillus* spp. 18, 25, and 95 AgNP, and 5 μg/mL after treatment with *Geobacillus* sp. 612 AgNP (**Table 3.2.**). To specify MICs, an experiment with more precise MIC values was conducted (see **Table 2.2.**), and the performed experiment confirmed the previously determined MIC values.

Geobacillus spp. AgNP MIC values were also determined against pathogenic skin bacteria. For *S. aureus* AgNP of *Geobacillus* spp. 25 and 612 had MIC values of 2.6 ± 0.83 μg/mL and AgNP of *Geobacillus* spp. 18 and 95 AgNP had MIC values of 4.17 ± 1.67 μg/mL (**Fig. 3.4a** and **Table 3.2.**).

In the case of *S. pyogenes*, the lowest MIC values were determined using *Geobacillus* spp. 95 and 612 AgNP. The MIC values of these particles were 1.30 ± 0.42 μg/mL and 1.04 ± 0.42 μg/mL respectively. The highest MIC value was 4.17 ± 1.67 μg/mL of *Geobacillus* sp. 18 and 25 AgNP (**Fig. 3.4b** and **Table 3.2.**).

For *P. aeruginosa* the most effective AgNP was *Geobacillus* sp. 612 AgNP a with a MIC value of 2.09 ± 0.83 μg/mL. MIC values of *Geobacillus* spp. 18, 25, and 95 AgNP against *P. aeruginosa* were 10.42 ± 3.33 μg/mL, 5.21 ± 1.67 μg/mL, and 4.17 ± 1.67 μg/mL, respectively (**Fig. 3.4c** and **d**, and **Table 3.2.**).

Table 3.2. The minimum inhibitory concentrations (μg/mL) of *Geobacillus* spp. strains 18, 25, 95, and 612 AgNP against skin pathogens.

Geobacillus spp. strain / Microorganism	18	25	95	612
S. aureus	4.17 ± 1.67	2.60 ± 0.83	4.17 ± 1.67	2.60 ± 0.83
S. pyogenes	4.17 ± 1.67	4.17 ± 1.67	1.30 ± 0.42	1.04 ± 0.42
P. aeruginosa	10.42 ± 3.33	5.21 ± 1.67	4.17 ± 1.67	2.09 ± 0.83
C. guilliermondii	10.00 ± 3.33	10.00 ± 3.33	10.00 ± 3.33	5.00 ± 1.67

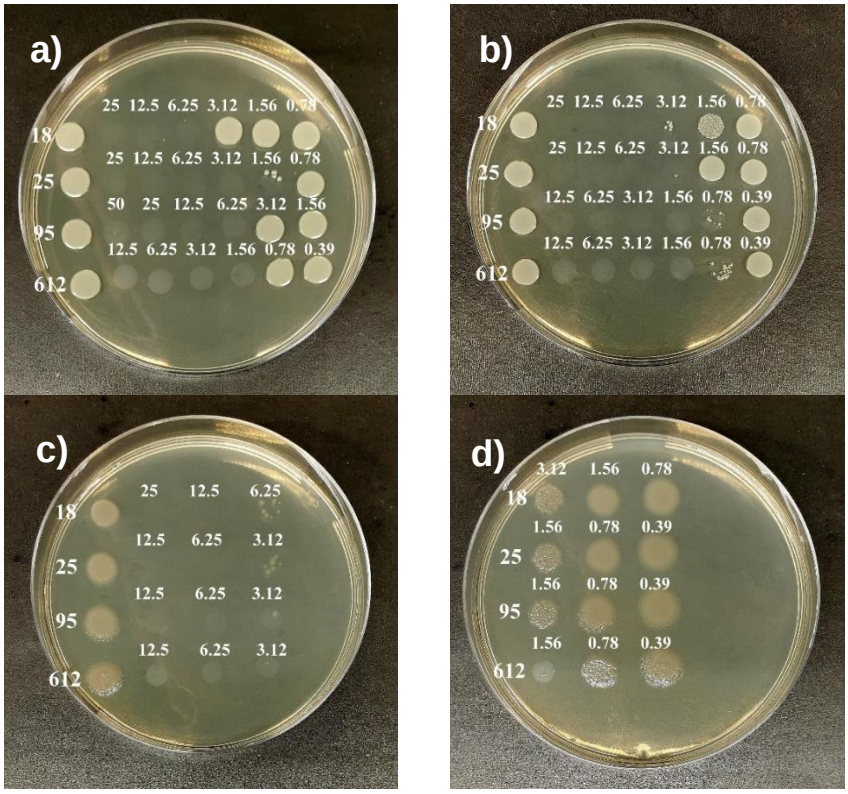

Fig. 3.4. The evaluation of *Geobacillus* spp. AgNP MICs for pathogenic skin bacteria. Concentrations (μg/mL) of AgNP are shown as numbers above; numbers on the left side refer to *Geobacillus* spp. strain number of AgNP. **a** - *S. aureus*; **b** - *S. pyogenes*; **c** and **d** - *P. aeruginosa*. These pictures are representative of one of three replicates performed.

The obtained results show that lower concentrations of AgNP are needed against prokaryotic microorganisms than against eukaryotic ones. However, according to the literature, AgNP should work more effectively against gram-negative bacterial cells than gram-positive ones, and during the tests, it was found that the MIC values against gram-positive *S. aureus* and *S. pyogenes* bacteria are lower than against gram-negative *P. aeruginosa*. This could be explained by the fact that *P. aeruginosa* formed a biofilm during the experiments, so a separate study was conducted with the biofilms of this bacterium.

3.3. Antifungal properties against pathogenic skin yeast

This section describes the part of the study carried out with pathogenic skin yeast *C. guilliermondii* and some experiments were done with the model yeast species *S. cerevisiae*. These two yeast species were chosen because *S. cerevisiae* has well-described programmed cell death mechanisms and is frequently analysed as a model system, that could be used for the comparison of the similar processes undergoing in the *C. guilliermondii* yeast. In addition, *C. guilliermondii* yeast is highly resistant to various environmental conditions as well as antifungal drugs and it is described as one of the most resistant species in *Candida* genera [7,87].

3.3.1. Enhancing silver nanoparticles effects using the electroporation

C. guilliermondii cells were eliminated statistically significantly following electroporation at various electroporation parameters (10, 12.5, and 15 kV/cm) even in the absence of AgNP. At an electric field strength (PEF) of 15 kV/cm, the most noticeable effect of electroporation was found in comparison to the control (unaffected cells). Cell viability was reduced significantly, reaching 35.63 ± 2.26%.

Initially, the effect of electroporation and AgNP was investigated using AgNP MIC (10 μg/mL for *Geobacillus* spp. 18, 25, and 95 AgNP and 5 μg/mL for *Geobacillus* sp. 612 AgNP). The impact, however, was severe, resulting in the absence of colonies growth on the agarized medium. As a result, in order to evaluate the elimination results in percentages, AgNP concentrations had to be reduced by 10 times (1 μg/mL for *Geobacillus* spp. 18, 25, and 95 AgNP and 0.5 μg/mL for *Geobacillus* sp. 612 AgNP) (**Fig. 3.5.**). Statistically significant cell elimination was detected at varied PEF ranging from 2.5 to 15 kV/cm with all tested *Geobacillus* spp. AgNP (18, 25, 95, and 612). When

compared to the control group, 15 kV/cm PEF induced a considerable reduction in *C. guilliermondii* cell population, 6.85 ± 5.87%, 4.40 ± 2.07%, 3.06 ± 0.96%, and 2.67 ± 1.82% of viable cells remained compared to negative control.

In addition, it was found that the combination of PEF and AgNP reduced cell viability significantly compared to the effect of PEF or AgNP alone (**Fig. 3.5.**). According to these results, it can be assumed that the increase of dead cells is decisive for both electroporation and AgNP, hence electroporation enhances the antifungal properties of AgNP.

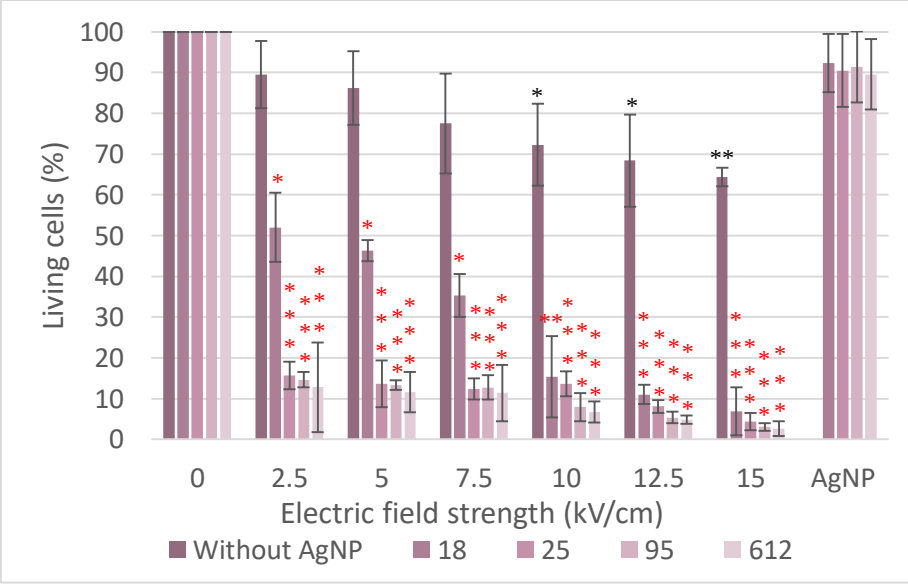

Fig. 3.5. The effect of *Geobacillus* spp. AgNP and electroporation on *C. guilliermondii* yeast cells. *C. guilliermondii* cells were treated with electroporation or a combination of AgNP and electroporation. The control group consisted of cells that were not subjected to electroporation or AgNP or AgNP only. The experimental group was treated with AgNP derived from *Geobacillus* sp., as it is indicated numerically in the figure. p-values: * <0.05; ** <0.005; *** <0.0005; black asterisks refer to p-values compared to negative control; red asterisk refer to p-values compared between cells which were electroporated and electroporated together with AgNP.

In collaboration with scientists from the Center for Physical Sciences and Technology, the effect of AgNP and electroporation was visualized by SEM. For SEM, the *C. guilliermondii* yeasts, *Geobacillus* sp. 25 AgNP, and 10 kV/cm PEF were selected. The obtained results are shown in **Fig. 3.6.**

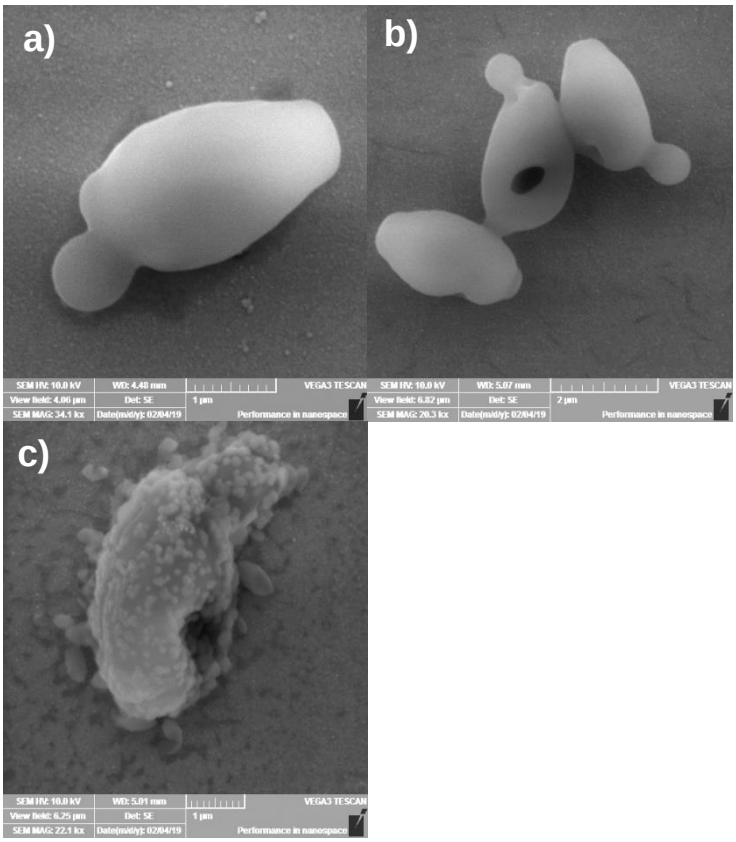

Fig. 3.6. SEM images of *C. guilliermondii*. **a -** unaffected cell; **b -** cells exposed to 10 kV/cm electric field strength; **c** – cells exposed to 5 μg/mL of *Geobacillus* sp. 25 AgNP and 10 kV/cm electric field strength.

Fig. 3.6b and **c** show severe damage to the cell wall and membrane after exposure to an electroporation which leads to cell death. In addition, it is shown in **Fig. 3.6c** that AgNP uniformly cover the yeast cell surface.

3.3.2. Fluorescence microscopy and flow cytometry analysis of ROS generation following treatment with silver nanoparticles

The DCFDA/H_2DCFDA-Cellular ROS Assay Kit (ab113851) was employed to ascertain the production of ROS in *C. guilliermondii* following exposure to AgNP. A fluorescent dye called DCFDA (2',7'-dichlorofluorescein diacetate) is used to measure the cell ROS activity. Cellular esterases convert the dye that enters the cells into a non-fluorescent substance. This substance changes into the fluorescent molecule DCF (2',7'-dichlorofluorescein) when it is exposed to ROS [276].

The DCFDA/H_2DCFDA-Cellular ROS Assay Kit (ab113851) protocol was adjusted to fit the current experiment before performing additional flow cytometric quantitative ROS assessments. Consequently, 2 hours was found to be an appropriate amount of time for yeast to be incubated with the DCFDA dye. Based on whether the test samples displayed fluorescence in comparison to the negative control, the experiment's success was determined. In contrast to the negative control, which showed no fluorescence, AgNP-treated *C. guilliermondii* cells showed fluorescence that could be seen and recorded (**Fig. 3.7.**).

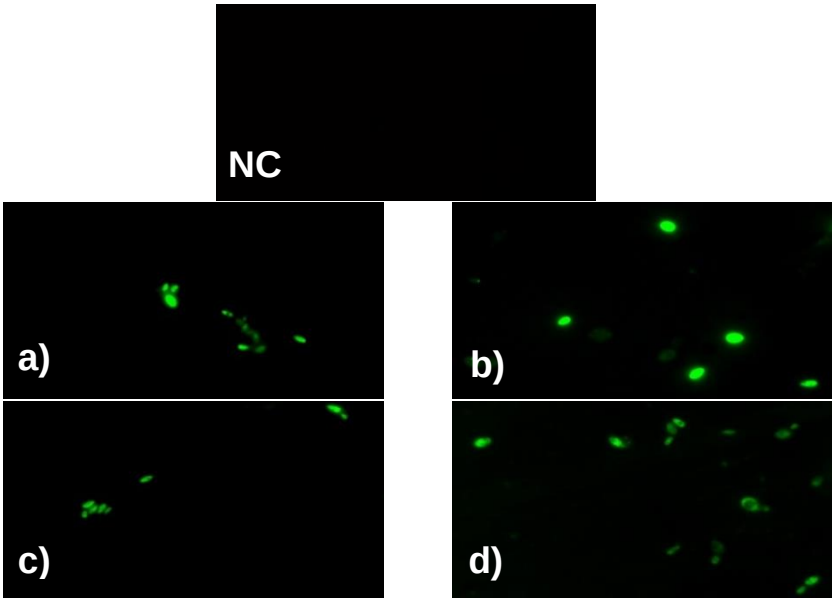

Fig. 3.7. Fluorescence microscopy of DCF in *C. guilliermondii*. The occurrence of ROS generation in *C. guilliermondii* cells after treatment of *Geobacillus* spp. AgNP was indicated by the green fluorescence. **NC** - negative control, unaffected *C. guilliermodii* cells; **a** - treatment with *Geobacillus* sp. 18; **b** - with *Geobacillus* sp. 25 AgNP; **c** - with *Geobacillus* sp. 95; **d** - with *Geobacillus* sp. 612 AgNP.

The AgNP produced by *Geobacillus* spp. strains 25 and 612 caused the highest increase in ROS generation, which was measured using a flow cytometer. The mean fluorescence increases of three independent samples in A.U. (arbitrary units) was found to be 7.73 ± 0.64 6.20 ± 1.07, respectively compared to the negative control, which was unaffected by AgNP. AgNP made by *Geobacillus* spp. 18 and 95 were also used in the experiments, and the results showed that they increased A.U. by 3.44 ± 0.49 and 3.03 ± 0.33 (**Fig. 3.8.**).

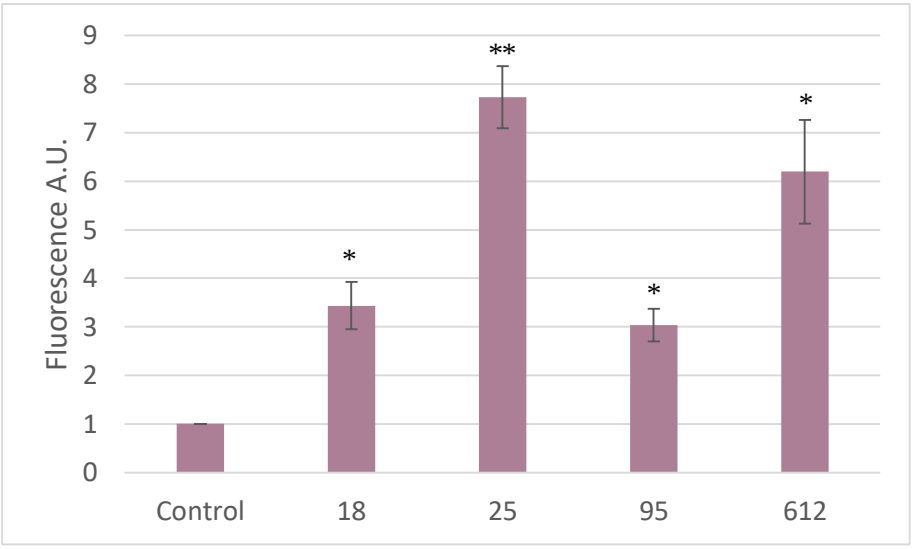

Fig. 3.8. The average green fluorescence intensity increased by a factor of two compared to the negative control equalized to 1 of intracellular ROS. Control – unaffected *C. guilliermondii* cells; number refers to the respective *Geobacillus* spp. strain AgNP. p-values: * <0.05; ** <0.005.

In the case of *S. cerevisiae*, no statistically significant increase in ROS levels was found with AgNP of either strain (**Fig.3.9.**).

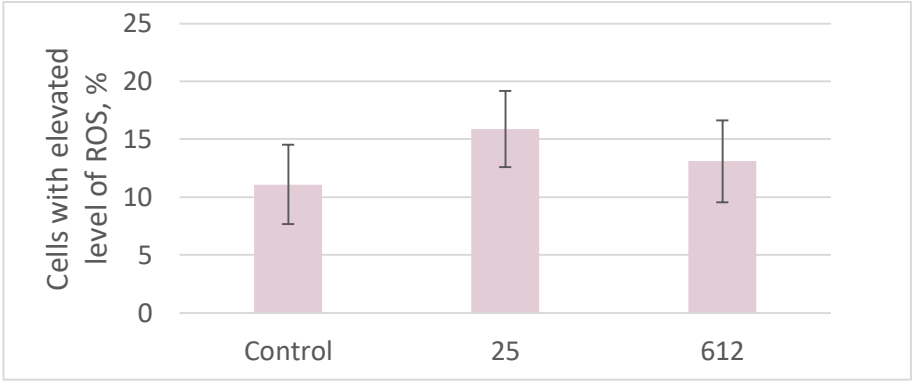

Fig. 3.9. Estimation of number of *S. cerevisiae* cells with elevated level of ROS after 1 h incubation with *Geobacillus* spp. 25 and 612 AgNP. Control - unaffected cells, number refers to the respective *Geobacillus* spp. strain.

3.3.3. Fluorescence microscopy analysis of ROS generation following treatment with silver nanoparticles and electroporation

The generation of ROS in *C. guilliermondii* cells after electroporation and the synergistic effect of electroporation and AgNP were both studied using the DCFDA assay kit.

No fluorescence was seen in the negative control samples during the fluorescence microscopy study, but fluorescence was seen and recorded in *C. guilliermondii* cells after electroporation or electroporation combined with AgNP, comparable to the previous research (**Fig. 3.10.**). The cells treated with the positive control, TBHP (*tert*-butyl hydroperoxide), exhibited the brightest fluorescence.

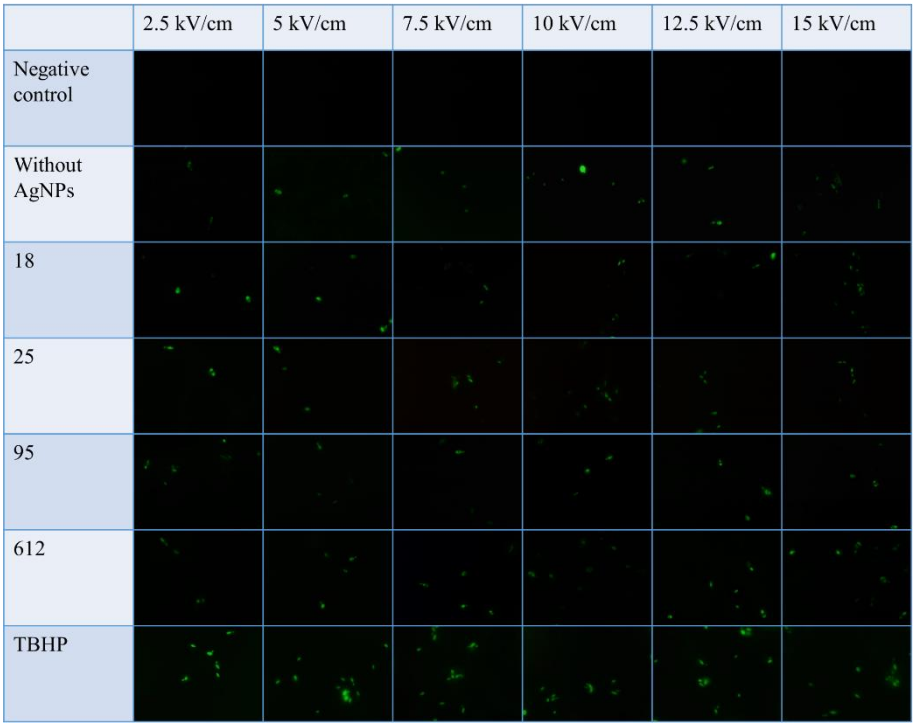

Fig. 3.10. The fluorescence microscopy analysis of DCF. The presence of ROS generation in *C. guilliermondii* cells after electroporation or the synergistic effect with electroporation and *Geobacillus* spp. AgNP is indicated by the green fluorescence. The *Geobacillus* spp. strains that formed AgNP are identified by the numbers on the left side. The electric field strength is shown at the top.

Following the electroporation study covered in Section 2.4.5., the synergistic impact of AgNP and electroporation on ROS generation was

examined (**Fig. 3.11.**). The AgNP concentration used in this study were the same. *Geobacillus* sp. 18 AgNP and 10 kV/cm, *Geobacillus* sp. 25 AgNP and 12.5 kV/cm, *Geobacillus* sp. 95 AgNP and 12.5 kV/cm, and *Geobacillus* sp. 612 AgNP and 2.5 kV/cm, 7.5 kV/cm or 12.5 kV/cm PEF all had statistically significant synergistic effects on ROS generation compared to negative control. The formation of ROS was not statistically increased by electroporation alone in the absence of AgNP. The trend, though, shows that ROS generation becomes apparent at higher voltage PEF. Almost all AgNP produce a statistically significant increase in ROS generation at PEF of 12.5 kV/cm. When using *Geobacillus* sp. 25 AgNP, the average ROS increase in folds was 3.34 ± 1.06, *Geobacillus* sp. 95 AgNP - 2.72 ± 0.75, and *Geobacillus* sp. 612 AgNP - 3.74 ± 1.41 at this PEF. The ROS level increases by 4.14 ± 1.60 times in comparison to the negative control at 7.5 kV/cm with *Geobacillus* sp. 612 AgNP.

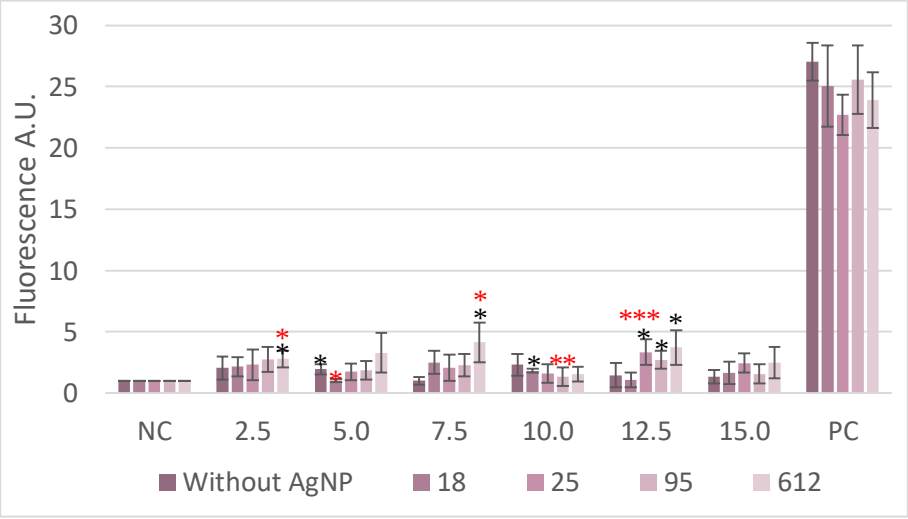

Fig. 3.11. The qualitative evaluation of DCF fluorescence observed by fluorescent microscopy. *C. guilliermondii* cells were electroporated or electroporated together with *Geobacillus* spp. AgNP. NC – negative control, *C. guilliermondii* cells unaffected with AgNP or electroporation; PC – positive control, *C. guilliermondii* cells treated with TBHP; numbers under the histogram refer to PEF (kV/cm); numbers in the legend refer to *Geobacillus* spp. strain AgNP. p-values: * <0.05; **<0.005; ***<0.0005; black asterisks refer to p-values compared to negative control; red asterisk refer to p-values compared between cells which were electroporated and electroporated together with AgNP.

In addition, it was found that the increase in the amount of ROS using *Geobacillus* sp. 95 AgNP and the PEF of 12.5 kV/cm and *Geobacillus* sp. 612 AgNP and the PEF of 2.5 and 7.5 kV/cm is statistically significantly different from the amount of ROS produced when the cells are exposed only to the respective values of the PEF (**Fig. 3.11.**). According to these results, it can be assumed that the increase of ROS is decisive for both electroporation and AgNP.

To determine whether the experimental settings were properly chosen and whether DCFDA accurately represented ROS generation, TBHP was used as the study's positive control. The data in this study showed that ROS in the positive control was effectively identified, with an increase in folds ranging from 22.69 to 27.03 ± 2.31 when compared to the negative control.

3.3.4. Fluorescence microscopy analysis of lipid peroxidation following treatment with silver nanoparticles

ROS generation is known to be linked to lipid peroxidation [277]. In this work, the Click-iT® Lipid Peroxidation Detection with Linoleamide Alkyne (LAA) kit was used to analyse this process. When Clik-iT® LAA is introduced to cells, it permeates and integrates into their membranes. The tagged LAA is oxidized as the membranes undergo lipid peroxidation, resulting in the generation of hydroperoxides. These hydroperoxides then degrade into α,β-unsaturated aldehydes, which could alter proteins in cells. These changes in proteins with the alkyne group can be recognized and evaluated utilizing Click-iT® chemistry [278].

In contrast to the DCFDA/H_2DCFDA-Cellular ROS Assay Kit (ab113851), qualitative assessment using fluorescence microscopy found fluorescence in the negative control. The difference can be explained by the fact that, unlike DCFDA, the fluorophore utilized in this assay is fluorescent from the start, whereas DCFDA requires a reaction to occur before it becomes fluorescent. This variation is consistent with the scientific literature and is regarded as acceptable [279]. Similar to the previous study, fluorescence was noticed and captured in yeast cells impaired by AgNP, as seen in **Figure 3.12**. The strongest fluorescence was found again in the positive control impacted by Cumene hydroperoxide (**Fig. 3.12P**).

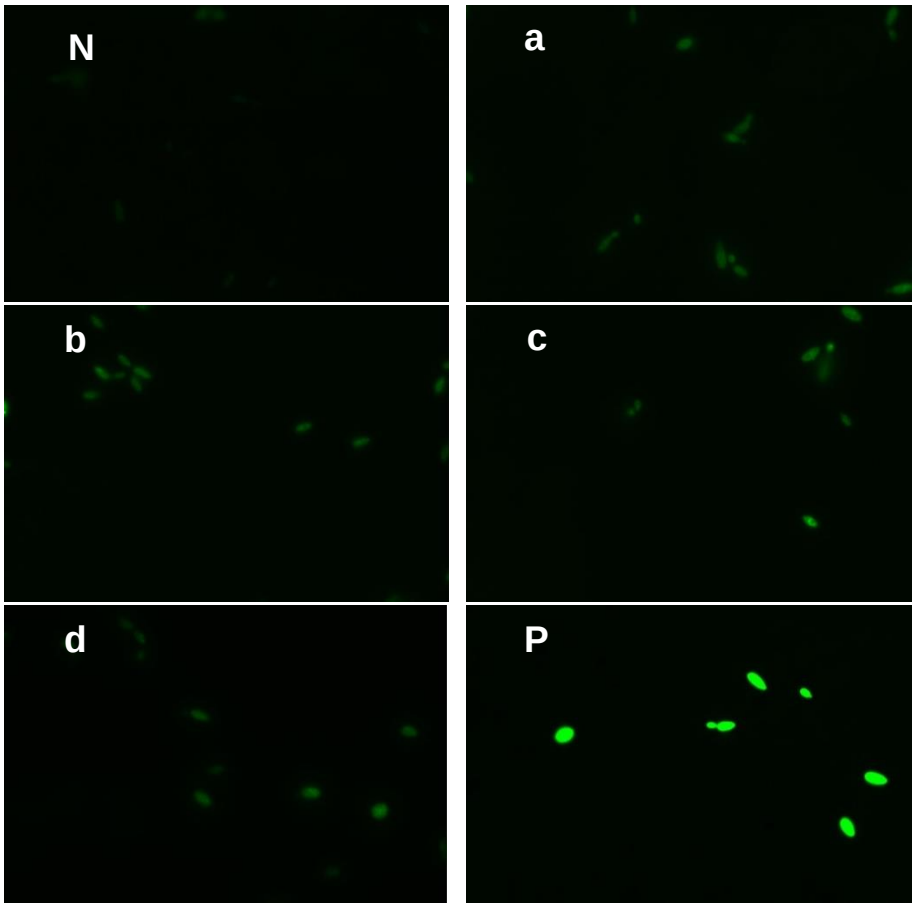

Fig. 3.12. Alexa Fluor® 488 observation by fluorescence microscopy. Following exposure to *Geobacillus* spp. AgNP, the green fluorescence shows that lipid peroxidation has occurred in the *C. guilliermondii* cells. **N** - negative control, unaffected *C. guilliermodii* cells; **a** - treatment with *Geobacillus* sp. 18; **b** - with *Geobacillus* sp. 25 AgNP; **c** - with *Geobacillus* sp. 95; **d** - with *Geobacillus* sp. 612 AgNP; **P** – positive control, *C. guilliermondii* cells impacted by Cumene hydro peroxide.

Increased lipid peroxidation after exposure to AgNP compared to negative control was found using AgNP of all four *Geobacillus* spp. strains. The mean fluorescence increase of three independent repetitions was determined to be 2.53 ± 0.76, 3.05 ± 0.66, 2.49 ± 0.57, and 3.10 ± 1.10 A. U. compared to negative control after treatment with *Geobacillus* spp. strains 18, 25, 95, and 612 respectively (**Fig. 3.13.**).

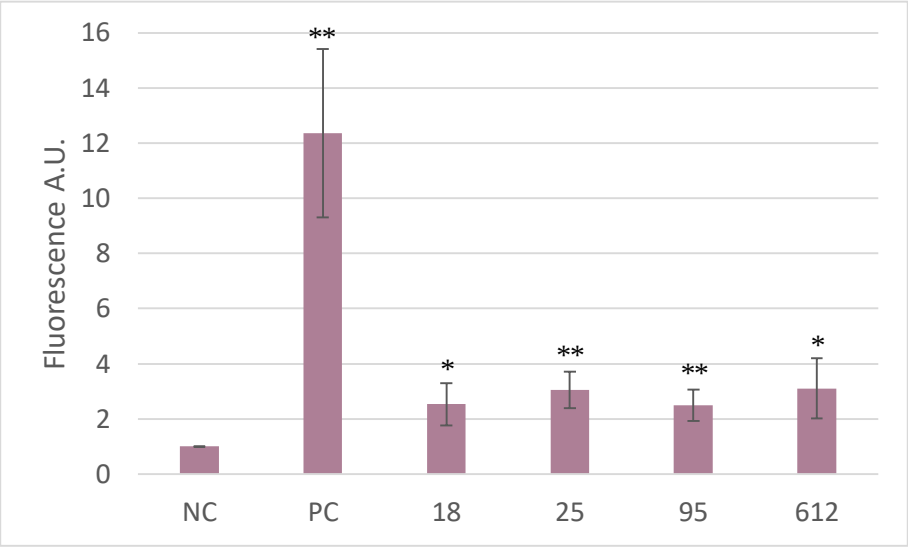

Fig. 3.13. The average green fluorescence intensity increased by a factor of two compared to the negative control equalized to 1 of lipid peroxidation. NC – unaffected *C. guilliermondii* cells; PC - cells affected with Cumene hydro peroxide; number refers to the respective *Geobacillus* spp. strain AgNP. p-values: * <0.05; ** <0.005.

3.3.5. Fluorescence microscopy analysis of lipid peroxidation following treatment with electroporation and silver nanoparticles

PEF is known to cause ROS production in affected cells. These ROS can contribute to lipid peroxidation. The breakdown of these lipids affects the stability of the pores formed during the electroporation process [228].

The occurrence of lipid peroxidation in *C. guilliermondii* cells after electroporation and the combination of electroporation and AgNP was investigated using the Click-iT® Lipid Peroxidation Detection with Linoleamide Alkyne (LAA) kit. Fluorescence microscopy indicated the presence of fluorescence in the negative control, but it was weaker than in the positive control. Analogously to results obtained when analysing the effect of AgNP alone, fluorescence was detected and captured in *C. guilliermondii* cells impacted by electroporation or the combination of electroporation and AgNP, as seen in **Figure 3.14**. Yet again, the positive control treated with Cumene hydroperoxide produced the brightest fluorescence signal. Cumene hydroperoxide was used as a positive control to determine if the experimental conditions were chosen correctly and if Alexa Fluor® 488 accurately presented lipid peroxidation. According to the findings in this study, the

positive control's lipid peroxidation was efficiently detected, with an increase in folds ranging from 10.00 to 13.03 ± 2.23 A.U. when compared to the negative control.

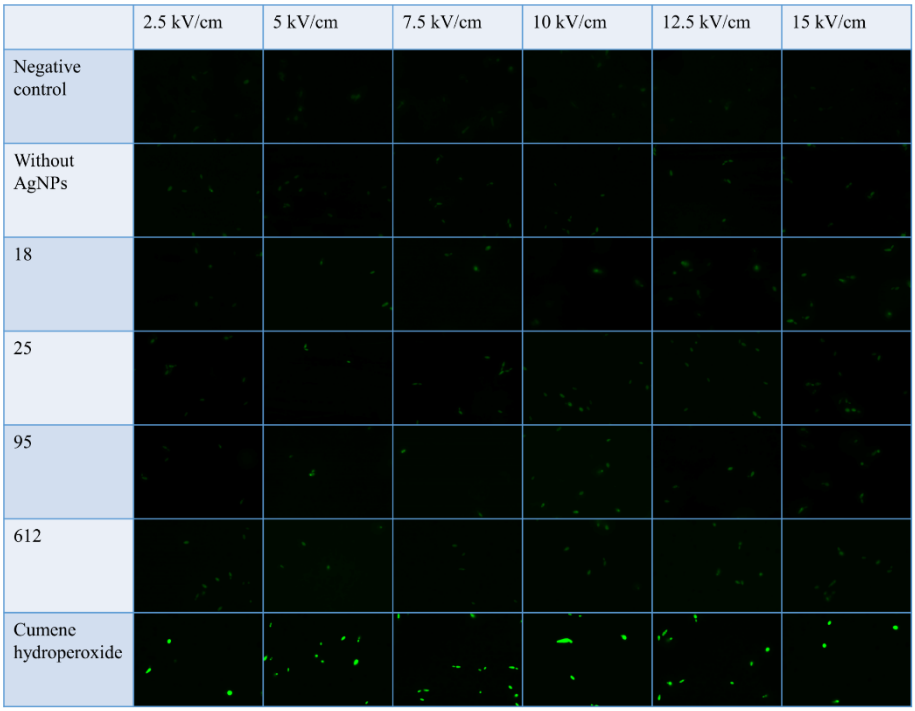

Fig. 3.14. The fluorescence microscopy analysis of Alexa Fluor® 488. The presence of lipid peroxidation in *C. guilliermondii* cells after electroporation or the synergistic effect with electroporation and *Geobacillus* spp. AgNP is indicated by the green fluorescence. The *Geobacillus* spp. strains that formed AgNP are identified by the numbers on the left side. The electric field strength is shown at the top.

Following the electroporation study mentioned above in Section 2.4.5., the same amounts of AgNP were used to conduct a study on the synergistic effect of electroporation and AgNP on lipid peroxidation occurrence (**Fig. 3.15.**). The statistically significant increase in lipid peroxidation after electroporation alone was not detected. The pattern continues to be that as the strength of the electroporation grows, so does the formation of ROS and consequent lipid peroxidation. The synergistic effect of electroporation and AgNP on lipid peroxidation formation was statistically significant at 7.5 and 15 kV/cm for *Geobacillus* sp. 18, 10 and 15 kV/cm for *Geobacillus* sp. 25, 10, 12.5, and 15 kV/cm for *Geobacillus* sp 95, and 15 kV/cm for *Geobacillus* sp.

612 AgNP. The PEF that produced the most consistent increase in lipid peroxidation when compared to the negative control was 15 kV/cm. The average-fold increase in lipid peroxidation with AgNP of *Geobacillus* spp. 18, 25, 95, and 612 was 2.29 ± 0.31, 2.63 ± 0.85, 1.59 ± 0.15, and 2.63 ± 0.87, respectively, at this PEF. The greatest increase in ROS was seen with *Geobacillus* sp. 612 AgNP at 12.5 kV/cm, resulting in a 2.96 ± 0.55-fold increase in lipid peroxidation as compared to the negative control (**Fig. 3.15.**).

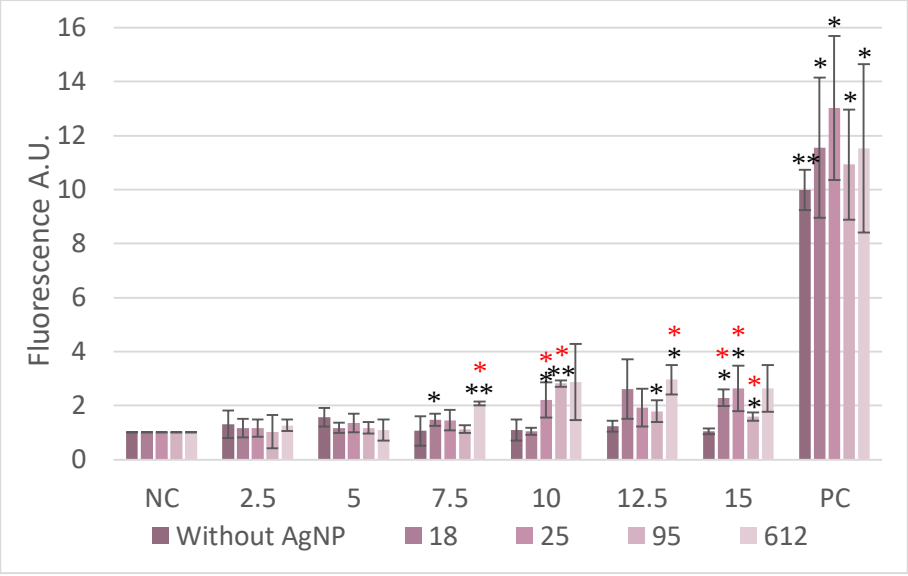

Fig. 3.15. The qualitative assessment of Alexa Fluor® 488 fluorescence was observed under a fluorescence microscope. *C. guilliermondii* cells were electroporated or electroporated together with *Geobacillus* spp. AgNP. NC – negative control, *C. guilliermondii* cells unaffected with AgNP or electroporation; PC – positive control, *C. guilliermondii* cells treated with Cumene hydro peroxide; numbers under the histogram refer to electric field strength (kV/cm); numbers in the legend refer to *Geobacillus* spp. strain AgNP. p-values: * <0.05; **<0.005; black asterisks refer to p-values compared to negative control; red asterisks refer to p-values compared between cells that were electroporated and electroporated together with AgNP.

In addition, it was found that the increase in the amount of lipid peroxidation using *Geobacillus* sp. 18 AgNP and the PEF of 15 kV/cm, *Geobacillus* sp. 25 and 95 AgNP and 10 and 15 kV/cm, *Geobacillus* sp. 612 AgNP and 7.5 and 12.5 kV/cm is statistically significantly different from the amount of lipid peroxidation caused when the cells are exposed only to the respective values of the PEF (**Fig. 3.15.**). According to these results, it can be

assumed that the increase in lipid peroxidation is decisive for both electroporation and AgNP.

3.3.6. Evaluation of changes in membrane permeability

When yeast cells are exposed to AgNP, their membranes can change with the loss of integrity making the cell membrane permeable. This feature is characteristic of late apoptosis or necrosis. Changes in membrane permeability in this work were assessed by staining cells with PI, which intercalates with DNA when inside cells and stains yeast red (**Fig. 3.16.**). Membrane permeability was tested after exposure to *Geobacillus* spp. 25 and 612 AgNP, as they exhibited the highest ROS generation.

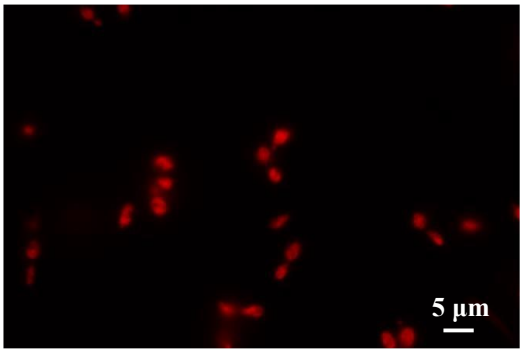

Fig. 3.16. Evaluation of membrane permeability in yeast *C. guilliermondii* exposed to *Geobacillus* sp. 25 AgNP. Yeast cells that are permeable to PI are stained in red.

Statistically reliable changes were detected after 30 min of exposure to 10 µg/mL concentration of *Geobacillus* sp. 25 and 5 µg/mL *Geobacillus* sp. 612 AgNP with both *C. guilliermondii* and *S. cerevisiae* yeast cells. In the case of *C. guilliermondii* 65.29 ± 0.51% cells with permeable membranes were found after treatment with *Geobacillus* sp. 25 AgNP, and 61.00 ± 5.72% cells with permeable membranes after exposure to *Geobacillus* sp. 612 AgNP (**Fig. 3.17.**). In the case of *S. cerevisiae* 58.98 ± 4.69% and 72.93 ± 4.80% cells with permeable membranes were found after the treatment with *Geobacillus* spp. 25 and 612 respectively.

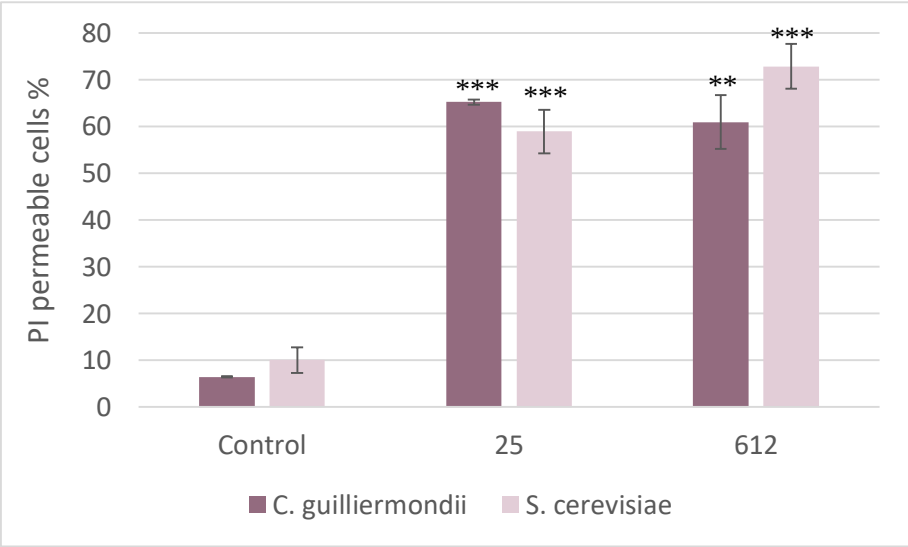

Fig. 3.17. Estimation of number of *C. guilliermondii* and *S. cerevisiae* cells with permeable membranes after 30 min incubation with *Geobacillus* spp. 25 and 612 AgNP. Control - unaffected cells, numbers refer to *Geobacillus* sp. strain. p-values: **<0.005; ***<0.0005.

3.4. Detection of cell death in yeast cells

This section will discuss the evaluation of the type of yeast death following *Geobacillus* spp. AgNP exposure. The active caspases were analysed after treatment with *Geobacillus* spp. 25 and 612 AgNP with the highest ROS generation. The DNA fragmentation was analysed with *Geobacillus* spp. 25 and 95 AgNP because for active caspases, the AgNP used showed no difference (comparing effects with 25 and 612 AgNP).

3.4.1. Identification of active caspases

The FITC-VAD-FMK in situ label (FITC), which is conjugated to the caspase inhibitor VAD-FMK, was used to identify active caspases. When this marker enters cells and binds to activated caspases, fluorescence is observed, which serves as a marker of apoptosis. Cells with activated caspases stain green, while cells with no active caspases do not (**Fig. 3.18.**).

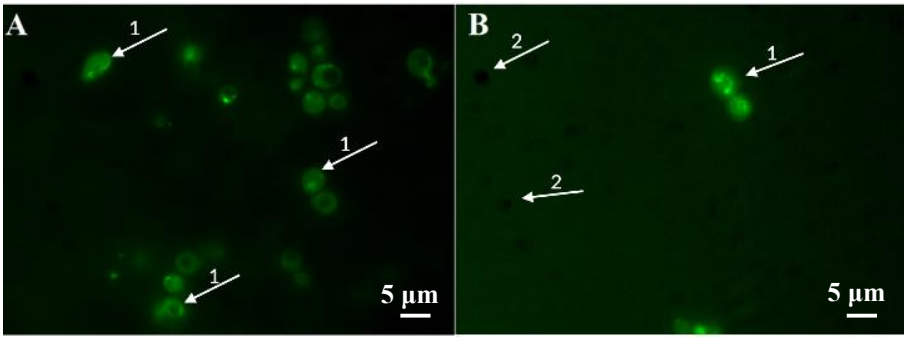

Fig. 3.18. Detection of active caspases in *C. guilliermondii* (**A**) and *S. cerevisiae* (**B**) after 2 h incubation with 50 µg/mL concentration of *Geobacillus* sp. 25 AgNP. **1** - cells with active caspases are stained green; **2** - cells without active caspases do not stain.

After exposing *C. guilliermondii* yeast cells to *Geobacillus* spp. 25 and 612 AgNP (10 and 5 µg/mL concentration respectively) for 1 hour, it was found that 44.69 ± 5.22% of cells with active caspases were identified for *Geobacillus* sp. 25 AgNP, and *Geobacillus* sp. 612 AgNP 32.71 ± 4.87% (**Fig. 3.19.**). In the case of *S. cerevisiae* after exposure to the same concentrations of *Geobacillus* spp. 25 and 612 AgNP, 72.35 ± 8.95% and 66.64 ± 10.52% cells with active caspases were identified, respectively (**Fig. 3.19.**). In all cases, the change in cells with active caspases was statistically significant ($p < 0.05$).

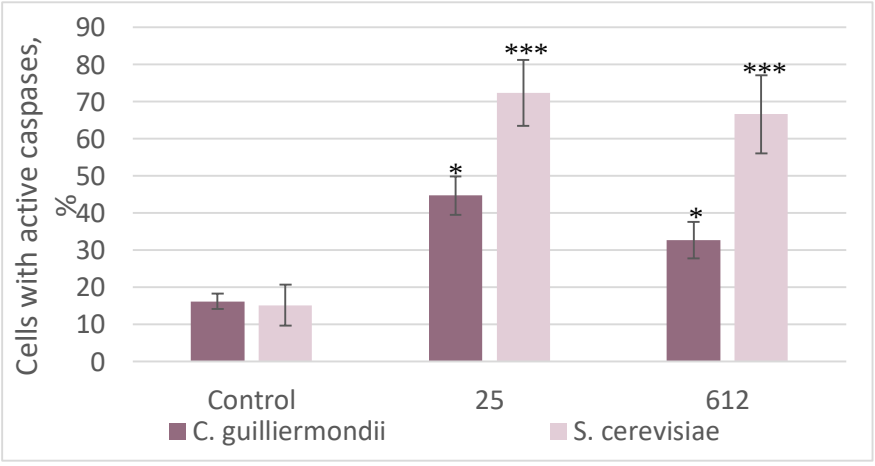

Fig. 3.19. Estimation of number (%) of *C. guilliermondii* and *S. cerevisiae* cells with active caspases after 1 h incubation with *Geobacillus* spp. 25 and 612 AgNP. Control - unaffected cells, numbers refer to *Geobacillus* spp. strains. p-values: *<0.05; ***<0.0005.

3.4.2. Assessment of DNA fragmentation

The formation of DNA breaks is a marker of early apoptosis. In this work, DNA fragmentation was assessed qualitatively. During apoptosis, after fractionation of yeast genomic DNA in agarose gel, DNA fragmentation or DNA ladder formation is observed. After 2 h of exposure to *Geobacillus* sp. 25 and 95 AgNP (concentration of 25 and 70 μg/mL, respectively) in YPD medium DNA fragmentation was not detected. In the gel electrophotogram, the control and test samples were of the same size, the DNA ladder characteristic of apoptosis was not formed, and no DNA fragments of smaller size were observed.

The same results were obtained by incubating yeast cells with a 10-fold lower concentration of AgNP for 1 h. The results show that DNA fragmentation did not occur under the tested conditions. It is important to mention that single-stranded DNA breaks are also possible during apoptosis, which are not detected by this method.

3.5. Antibacterial properties against pathogenic skin bacteria

This section describes the part of the study carried out with pathogenic skin bacteria *S. aureus*, *S. pyogenes*, and *P. aeruginosa*. Only *Geobacillus* spp. 25 and 612 AgNP were used for this section of thesis, because these AgNP had lowest MICs. AgNP exposure has also been combined with electroporation in the hope of shortening the exposure time. Electroporation increases membrane permeability, so it may improve the entry of AgNP into the cell [233]. In addition, electroporation is suitable for the treatment of wounds and scars, so it is safe to use [238].

3.5.1. Enhancing silver nanoparticles effect using the electroporation against skin pathogenic bacteria

The results obtained during the study with *S. aureus* bacterial cells show that the electroporation enhanced the antibacterial effect of AgNP and significantly reduces the number of viable cells (**Fig. 3.20.**). The MIC of *Geobacillus* sp. 612 AgNP (2.5 μg/mL) for *S. aureus* cells was used in this study. The best results were obtained using an electric field of 15 kV/cm together with AgNP in which the number of viable cells decreases to 13.34 ± 5.65%. A decrease in cell viability is also observed when they are only

exposed to an electric field. Using a PEF of 15 kV/cm reduces the number of viable cells to 61.94 ± 14.09%.

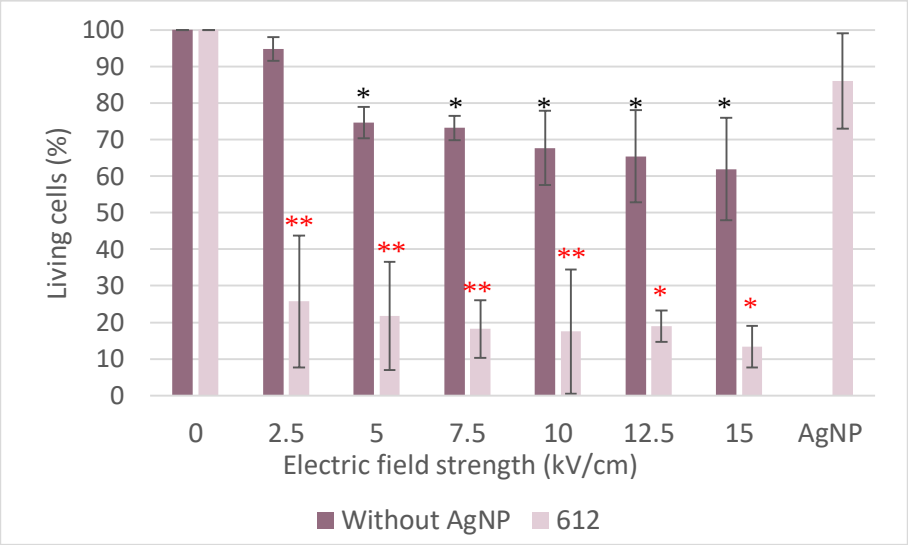

Fig. 3.20. The effect of *Geobacillus* sp. AgNP and electroporation on *S. aureus* bacteria cells. *S. aureus* cells were treated with electroporation or a combination of AgNP and electroporation. The control group consisted of cells that were not subjected to electroporation or AgNP or AgNP only. The experimental group was treated with AgNP derived from *Geobacillus* sp., as it is indicated numerically in the figure. p-values: * <0.05; ** <0.005; black asterisks refer to p-values compared to negative control; red asterisk refer to p-values compared between cells which were electroporated and electroporated together with AgNP.

The results of the experiment performed with *S. pyogenes* bacterial cells show that the combined effect of electroporation and AgNP significantly reduce cell viability (**Fig. 3.21.**). The best result is observed when the MIC of *Geobacillus* sp. 612 AgNP (1 μg/mL) is combined with a PEF of 15 kV/cm, in which case the number of viable cells is reduced to 16.53 ± 10.10%. Cell viability was also observed to decrease when subjected to electroporation alone and was obtained with a PEF of 15 kV/cm, a decrease in the number of viable cells in this case to 56.46 ± 7.18%.

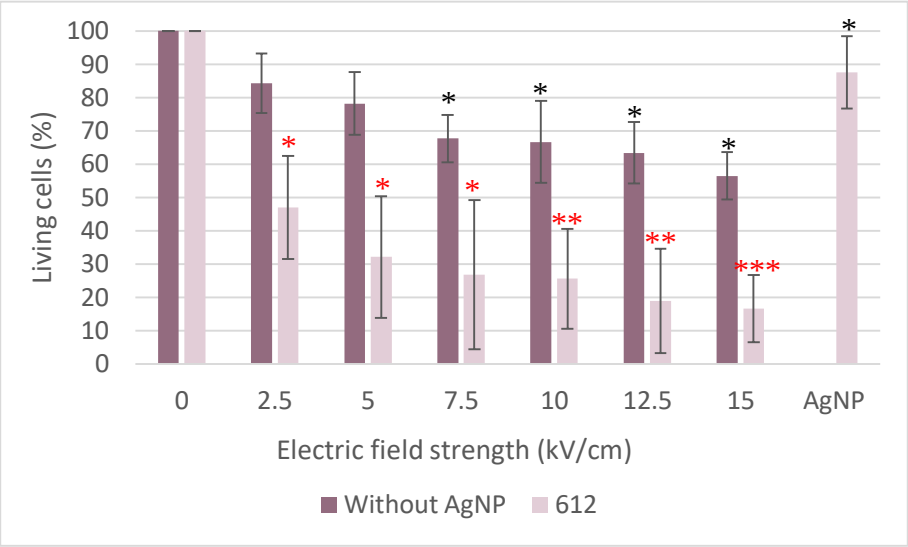

Fig. 3.21. The effect of *Geobacillus* sp. AgNP and electroporation on *S. pyogenes* bacteria cells. *S. pyogenes* cells were treated with electroporation or a combination of AgNP and electroporation. The control group consisted of cells that were not subjected to electroporation or AgNP or AgNP only. The experimental group was treated with AgNP derived from *Geobacillus* sp., as it is indicated numerically in the figure. p-values: * <0.05; ** <0.005; *** <0.0005; black asterisks refer to p-values compared to negative control; red asterisk refer to p-values compared between cells which were electroporated and electroporated together with AgNP.

The results of the experiment performed with *P. aeruginosa* bacterial cells show that the combined effect of electroporation and AgNP significantly reduce cell viability (**Fig. 3.22.**). When cells are exposed to electroporation alone, the greatest reduction in the number of viable cells is achieved at an applied PEF of 15 kV/cm (55.78 ± 3.55%), whereas when the MIC of *Geobacillus* sp. 612 AgNP (2 μg/mL) is combined with a PEF of 15 kV/cm, in which case the number of viable cells is reduced by 32.59 ± 12.98%.

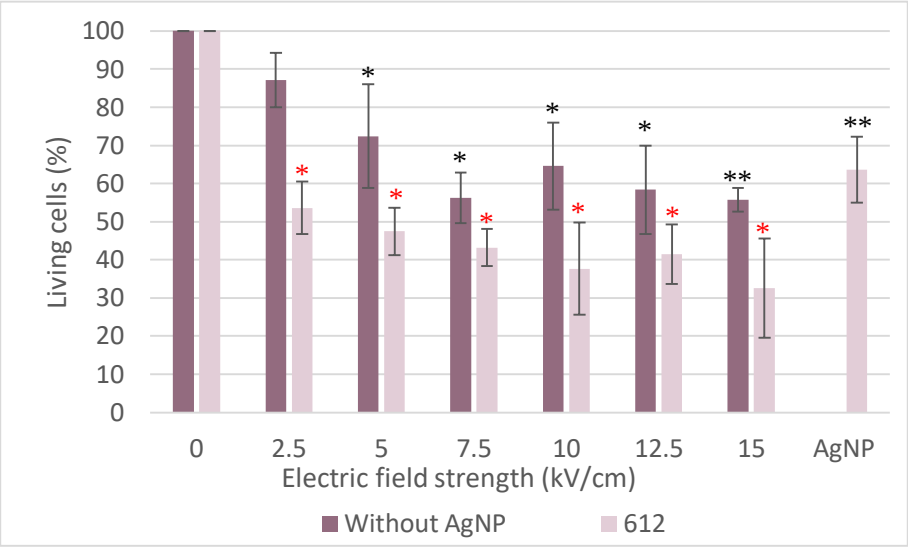

Fig. 3.22. The effect of *Geobacillus* sp. AgNP and electroporation on *P. aeruginosa* bacteria cells. *P. aeruginosa* cells were treated with electroporation or a combination of AgNP and electroporation. The control group consisted of cells that were not subjected to electroporation or AgNP or AgNP only. The experimental group was treated with AgNP derived from *Geobacillus* sp., as it is indicated numerically in the figure. p-values: * <0.05; ** <0.005; black asterisks refer to p-values compared to negative control; red asterisk refer to p-values compared between cells which were electroporated and electroporated together with AgNP.

Moreover, it was observed that the increased number of dead cells when *Geobacillus* sp. 612 AgNP and with all electroporation electric field strength are used is statistically significantly different from the number of dead cells when the cells are exposed only to the respective values of the PEF or AgNP alone (**Fig. 3.20.**, **Fig. 3.21.**, and **Fig. 3.22.**). According to these results, it can be assumed that the increase of dead cells is decisive for both electroporation and AgNP, hence electroporation enhances the antibacterial properties of AgNP.

3.5.2. Evaluation of silver nanoparticles and electroporation effect on *Pseudomonas aeruginosa* biofilms

To determine the potential of AgNP in antimicrobial therapy, an assessment of their effect on *P. aeruginosa* biofilms over time was performed. AgNP of *Geobacillus* sp. strain 25 with moderate antimicrobial properties against planktonic *P. aeruginosa* cells were selected for this study, and AgNP

concentration was increased twofold. The results of the time assessment of the antimicrobial activity showed that incubating *P. aeruginosa* in 1 M sorbitol together with 10 µg/mL concentration of *Geobacillus* sp. 25 AgNP successfully reduced bacterial viability depending on the incubation time (**Fig. 3.23.**). When *P. aeruginosa* was exposed to AgNP, the number of living cells compared to the control decreased to 75.00 ± 2.00% immediately after adding AgNP, 33.33 ± 5.35% after 2 h, 18.00 ± 0.84% after 4 h, and 1.67 ± 0.37% after 6 h. After incubation of biofilms with AgNP for 24 h the viability of the cells was practically destroyed (99.67 ± 0.11%).

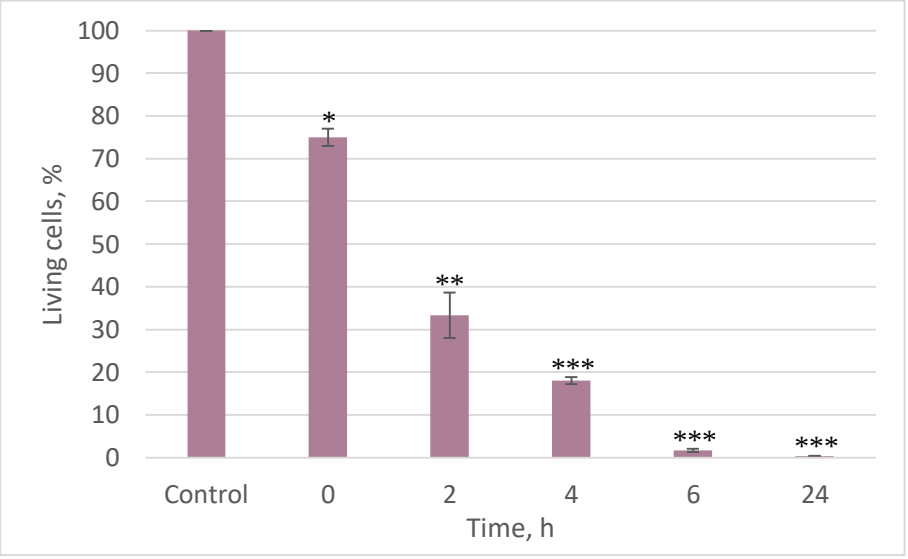

Fig. 3.23. Effect of *Geobacillus* sp. 25 AgNP on *P. aeruginosa* biofilms after different periods of incubation. The number of viable *P. aeruginosa* cells in biofilms expressed as a percentage. Control - biofilms unaffected by AgNP. p-values: * <0.05; **<0.005; ***<0.0005.

To evaluate the effect of electroporation and AgNP, a study was conducted in which *P. aeruginosa* biofilms were exposed to eight impulses of different PEF values together with a 5 µg/mL concentration of *Geobacillus* sp. 25 AgNP.

The results of the experiment showed that electroporation together with *Geobacillus* sp. 25 AgNP statistically significantly reduced the number of viable cells in *P. aeruginosa* biofilms under all experimental conditions (**Fig. 3.24.**). Using only the PEF of values 15, 20, and 25 kV/cm, the number of viable cells decreased accordingly to 91.67 ± 1.67%, 85.67 ± 1.67%, and 83.33 ± 0.83%, whereas when added 5 µg/mL concentration of *Geobacillus* sp. 25

AgNP the number of viable cells in *P. aeruginosa* biofilms decreased to 76.67 ± 3.33%, 33.07 ± 5.20%, and 20.26 ± 0.27%, respectively.

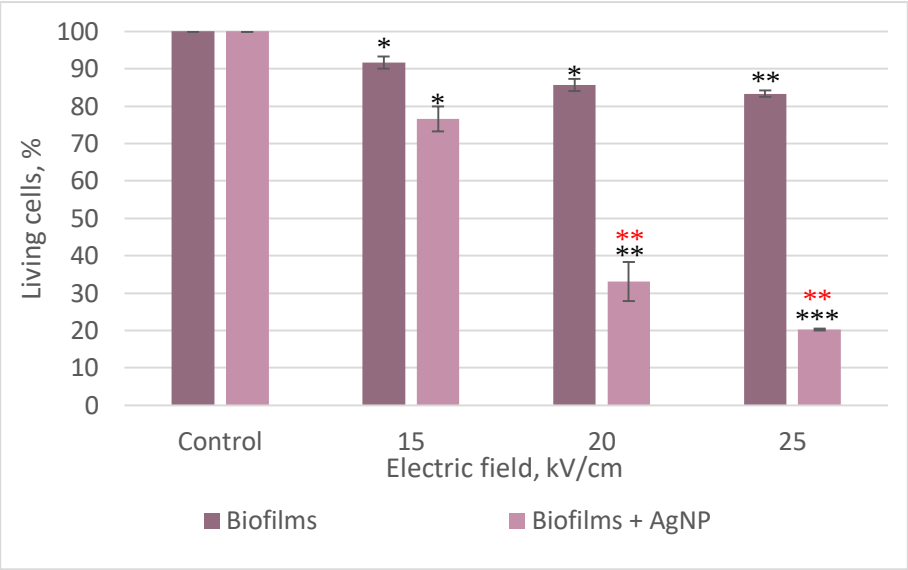

Fig. 3.24. The effect of *Geobacillus* sp. strain 25 AgNP and electroporation on *P. aeruginosa* biofilms. The number of viable *P. aeruginosa* cells in biofilms expressed as a percentage. Control – biofilms unaffected by AgNP and electroporation. p-values: * <0.05; **<0.005; ***<0.0005; black asterisks refer to p-values compared to control; red asterisk refer to p-values compared between biofilms which were only electroporated and only affected with AgNP, and electroporated together with AgNP.

Evaluating the effect of electroporation on biofilms showed that using even eight 100 µs impulses and 25 kV/cm PEF, the number of viable cells of *P. aeruginosa* in biofilms is reduced by only about 20%. However, after adding 5 µg/mL concentration of *Geobacillus* sp. 25 AgNP and applying a PEF of 25 kV/cm, the number of viable cells in the biofilm is reduced to a similar extent as cells exposed to 10 µg/mL of the same AgNP for 6 h. Moreover, it was found that when applying eight impulses of PEF of 20 and 25 kV/cm and 5 µg/mL concentration of *Geobacillus* sp. 25 AgNP, the number of viable cells in *P. aeruginosa* biofilms is statistically reliably different from those biofilms that were only exposed to electroporation impulses of the corresponding values or those that were only for a short time exposed to 10 µg/mL concentration of AgNP (**Fig. 3.24.**). These results suggest that the electroporation enhanced the antibacterial effect of *Geobacillus* AgNP and decreased the number of viable cells in biofilms.

3.5.3. Flow cytometry analysis of ROS generation in bacteria following treatment with silver nanoparticles

The evaluation of ROS generation was assessed by staining cells with DCFDA. This substance changes into the fluorescent molecule DCF when it is exposed to ROS [276].

Statistically reliable changes were detected after 1 hour of exposure to MIC of *Geobacillus* spp. 25 and 612 AgNP with all tested bacteria (*S. aureus*, *S. pyogenes*, and *P. aeruginosa*). In the case of *S. aureus* 72.25 ± 15.76% cells with elevated levels of ROS were found after affecting cells with 2.6 µg/mL *Geobacillus* sp. 25 AgNP, and 80.65 ± 6.71% cells with elevated levels of ROS after exposure to 2.6 µg/mL *Geobacillus* sp. 612 AgNP (**Fig. 3.25.**). In the case of *S. pyogenes* 56.54 ± 18.21% and 46.04 ± 6.36% cells with elevated levels of ROS were found after the exposure to *Geobacillus* spp. 25 (4.17 µg/mL) and 612 (1.04 µg/mL) respectively, and in the case of *P. aeruginosa* - 26.36 ± 5.75% and 49.03 ± 3.34% cells with permeable membranes were found after the treatment with *Geobacillus* spp. 25 (5.21 µg/mL) and 612 (2.09 µg/mL) respectively.

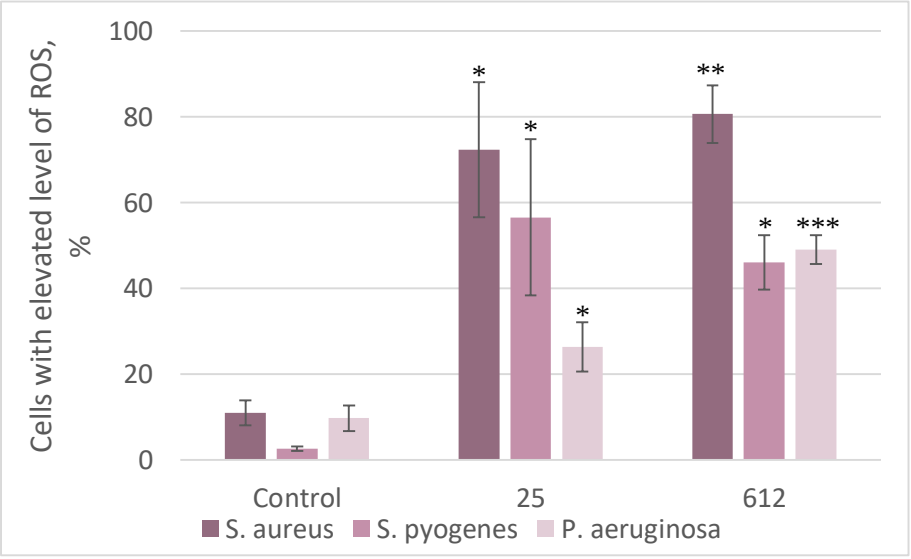

Fig. 3.25. Estimation of number of *S. aureus*, *S. pyogenes*, and *P. aeruginosa* cells with elevated level of ROS after 1 h incubation with *Geobacillus* spp. 25 and 612 AgNP. Control - unaffected cells, numbers refer to *Geobacillus* sp. strain. p-values: *<0.05; **<0.005; ***<0.0005.

3.5.4. Evaluation of changes in membrane permeability

Changes in membrane permeability in this work were assessed by staining cells with PI, which intercalates with DNA when inside cells. Membrane permeability was tested after exposure to *Geobacillus* spp. 612 and 25 AgNP, because one demonstrated the lowest MIC values and the other the middle MIC value compared to other AgNP.

Statistically reliable changes were detected after 30 min of exposure to MIC of *Geobacillus* spp. 25 and 612 AgNP with all tested bacteria (*S. aureus*, *S. pyogenes*, and *P. aeruginosa*). In the case of *S. aureus* 34.65 ± 10.60% cells with permeable membranes were found after exposure to 2.6 μg/mL *Geobacillus* sp. 25 AgNP, and 33.37 ± 6.66% cells with permeable membranes after exposure to 2.6 μg/mL *Geobacillus* sp. 612 AgNP (**Fig. 3.26.**). In the case of *S. pyogenes* 39.55 ± 1.96% and 23.68 ± 6.75% cells with permeable membranes were found after the exposure to *Geobacillus* spp. 25 (4.17 μg/mL) and 612 (1.04 μg/mL) respectively, and in the case of *P. aeruginosa* - 82.81 ± 0.86% and 57.59 ± 2.79% cells with permeable membranes were found after the exposure to *Geobacillus* spp. 25 (5.21 μg/mL) and 612 (2.09 μg/mL) respectively.

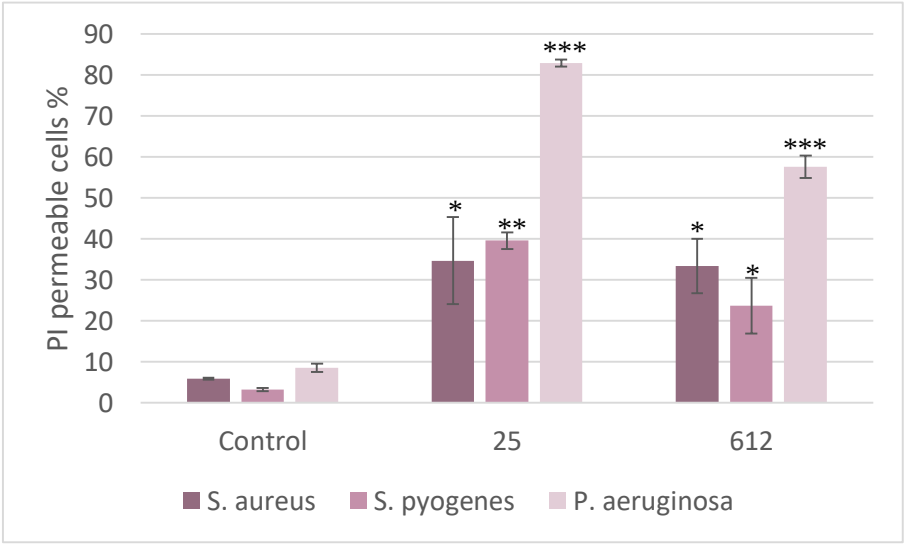

Fig. 3.26. Estimation of number of *S. aureus*, *S. pyogenes*, and *P. aeruginosa* cells with permeable membranes after 30 min incubation with *Geobacillus* spp. 25 and 612 AgNP. Control - unaffected cells, numbers refer to *Geobacillus* sp. strain. p-values: *<0.05; **<0.005; ***<0.0005.

3.6. Effects of silver nanoparticles on keratinocyte cell culture

This section will discuss the results obtained by exposure of keratinocyte (Ker-CT) cell culture to *Geobacillus* sp. strain 612 AgNP that were selected as having the lowest MIC values against all tested pathogenic microorganisms. This section was carried out in collaboration with the Department of Biological Models of the Institute of Biochemistry of VU LSC.

3.6.1. Evaluation of cytotoxicity of silver nanoparticles to keratinocytes

In order to determine the effect of *Geobacillus* sp. AgNP in cell culture, a study of their cytotoxicity on Ker-CT cell culture was performed. The results are compared with Ker-CT cells unaffected by AgNP. The lowest concentration of *Geobacillus* sp. strain 612 AgNP tested coincides with the highest MIC value determined (against *C. guilliermondii*). The results show that this concentration is not cytotoxic to the examined Ker-CT cells (**Fig. 3.27.** and **3.28.**). Increasing the concentration of AgNP results in a cytotoxic effect on Ker-CT cells.

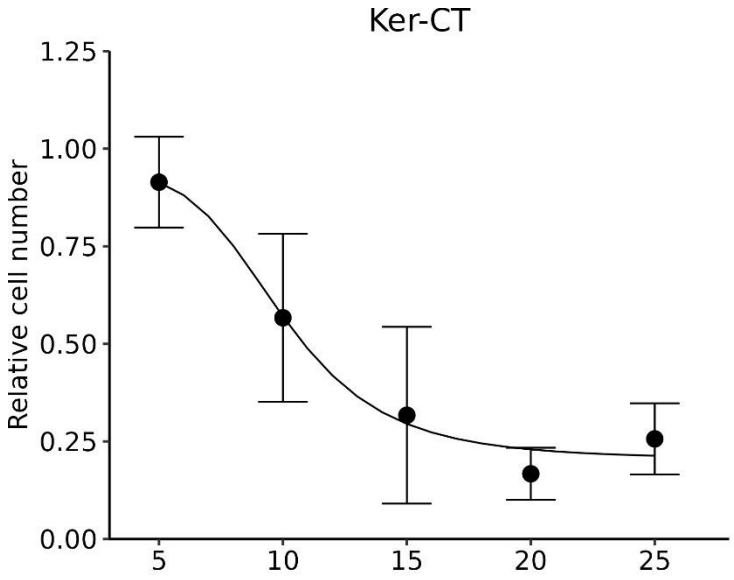

Fig. 3.27. *Geobacillus* sp. 612 AgNP cytotoxicity assessment on Ker-CT cell culture. This effect is expressed as relative units compared to unaffected cells. The numbers at the bottom indicate the concentrations of AgNP (μg/mL) used.

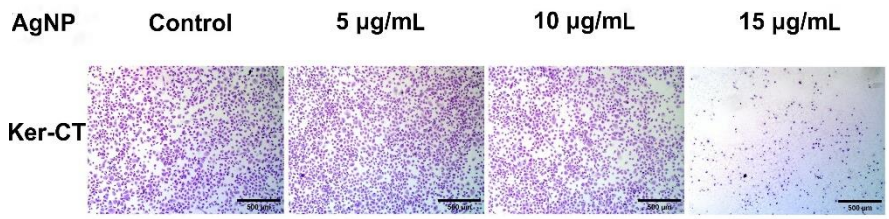

Fig. 3.28. Crystal violet photographs of Ker-CT cells treated with different concentrations of *Geobacillus* sp. 612 AgNP for 24 hours.

3.6.2. Evaluation of cell proliferation of silver nanoparticles to keratinocytes

After determining the cytotoxic effect of *Geobacillus* sp. 612 AgNP on Ker-CT cell culture, the proliferative activity of Ker-CT at different AgNP concentrations was investigated (**Fig. 3.29.**). These results can be used to determine whether cells proliferate or die over time at these AgNP concentrations. The obtained results show that at a concentration of 5 µg/mL, Ker-CT cells neither proliferate nor die in 72 hours, but their proliferative activation decreases with the use of higher concentrations.

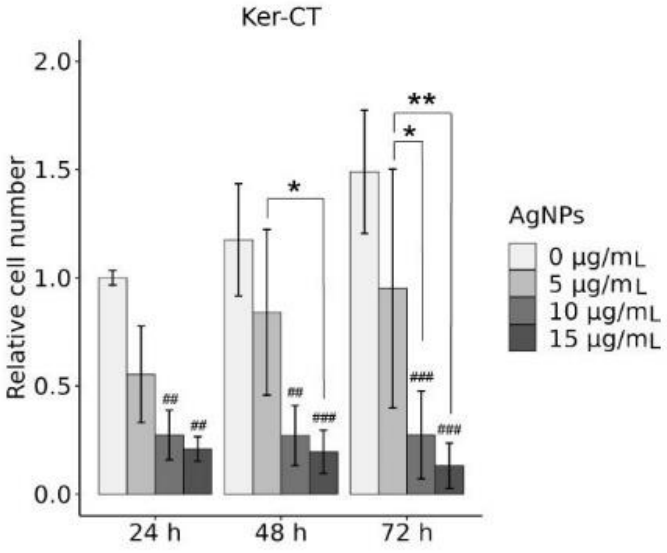

Fig. 3.29. *Geobacillus* sp. 612 AgNP proliferation assessment on Ker-CT cell culture. This effect is expressed as relative units compared to unaffected cells. The numbers at the bottom indicate the incubation time; number in the legend correspond to concentrations of AgNP (µg/mL) used.

3.6.3. Evaluation of wound healing process after treatment with silver nanoparticles

Ker-CT cells were investigated for epithelial wound healing after treatment with *Geobacillus* sp. 612 AgNP (0, 5, 10, and 15 μg/mL concentrations). Lipopolysaccharides (4 μg/mL) were used as a control. The results show that without the addition of AgNP and with the addition of LPS, the wound completely shrinks within 24 h (**Fig. 3.30.**). The addition of 5 μg/mL AgNP shows cell migration after 24 h, and the wound shrinks completely within 48 h, whereas exposure to AgNP at concentrations of 10 and 15 μg/mL results in no wound shrinkage during this period (no cell migration occurs with the concentration of 15 μg/mL) (**Fig. 3.30.**).

Quantitative measurements of wound closure (Ker-CT cells migration) after exposure to AgNP show that wound area, wound closure (%), wound width, and wound healing rate remain the same after affecting Ker-CT with AgNP concentrations of 10 and 15 μg/mL compared to 0 h, indicating that cell migration does not occur within 48 h (**Fig. 3.31**). However, 5 μg/mL concentration of AgNP only slows down the healing of the wound - the wound completely shrinks within 48 h compared to 24 h in the control sample (**Fig. 3.31.**).

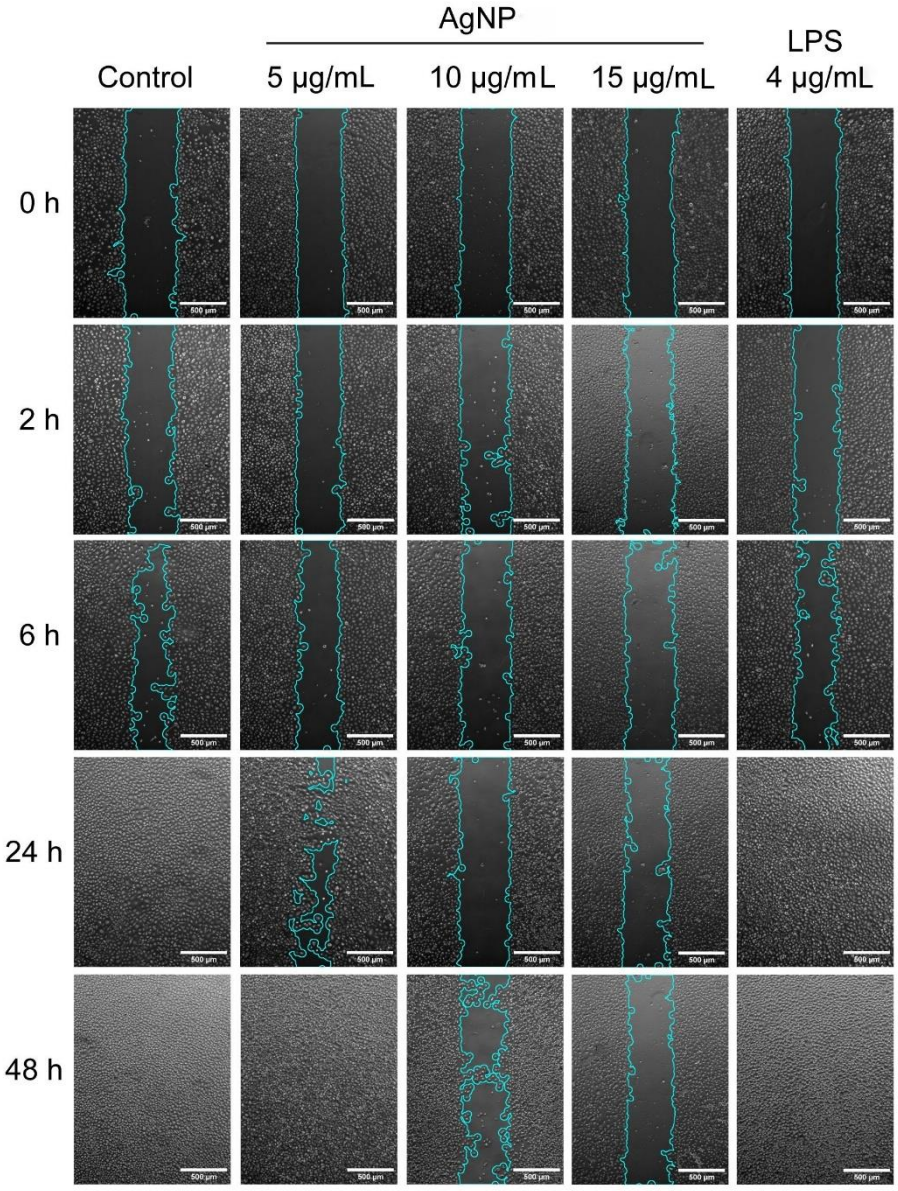

Fig. 3.30. Effect of AgNP on Ker-CT cell migration. Pictures of Ker-CT cells at 0 h, 2 h, 6 h, 24 h and 48 h. Scale bar - 500 µm.

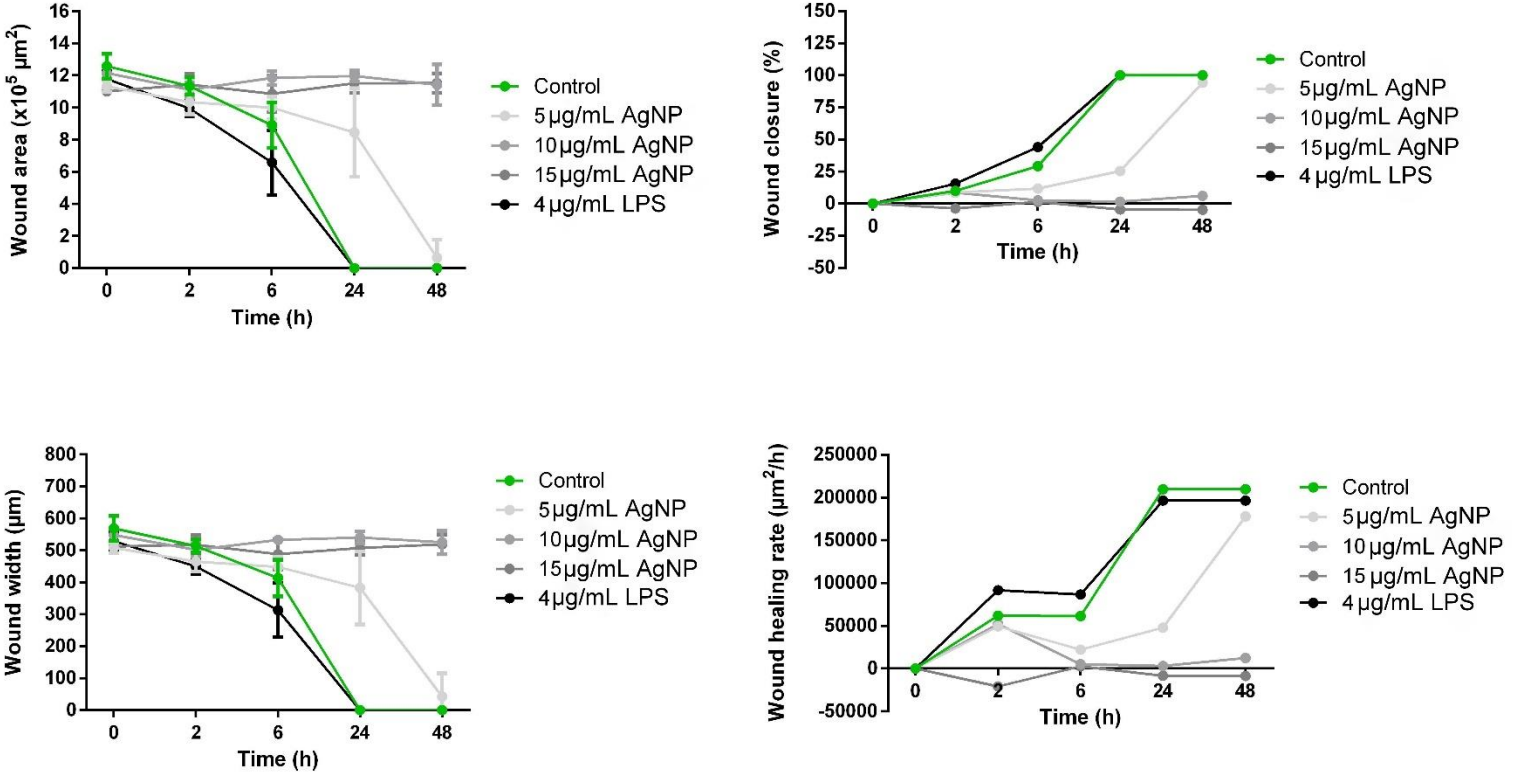

Fig. 3.31. The quantitative analyses of cell migration. Notes: each point represents the mean ± SD (n=3). Graphs in the left side are represented as mean ± SD of three different fields of pseudo-"wound" view area. Right side graphs are represented as mean.

4. DISCUSSION

Silver nanoparticles, or AgNP, are particles with 20–15,000 silver atoms that are typically smaller than 100 nm. When compared to their bulk materials, AgNP have different physical, chemical, and biological characteristics. The superior antimicrobial activity of AgNP, which can aid in lowering the use of different antibiotics, has received the greatest focus in study and application. As such, the low-cost, low-complexity, and environmentally benign method of producing AgNP is critical. AgNP can be synthesized biologically as an alternative to chemical or physical synthesis. This study examined the supernarants of thermophilic *Geobacillus* spp. that synthesize AgNP extracellularly. Although these microorganisms have been used in the past to synthesize AgNP, this is the first work to fully investigate their potential and probable antimicrobial mechanism. Four *Geobacillus* sp. strains - 18, 25, 95, and 612 - have undergone more thorough testing for the synthesis of AgNP in this thesis. The primary nitrate reductase screening method was used to select all four strains (not included in this thesis) since it is the key enzyme involved in the production of AgNP from $AgNO_3$.

One of the primary methods for identifying AgNP synthesis is the colour shift in the media following a cell-free supernatants incubation with $AgNO_3$ [134]. When employing the cell-free supernatants of all four strains of *Geobacillus* spp., these alterations were identified at 2 mM $AgNO_3$. AgNP surface plasmon vibrations are excited, which results in a hue shift from light brown to dark brown [132,280–282]. AgNP shape, size, and dielectric environment all affect their surface plasmon resonance [283]. The resonance peaks were found in the 410–425 nm range, which has been identified as the AgNP surface plasmon resonance band [280,284]. For AgNP generated by cell-free extract of *Geobacillus stearothermophilus*, a comparable absorbance maximum was found. Transmission electron microscopy (TEM) images were used by Fayaz et al. to determine that the resultant AgNP have a diameter of 5–35 nm and are spherical [16]. This thesis' SEM investigation further revealed that while the generated AgNP have a spherical form, their particle size distribution is wider, with most of them being less than 100 nm. In addition, DLS analysis, a more precise technique, was employed to figure out the size of particles in aqueous dispersions and cultivation media of microorganisms.

The obtained AgNP zeta potentials were discovered to be negative, with values ranging from −25 to −31 mV (in aqueous dispersion). This is not unusual, as evidenced by numerous instances in the literature where negative

AgNP zeta potential values achieved through biological synthesis have been documented [285–287]. The binding of microorganisms or nutritional media constituents, such as proteins and amino acids from the supernatants to the surface of produced AgNP may be the cause of the negative potential values. This theory is also supported by the conducted measurements of AgNP zeta potential after incubation in nutrient media. Zeta potentials were more negative compared to those values after the synthesis (the values dropped by 0.94–6.7). It is noteworthy to mention that the zeta potential is a crucial metric that offers insights into the stability of the produced particles, especially in the context of aqueous dispersion. It has been shown that the generated colloids are stable in aqueous dispersion, meaning they do not agglomerate if the absolute zeta potential value is greater than 30 mV ($\xi > +30$ mV or $\xi < -30$ mV) [275].

AgNP synthesis can also be carried out by bacteria belonging to different genera. *Pseudomonas* and *Bacillus* are the most often examined genera of bacteria [288,289]. However, because these genera of bacteria are mesophilic, doing so could lower the cost of synthesis (lower temperatures would be used), but it also raises the possibility that the resulting AgNP will be contaminated with mesophilic microorganisms, which could produce undesirable products or even be pathogens. Thus far, reports have been made of the synthesis of AgNP employing thermophilic mould *Sporotrichum thermophile* [290], thermophilic *Thermus thermophilus* [291], and *Bacillus* sp. isolated from a hot spring [292]. The synthesis of AgNP can be made less likely to produce other microbiological byproducts and more resistant to contamination by using thermophilic bacteria like *Geobacillus*. As a result, AgNP produced with thermophilic microorganisms may find use in both industry and healthcare.

After obtaining AgNP using supernatants of *Geobacillus* spp. bacteria, their antimicrobial properties were tested. The results show that, overall, AgNP of *Geobacillus* sp. strain 612 kill the tested skin pathogenic microorganisms at the lowest concentrations (for *S. aureus* 2.60, *S. pyogenes* 1.04, *P. aeruginosa* 2.09, and *C. guilliermondii* 5.00 (μg/mL)). Prashik et al. tested commercially available AgNP (diameter of 5 nm) against *S. aureus*. Their result shows that the MIC of these AgNP is 0.625 mg/mL (about 240 times higher than established in this thesis) [293]. The MICs of AgNP obtained by biosynthesis against *S. aureus* were 20 μg/mL (using *Cotyledon orbiculata* extract; 7.7 times higher) [294], 32 μg/mL (using *Aspergillus oryzae*; 12.3 times higher) [295], 8 μg/mL (using *Syzygium polyanthum*; 3.1 times higher) [296]. Lara et al. found that the commercially available AgNP MIC against *S. pyogenes* was 7.2 μg/mL (6.9 times higher) [297]. The MICs of AgNP obtained by biosynthesis against *P. aeruginosa* were 5 μg/mL (using

Cotyledon orbiculata extract; 2.4 times higher) [294], 32 μg/mL (using *Aspergillus oryzae*; 15.3 times higher) [295], 15 μg/mL (using *Syzygium polyanthum*; 7.2 times higher) [296]. The MICs of AgNP obtained by biosynthesis against *C. guilliermondii* were 1.16 mg/mL (using beech bark extract; 232 times higher) [298]. Mare et al. demonstrated, that 100% of growth inhibition of *C. guilliermondii* is achieved with 90 μg/mL concentration of AgNP synthesized using spruce bark extract and silver acetate salt (18 times higher) and 80 μg/mL of AgNP using silver nitrate salt (16 times higher) [299]. From these results, a tendency can be seen that the antimicrobial properties of AgNP obtained by biological synthesis are stronger than those of other methods, which correlates with the literature [133] and the MIC of thermophilic *Geobacillus* spp. AgNP is lower than the concentrations obtained in other studies.

One aspect of concern is the potential cytotoxic effect of AgNP on human cells, so ways to reduce AgNP concentration and/or exposure time may be sought. To that end, *Geobacillus* AgNP were combined with electroporation. The obtained results show that after 10 min exposure of cells of pathogenic skin microorganisms to *Geobacillus* AgNP and a single 100 μs impulse of electroporation, cell viability decreases by more than 60% (*S. aureus* 86.66%, *S. pyogenes* 83.47%, *P. aeruginosa* 67.41%, *C. guilliermondii* 97.33%). In addition, electroporation enhances the effect of AgNP against *P. aeruginosa* biofilms (eight 25 kV/cm 100 μs impulses reduce the number of viable cells in biofilms by 79.74%).

Novickij et al. used a range of electric field strengths (2.5 to 25 kV/cm) and impulse lengths (100 and 200 μs) to examine the effects of pulsed electric field (PEF) on *C. albicans* yeast cells [300]. The cells showed signs of permeabilization between 7.5 and 12.5 kV/cm, with statistically significant permeabilization at 15 to 25 kV/cm of applied PEF. Also, they demonstrated that PEF enhanced naftifine hydrochloride effect against the drug-resistant *C. albicans*, however this effect was not observed with other antifungal drugs (fluconazole, terbinafine) [300]. By comparing these results with the findings of the study of this thesis, Novickij et al. showed that applying a PEF of 15 kV/cm (25–50 impulses of 250 μs) resulted in a viable cell number of approximately 5%, whereas applying single 100 μs impulse (PEF of 15 kV/cm) together with *Geobacillus* sp. 612 AgNP (0.5 μg/mL concentration) resulted in viable cell number to approximately 3%.

In a separate study, Novickij et al. also showed the effectiveness of electroporation against MRSA. They used eight 100 μs impulses and obtained results that revealed that 15 kV/cm PEF reduced viable cell number to approximately 45%. Also, they tested the combination of vancomycin and

IRE, which was not effective against this pathogen (it was concluded that the viable cell elimination was only because of the IRE), whereas IRE enhanced the antimicrobial effect of sulfamethoxazole, ciprofoxacin, doxycycline, and gentamicin [301]. Munoz et al. demonstrated that 60 impulses of 2700 V/cm (duration of 70 μs) eliminated *S. aureus* [302]. In comparison, a single 100 μs impulse, 15 kV/cm PEF, and *Geobacillus* sp. 612 AgNP (2.5 μg/mL) reduced viable cell number to about 13%. This shows that electroporation enhances the effect of AgNP and better results can be achieved in their combination (thus reducing the number of impulses).

Novickij et al. also showed the effectiveness of electroporation against *P. aeruginosa* [303]. It indicates that 500 impulses of 900 ns (PEF of 15 kV/cm) reduced viable cell number to approximately 35%. The combined effect of nanosecond PEF and acetic acid against *P. aeruginosa* almost eliminated viable *P. aeruginosa* cells in contaminated areas in mice models. A single 100 μs impulse (PEF of 15 kV/cm) and *Geobacillus* sp. 612 AgNP (2 μg/mL) had a weaker effect than Novickij et al. showed, but it should be emphasized that in their case, a much higher number of impulses is used.

The study of this thesis is a new method of applying the combination of electroporation and AgNP to pathogenic microorganisms. To date, there is only one published article testing this combination (against *Leishmania major*) [304]. Dolat et al. showed that four impulses of 700 V/cm (impulse duration 100 μs) and 2 μg/mL concentration of AgNP reduced viable parasite cell number to 34.6% (electroporation or AgNP itself did not have statistically reliable results in reduction of viable cell number). It can be concluded that the combination of AgNP and electroporation has good potential in the fight against skin pathogenic microorganisms and parasites, but it needs to be investigated in more detail.

After the MICs were determined, the permeability of the microbial membranes to *Geobacillus* spp. 25 and 612 AgNP were investigated. The results revealed that in the case of the exposure to *Geobacillus* sp. 25 AgNP, 34.65% of *S. aureus*, 39.55% of *S. pyogenes*, 82.81% of *P. aeruginosa*, 65.29% of *C. guilliermondii*, and 58.98% of *S. cerevisiae* cells had permeable membranes. In the case of *Geobacillus* sp. 612 AgNP, 33.37%, 23.68%, 57.59%, 61.00%, and 72.93% of cells had permeable membranes, respectively. Vazquez-Munoz et al. showed that after exposure 10 μg/mL concentration of commercially available AgNP for 1 hour to *S. aureus* resulted in approximately 25% of cells with permeable membranes [305]. Lee et al. demonstrated, that commercially available AgNP of 5 and 100 nm diameter, increase cell number with permeable membranes in *C. albicans* (up to approximately 60% after 24 h of exposure) but do not change the cell number

with permeable membranes in *S. cerevisiae* [306]. Zhou et al. also showed that AgNP synthesized using iturin from *B. subtilis* increased cell membrane permeability in *C. albicans* [307]. It should be noted that exposure to *Geobacillus* spp. AgNP for a shorter time (30 min) and with smaller concentration resulted in more cells with permeable membranes, which supports the hypothesis that biologically synthesized AgNP can be successfully used for the biocontrol of microorganisms.

One of the well-known mechanisms of antimicrobial AgNP is the disruption of the respiratory chain and the resulting oxidative stress (that is, ROS generation). It was found, that *Geobacillus* sp. 25 AgNP induce ROS generation in 72.25% of *S. aureus*, 56.54 % of *S. pyogenes*, 26.36% of *P. aeruginosa*, 15.89 % of *S. cerevisiae* cells, and increases up to 8 times in *C. guilliermondii*. *Geobacillus* sp. 612 AgNP induce ROS generation in 80.65%, 46.04 %, 49.03%, 13.11 %, and up to 6 times, respectively (only the results with *S. cerevisiae* had no statistical reliability). Lee et al. demonstrated, that commercially available 5 nm AgNP increased intracellular ROS levels in *C. albicans* (less than two times after the 30 min exposure to AgNP) and did not increase ROS levels in *S. cerevisiae* [306]. Zhou et al. demonstrated, that biosynthesized AgNP increase ROS levels in *C. albicans* cells after 1 h of exposure and after 4 h exposure all cells had elevated levels of ROS [307].

From obtained results the antimicrobial mechanism of *Geobacillus* spp. AgNP may differ among different types of microorganisms. In the case of gram-positive bacteria, the membrane permeability to AgNP is up to 40%, but the cells experience stronger oxidative stress compared to gram-negative bacteria. This can be explained by the fact that gram-positive bacteria have a thick layer of peptidoglycan, which can potentially trap AgNP, but this is sufficient to cause oxidative stress. On the other hand, gram-negative bacteria have a high membrane permeability to *Geobacillus* spp. AgNP (up to 82%), but ROS generation is at a lower level than in gram-positive bacteria. It is also interesting that in ROS studies, when performing flow cytometry measurements, significantly fewer gam-negative bacterial cells were collected after exposure to AgNP than in non-exposed samples (this was not observed in gram-positive bacterial samples), which may indicate ongoing cell lysis. This suggests that the effect on membranes is much stronger in gram-negative membranes than in the case of gram-positive bacteria. Thus, according to the available results, in the case of gram-positive bacteria, the main mechanism of cell death after exposure to *Geobacillus* spp. AgNP is the generation of ROS, while in the case of gram-negative bacteria, it is a direct effect on the cell membranes.

Lipid peroxidation analysis showed that the highest level of lipid peroxidation in *C. guilliermondii* yeast cells was induced after affecting them with *Geobacillus* spp. 25 and 612 AgNP which correlates with the highest levels of ROS generation. In a related investigation, AgNP made using bacterial cells were also used to detect lipid peroxidation in *C. albicans* yeast cells. To assess the degree of lipid peroxidation, the amount of MDA, a crucial indicator of this process, was evaluated. After incubation of *C. albicans* cells for 36 hours, the treated cells' MDA concentration was notably greater than that of the control cells [277]. This result, which is in line with this thesis' investigation, suggests that AgNP oxidized fatty acids in the cell membrane, which increased lipid peroxidation. It is also important to mention that in the study of Elbahnasawy et al. lipid peroxidation was determined after 36 hours of exposure to AgNP, while this thesis aimed to determine whether this process occurs after short-term (15 min) exposure to AgNP. The results show that lipid peroxidation indeed starts to take place in *C. guilliermondii* cells even after a short exposure to AgNP.

To determine whether *Geobacillus* spp. AgNP cause programmed death in yeast cells, it was tested whether caspase activation occurs after exposure to these AgNP. It was found that caspases indeed are activated after exposure to *Geobacillus* spp. AgNP and strain 25 AgNP induce higher rate activation than strain 612 AgNP. In addition, more cells with active caspases are detected in *S. cerevisiae* than in *C. guilliermondii*. Whether or not AgNP induce programmed cell death through caspase activation in yeast is still unknown. Only a few studies have been conducted. Hwang et al. showed that chemically obtained AgNP also activate caspases in *C. albicans* [308]. Prateeksha et al. also demonstrated that biosilver nanoclusters activate caspase in *C. albicans* [309]. Thus, it can be assumed that this thesis was the first to show that caspase activation occurs in *S. cerevisiae* and *C. guilliermondii* yeasts after exposure to AgNP, thus allowing the conclusion that programmed cell death occurs.

Although caspases are activated in yeast cells of both species of yeasts, the antifungal effects in pathogenic *C. guilliermondii* and model organism *S. cerevisiae* is different. Both yeast cell membranes are highly permeable to these AgNP, but a statistically significant increase in ROS generation occurs only in *C. guilliermondii*. There are no data in the literature on ROS levels in *C. guilliermondii* yeasts after exposure to AgNP and little data on this process in *S. cerevisiae* yeasts. In the case of *S. cerevisiae*, the data obtained are different. Lee et al. showed, as in this thesis, that ROS generation does not occur in *S. cerevisiae* but does in *C. albicans* [306]. On the other hand, Babele et al. showed that ROS generation intensifies when *S. cerevisiae* cells are exposed to increasing concentrations of AgNP [310]. Thus, according to the

available data, it can be stated that the antifungal mechanism of AgNP differs between different yeasts and possibly after exposure to differently obtained AgNP, and caspases may be activated depending or not on ROS generation.

Studies with human keratinocytes have shown that *Geobacillus* sp. strain 612 AgNP do not have a strong cytotoxic effect on these cells at the concentration that affects yeast *C. guilliermondii* (5 μg/mL). Moreover, this concentration does not statistically significantly interfere with the proliferation and migration of keratinocytes after wounding. However, it should be noted that higher concentrations have a negative effect on human keratinocyte cells, so it is necessary to carry out long-term exposure studies due to the possible accumulation of AgNP.

However, according to research conducted by other scientific groups, it can be assumed that *Geobacillus* sp. 612 AgNP have better antimicrobial properties compared to other studies, but also have a greater effect on human keratinocytes. Galandakova et al. concluded that for wound healing it is safe to use up to 25 μg/mL of AgNP synthesized by chemical method. Their results showed that AgNP did not have a significant effect on keratinocyte viability with AgNP concentrations up to 25 μg/mL after 24 h of exposure [311]. Salesa et al. demonstrated that concentrations of commercially available AgNP did not have a statistically reliable cytotoxic effect on human keratinocytes with up to 40 μg/mL concentrations after 24 h exposure and concentrations up to 20 μg/mL did not affect the proliferation of these cells [312]. Nonetheless, it is necessary to emphasize that other keratinocyte lines were used in the studies, which may affect the obtained results. As mentioned earlier, more detailed long-term exposure studies are needed to make more definite conclusions about whether *Geobacillus* sp. strain 612 AgNP are safe to use.

AgNP obtained using thermophilic *Geobacillus* spp. bacteria-induced synthesis are an excellent antimicrobial tool that can control pathogenic microbiota. They exhibit a complex action against both bacteria and yeast, affecting their membranes, increasing ROS generation, and causing programmed cell death in yeast cells. Moreover, the combination of electroporation and AgNP may shorten the exposure time, which would likely reduce the toxicity to human cells as well. Studies with human keratinocyte cells have shown that these AgNP are not harmful at low concentrations, which shows good potential for their application in microbiota biocontrol.

5. CONCLUSIONS

1. Thermophilic *Geobacillus* spp. bacteria are suitable for the production of stable AgNP exhibiting antimicrobial activity. Most of the AgNP are less than 100 nm in diameter and their zeta potentials are ranging from −25 to −31 mV;
2. Silver nanoparticles obtained by using *Geobacillus* spp. have antimicrobial properties against pathogenic skin bacteria and yeast. They cause damage to cell membranes, increase ROS levels, cause lipid peroxidation and activate caspases;
3. The electroporation enhances the antimicrobial effects of AgNP against skin pathogenic microorganisms. By applying both, electroporation and AgNP, the exposure time can be shortened;
4. Death mechanisms of *Geobacillus* spp. AgNP differ among different microorganisms. The main mechanism in gram-positive bacteria is elevated ROS generation, in gram-negative bacteria the direct damage to cell membranes. In yeasts these AgNP induce caspase-related programmed cell death;
5. The 5 μg/mL concentration of *Geobacillus* sp. 612 AgNP, which is effective against pathogenic yeasts, does not have a cytotoxic effect on human keratinocyte cells and does not reduce keratinocyte migration.

6. LITERATURE

1. Sanford, J.A.; Gallo, R.L. Functions of the Skin Microbiota in Health and Disease. *Semin Immunol* 2013, *25*, 370–377, doi:10.1016/j.smim.2013.09.005.
2. Byrd, A.L.; Belkaid, Y.; Segre, J.A. The Human Skin Microbiome. *Nat Rev Microbiol* 2018, *16*, 143–155, doi:10.1038/nrmicro.2017.157.
3. Lamoth, F.; Lockhart, S.R.; Berkow, E.L.; Calandra, T. Changes in the Epidemiological Landscape of Invasive Candidiasis. *J Antimicrob Chemother* 2018, *73*, i4–i13, doi:10.1093/jac/dkx444.
4. Statistics | Invasive Candidiasis | Candidiasis | Types of Diseases | Fungal Diseases | CDC Available online: https://www.cdc.gov/fungal/diseases/candidiasis/invasive/statistics.html (accessed on 5 March 2024).
5. Marak, M.B.; Dhanashree, B. Antifungal Susceptibility and Biofilm Production of *Candida* spp. Isolated from Clinical Samples. *Int J Microbiol* 2018, 1–5, doi:10.1155/2018/7495218.
6. Pfaller, M.A.; Diekema, D.J. Rare and Emerging Opportunistic Fungal Pathogens: Concern for Resistance beyond *Candida albicans* and *Aspergillus fumigatus*. *J Clin Microbiol* 2004, *42*, 4419–4431, doi:10.1128/JCM.42.10.4419-4431.2004.
7. Marcos-Zambrano, L.J.; Puig-Asensio, M.; Pérez-García, F.; Escribano, P.; Sánchez-Carrillo, C.; Zaragoza, O.; Padilla, B.; Cuenca-Estrella, M.; Almirante, B.; Martín-Gómez, M.T.; et al. *Candida guilliermondii* Complex Is Characterized by High Antifungal Resistance but Low Mortality in 22 Cases of Candidemia. *Antimicrob Agents Chemother* 2017, *61*, e00099-17, doi:10.1128/AAC.00099-17.
8. Kapoor, G.; Saigal, S.; Elongavan, A. Action and Resistance Mechanisms of Antibiotics: A Guide for Clinicians. *J Anaesthesiol Clin Pharmacol* 2017, *33*, 300, doi:10.4103/joacp.JOACP_349_15.
9. Grundmann, H.; Aires-de-Sousa, M.; Boyce, J.; Tiemersma, E. Emergence and Resurgence of Meticillin-Resistant *Staphylococcus aureus* as a Public-Health Threat. *The Lancet* 2006, *368*, 874–885, doi:10.1016/S0140-6736(06)68853-3.
10. Iravani, S.; Korbekandi, H.; Mirmohammadi, S.V.; Zolfaghari, B. Synthesis of Silver Nanoparticles: Chemical, Physical and Biological Methods. *Res Pharm Sci* 2014; Vol. 9, pp. 385–406.
11. Mikhailova, E.O. Silver Nanoparticles: Mechanism of Action and Probable Bio-Application. *JFB* 2020, *11*, 84, doi:10.3390/jfb11040084.
12. Wei, L.; Lu, J.; Xu, H.; Patel, A.; Chen, Z.-S.; Chen, G. Silver Nanoparticles: Synthesis, Properties, and Therapeutic Applications. *Drug Discov Today* 2015, *20*, 595–601, doi:10.1016/j.drudis.2014.11.014.

13. Noga, M.; Milan, J.; Frydrych, A.; Jurowski, K. Toxicological Aspects, Safety Assessment, and Green Toxicology of Silver Nanoparticles (AgNPs)—Critical Review: State of the Art. *IJMS* 2023, *24*, 5133, doi:10.3390/ijms24065133.
14. Tak, Y.K.; Pal, S.; Naoghare, P.K.; Rangasamy, S.; Song, J.M. Shape-Dependent Skin Penetration of Silver Nanoparticles: Does It Really Matter? *Sci Rep* 2015, *5*, 16908, doi:10.1038/srep16908.
15. Zhang, J.; Wang, F.; Yalamarty, S.S.K.; Filipczak, N.; Jin, Y.; Li, X. Nano Silver-Induced Toxicity and Associated Mechanisms. *IJN* 2022, *17*, 1851–1864, doi:10.2147/IJN.S355131.
16. Fayaz, A.M.; Girilal, M.; Rahman, M.; Venkatesan, R.; Kalaichelvan, P.T. Biosynthesis of Silver and Gold Nanoparticles Using Thermophilic Bacterium *Geobacillus stearothermophilus*. *Process Biochem* 2011, *46*, 1958–1962, doi:10.1016/j.procbio.2011.07.003.
17. Marples, M.J. Life on the Human Skin. *Sci Am* 1969, *220*, 108–115, doi:10.1038/scientificamerican0169-108.
18. Schauber, J.; Gallo, R.L. Antimicrobial Peptides and the Skin Immune Defense System. *Allergy Clin Immunol* 2009, *124*, R13–R18, doi:10.1016/j.jaci.2009.07.014.
19. Grice, E.A.; Segre, J.A. The Skin Microbiome. *Nat Rev Microbiol* 2011, *9*, 244–253, doi:10.1038/nrmicro2537.
20. Segre, J.A. Epidermal Barrier Formation and Recovery in Skin Disorders. *J Clin Investig* 2006, *116*, 1150–1158, doi:10.1172/JCI28521.
21. Rochat, A.; Kobayashi, K.; Barrandon, Y. Location of Stem Cells of Human Hair Follicles by Clonal Analysis. *Cell* 1994, *76*, 1063–1073, doi:10.1016/0092-8674(94)90383-2.
22. Frohm, M.; Agerberth, B.; Ahangari, G.; Ståhle-Bäckdahl, M.; Lidén, S.; Wigzell, H.; Gudmundsson, G.H. The Expression of the Gene Coding for the Antibacterial Peptide LL-37 Is Induced in Human Keratinocytes during Inflammatory Disorders. *J Biol Chem* 1997, *272*, 15258–15263, doi:10.1074/jbc.272.24.15258.
23. Harder, J.; Schröder, J.M. RNase 7, a Novel Innate Immune Defense Antimicrobial Protein of Healthy Human Skin. *J Biol Chem* 2002, *277*, 46779–46784, doi:10.1074/jbc.M207587200.
24. Gallo, R.L.; Hooper, L.V. Epithelial Antimicrobial Defence of the Skin and Intestine. *Nat Rev Immunol* 2012, *12*, 503–516, doi:10.1038/nri3228.
25. Dominguez-Bello, M.G.; Costello, E.K.; Contreras, M.; Magris, M.; Hidalgo, G.; Fierer, N.; Knight, R. Delivery Mode Shapes the Acquisition and Structure of the Initial Microbiota across Multiple Body Habitats in Newborns. *Proc Natl Acad Sci USA*, 2010, *107*, 11971–11975, doi:10.1073/pnas.1002601107.

26. Laubereau, B. Caesarean Section and Gastrointestinal Symptoms, Atopic Dermatitis, and Sensitisation during the First Year of Life. *Arc Dis Child* 2004, *89*, 993–997, doi:10.1136/adc.2003.043265.
27. Oh, J.; Byrd, A.L.; Park, M.; Kong, H.H.; Segre, J.A. Temporal Stability of the Human Skin Microbiome. *Cell* 2016, *165*, 854–866, doi:10.1016/j.cell.2016.04.008.
28. Jo, J.H.; Deming, C.; Kennedy, E.A.; Conlan, S.; Polley, E.C.; Ng, W.I.; Segre, J.A.; Kong, H.H. Diverse Human Skin Fungal Communities in Children Converge in Adulthood. *J Investig Dermatol* 2016, *136*, 2356–2363, doi:10.1016/j.jid.2016.05.130.
29. Boxberger, M.; Cenizo, V.; Cassir, N.; La Scola, B. Challenges in Exploring and Manipulating the Human Skin Microbiome. *Microbiome* 2021, *9*, 125, doi:10.1186/s40168-021-01062-5.
30. Özcelik, S.; Kulac, I.; Yazici, M.; Ocal, E. Distribution of Childhood Skin Diseases According to Age and Gender, a Single Institution Experience. *Turk Pediatri Ars* 2018, *53*, 105–112, doi:10.5152/TurkPediatriArs.2018.6431.
31. Grice, E.A.; Kong, H.H.; Conlan, S.; Deming, C.B.; Davis, J.; Young, A.C.; NISC Comparative Sequencing Program; Bouffard, G.G.; Blakesley, R.W.; Murray, P.R.; et al. Topographical and Temporal Diversity of the Human Skin Microbiome. *Science* 2009, *324*, 1190–1192, doi:10.1126/science.1171700.
32. Egert, M.; Simmering, R.; Riedel, C. The Association of the Skin Microbiota With Health, Immunity, and Disease. *Clin Pharmacol Ther*, 2017, *102*, 62–69, doi:10.1002/cpt.698.
33. Nakatsuji, T.; Chiang, H.-I.; Jiang, S.B.; Nagarajan, H.; Zengler, K.; Gallo, R.L. The Microbiome Extends to Subepidermal Compartments of Normal Skin. *Nat Commun* 2013, *4*, 1431, doi:10.1038/ncomms2441.
34. Belkaid, Y.; Segre, J.A. Dialogue between Skin Microbiota and Immunity. *Science* 2014, *346*, 954–959, doi:10.1126/science.1260144.
35. Costello, E.K.; Lauber, C.L.; Hamady, M.; Fierer, N.; Gordon, J.I.; Knight, R. Bacterial Community Variation in Human Body Habitats Across Space and Time. *Science* 2009, *326*, 1694–1697, doi:10.1126/science.1177486.
36. Findley, K.; Oh, J.; Yang, J.; Conlan, S.; Deming, C.; Meyer, J.A.; Schoenfeld, D.; Nomicos, E.; Park, M.; et al. Topographic Diversity of Fungal and Bacterial Communities in Human Skin. *Nature* 2013, *498*, 367–370, doi:10.1038/nature12171.
37. Fierer, N.; Hamady, M.; Lauber, C.L.; Knight, R. The Influence of Sex, Handedness, and Washing on the Diversity of Hand Surface Bacteria. *Proc Natl Acad Sci USA*, 2008, *105*, 17994–17999, doi:10.1073/pnas.0807920105.
38. Egert, M.; Simmering, R. The Microbiota of the Human Skin. In *Microbiota of the Human Body*; Schwiertz, A., Ed.; Advances in

Experimental Medicine and Biology; Springer International Publishing: Cham, 2016; Vol. 902, pp. 61–81 ISBN 978-3-319-31246-0.
39. Belkaid, Y.; Hand, T.W. Role of the Microbiota in Immunity and Inflammation. *Cell* 2014, *157*, 121–141, doi:10.1016/j.cell.2014.03.011.
40. Scharschmidt, T.C.; Fischbach, M.A. What Lives on Our Skin: Ecology, Genomics and Therapeutic Opportunities of the Skin Microbiome. *Drug Discov Today Dis Mech* 2013, *10*, e83–e89, doi:10.1016/j.ddmec.2012.12.003.
41. Holland, C.; Mak, T.N.; Zimny-Arndt, U.; Schmid, M.; Meyer, T.F.; Jungblut, P.R.; Brüggemann, H. Proteomic Identification of Secreted Proteins of *Propionibacterium acnes*. *BMC Microbiol* 2010, *10*, 230, doi:10.1186/1471-2180-10-230.
42. Brüggemann, H.; Henne, A.; Hoster, F.; Liesegang, H.; Wiezer, A.; Strittmatter, A.; Hujer, S.; Dürre, P.; Gottschalk, G. The Complete Genome Sequence of *Propionibacterium acnes*, a Commensal of Human Skin. *Science* 2004, *305*, 671–673, doi:10.1126/science.1100330.
43. Wu, G.; Zhao, H.; Li, C.; Rajapakse, M.P.; Wong, W.C.; Xu, J.; Saunders, C.W.; Reeder, N.L.; Reilman, R.A.; Scheynius, A.; et al. Genus-Wide Comparative Genomics of *Malassezia* Delineates Its Phylogeny, Physiology, and Niche Adaptation on Human Skin. *PLoS Genet* 2015, *11*, e1005614, doi:10.1371/journal.pgen.1005614.
44. Wang, X.; Zhou, H.; Chen, D.; Du, P.; Lan, R.; Qiu, X.; Hou, X.; Liu, Z.; Sun, L.; Xu, S.; et al. Whole-Genome Sequencing Reveals a Prolonged and Persistent Intrahospital Transmission of Corynebacterium Striatum, an Emerging Multidrug-Resistant Pathogen. *J Clin Microbiol* 2019, *57*, e00683-19, doi:10.1128/JCM.00683-19.
45. Kluytmans, J. Nasal Carriage of *Staphylococcus aureus*: Epidemiology, Underlying Mechanisms, and Associated Risks. *Clin Microbiol Rev* 1997, *10*, doi: 10.1128/CMR.10.3.50.
46. Prescott, S.L.; Larcombe, D.L.; Logan, A.C.; West, C.; Burks, W.; Caraballo, L.; Levin, M.; Etten, E.V.; Horwitz, P.; Kozyrskyj, A.; et al. The Skin Microbiome: Impact of Modern Environments on Skin Ecology, Barrier Integrity, and Systemic Immune Programming. *World Allergy Organ J* 2017, *10*, 29, doi:10.1186/s40413-017-0160-5.
47. Giudice, P. Skin Infections Caused by *Staphylococcus aureus*. *Acta Derm Venerol* 2020, *100*, adv00110-215, doi:10.2340/00015555-3466.
48. Cheung, G.Y.C.; Bae, J.S.; Otto, M. Pathogenicity and Virulence of *Staphylococcus aureus*. *Virulence* 2021, *12*, 547–569, doi:10.1080/21505594.2021.1878688.

49. Otto, M. Community-Associated MRSA: What Makes Them Special? *Int J Med Microbiol* 2013, *303*, 324–330, doi:10.1016/j.ijmm.2013.02.007.
50. Fiedler, T.; Köller, T.; Kreikemeyer, B. *Streptococcus pyogenes* Biofilms-formation, Biology, and Clinical Relevance. *Front Cell Infect Microbiol* 2015, *5*, doi:10.3389/fcimb.2015.00015.
51. Cunningham, M.W. Pathogenesis of Group A *Streptococcal* Infections. *Clin Microbiol Rev* 2000, *13*, doi:10.1128/CMR.13.3.470.
52. Tan, L.K.K.; Eccersley, L.R.J.; Sriskandan, S. Current Views of Haemolytic *Streptococcal* Pathogenesis. *Curr Opin Infect Dis* 2014, *27*, 155–164, doi:10.1097/QCO.0000000000000047.
53. Passàli, D.; Lauriello, M.; Passàli, G.C.; Passàli, F.M.; Bellussi, L. Group A *Streptococcus* and Its Antibiotic Resistance. *Acta Otorhinolaryngol Ital* 2007, *27*, 27–32.
54. Yu, D.; Zheng, Y.; Yang, Y. Is There Emergence of β-Lactam Antibiotic-Resistant *Streptococcus pyogenes* in China? *IDR* 2020, *13*, 2323–2327, doi:10.2147/IDR.S261975.
55. Vannice, K.S.; Ricaldi, J.; Nanduri, S.; Fang, F.C.; Lynch, J.B.; Bryson-Cahn, C.; Wright, T.; Duchin, J.; Kay, M.; Chochua, S.; et al. *Streptococcus pyogenes* Pbp2x Mutation Confers Reduced Susceptibility to β-Lactam Antibiotics. *Clin Infect Dis* 2020, *71*, 201–204, doi:10.1093/cid/ciz1000.
56. Imöhl, M.; Van Der Linden, M. Antimicrobial Susceptibility of Invasive *Streptococcus pyogenes* Isolates in Germany during 2003-2013. *PLoS ONE* 2015, *10*, e0137313, doi:10.1371/journal.pone.0137313.
57. Thi, M.T.T.; Wibowo, D.; Rehm, B.H.A. *Pseudomonas aeruginosa* Biofilms. *IJMS* 2020, *21*, 8671, doi:10.3390/ijms21228671.
58. Sadikot, R.T.; Blackwell, T.S.; Christman, J.W.; Prince, A.S. Pathogen–Host Interactions in *Pseudomonas aeruginosa* Pneumonia. *Am J Respir Crit Care Med* 2005, *171*, 1209–1223, doi:10.1164/rccm.200408-1044SO.
59. Pachori, P.; Gothalwal, R.; Gandhi, P. Emergence of Antibiotic Resistance *Pseudomonas aeruginosa* in Intensive Care Unit; a Critical Review. *Genes Dis* 2019, *6*, 109–119, doi:10.1016/j.gendis.2019.04.001.
60. Yamin, D.H.; Husin, A.; Harun, A. Risk Factors of Candida Parapsilosis Catheter-Related Bloodstream Infection. *Front Public Health* 2021, *9*, 631865, doi:10.3389/fpubh.2021.631865.
61. Rasoulpoor, S.; Shohaimi, S.; Salari, N.; Vaisi-Raygani, A.; Rasoulpoor, S.; Shabani, S.; Jalali, R.; Mohammadi, M. *Candida albicans* Skin Infection in Patients with Type 2 Diabetes: A Systematic Review and Meta-Analysis. *J Diabetes Metab Disord* 2021, *20*, 665–672, doi:10.1007/s40200-021-00797-0.

62. Thomas-Rüddel, D.O.; Schlattmann, P.; Pletz, M.; Kurzai, O.; Bloos, F. Risk Factors for Invasive *Candida* Infection in Critically Ill Patients. *Chest* 2022, *161*, 345–355, doi:10.1016/j.chest.2021.08.081.
63. Wisplinghoff, H.; Ebbers, J.; Geurtz, L.; Stefanik, D.; Major, Y.; Edmond, M.B.; Wenzel, R.P.; Seifert, H. Nosocomial Bloodstream Infections Due to *Candida* spp. in the USA: Species Distribution, Clinical Features and Antifungal Susceptibilities. *Int J Antimicrob Agents* 2014, *43*, 78–81, doi:10.1016/j.ijantimicag.2013.09.005.
64. Sudbery, P.E. Growth of *Candida albicans* Hyphae. *Nat Rev Microbiol* 2011, *9*, 737–748, doi:10.1038/nrmicro2636.
65. Wakade, R.S.; Krysan, D.J. The Cbk1-Ace2 Axis Guides *Candida albicans* from Yeast to Hyphae and Back Again. *Curr Genet* 2021, *67*, 461–469, doi:10.1007/s00294-020-01152-1.
66. Sudbery, P.E. The Germ Tubes of Candida Albicans Hyphae and Pseudohyphae Show Different Patterns of Septin Ring Localization: Septin Ring Localization in *C. albicans* Germ Tubes. *Mol Microbiol* 2001, *41*, 19–31, doi:10.1046/j.1365-2958.2001.02459.x.
67. Merson-Davies, L.A.; Odds, F.C. A Morphology Index for Characterization of Cell Shape in *Candida albicans*. *J Gen Microbiol* 1989, *135*, 3143–3152, doi:10.1099/00221287-135-11-3143.
68. Dalle, F.; Wächtler, B.; L'Ollivier, C.; Holland, G.; Bannert, N.; Wilson, D.; Labruère, C.; Bonnin, A.; Hube, B. Cellular Interactions of *Candida albicans* with Human Oral Epithelial Cells and Enterocytes. *Cell Microbiol* 2010, *12*, 248–271, doi:10.1111/j.1462-5822.2009.01394.x.
69. Uwamahoro, N.; Verma-Gaur, J.; Shen, H.-H.; Qu, Y.; Lewis, R.; Lu, J.; Bambery, K.; Masters, S.L.; Vince, J.E.; Naderer, T.; et al. The Pathogen *Candida albicans* Hijacks Pyroptosis for Escape from Macrophages. *mBio* 2014, *5*, e00003-14, doi:10.1128/mBio.00003-14.
70. Boland, J.M.; Chung, H.H.; Robberts, F.J.L.; Wilson, W.R.; Steckelberg, J.M.; Baddour, L.M.; Miller, D.V. Fungal Prosthetic Valve Endocarditis: Mayo Clinic Experience with a Clinicopathological Analysis: Fungal Endocarditis. *Mycoses* 2011, *54*, 354–360, doi:10.1111/j.1439-0507.2010.01884.x.
71. Vitális, E.; Nagy, F.; Tóth, Z.; Forgács, L.; Bozó, A.; Kardos, G.; Majoros, L.; Kovács, R. *Candida* Biofilm Production Is Associated with Higher Mortality in Patients with Candidaemia. *Mycoses* 2020, *63*, 352–360, doi:10.1111/myc.13049.
72. Buffo, J.; Herman, M.A.; Soll, D.R. A Characterization of pH-Regulated Dimorphism in Candida Albicans. *Mycopathologia* 1984, *85*, 21–30, doi:10.1007/BF00436698.
73. Oh, S.H.; Schliep, K.; Isenhower, A.; Rodriguez-Bobadilla, R.; Vuong, V.M.; Fields, C.J.; Hernandez, A.G.; Hoyer, L.L. Using Genomics to Shape the Definition of the Agglutinin-Like Sequence (ALS) Family

in the *Saccharomycetales*. *Front Cell Infect Microbiol* 2021, *11*, 794529, doi:10.3389/fcimb.2021.794529.
74. Green, C.B.; Cheng, G.; Chandra, J.; Mukherjee, P.; Ghannoum, M.A.; Hoyer, L.L. RT-PCR Detection of *Candida albicans* ALS Gene Expression in the Reconstituted Human Epithelium (RHE) Model of Oral Candidiasis and in Model Biofilms. *Microbiology* 2004, *150*, 267–275, doi:10.1099/mic.0.26699-0.
75. Klotz, S.A.; Gaur, N.K.; De Armond, R.; Sheppard, D.; Khardori, N.; Edwards, J.E.; Lipke, P.N.; El-Azizi, M. *Candida albicans* Als Proteins Mediate Aggregation with Bacteria and Yeasts. *Med Mycol* 2007, *45*, 363–370, doi:10.1080/13693780701299333.
76. Nobile, C.J.; Schneider, H.A.; Nett, J.E.; Sheppard, D.C.; Filler, S.G.; Andes, D.R.; Mitchell, A.P. Complementary Adhesin Function in *C. albicans* Biofilm Formation. *Curr Biol* 2008, *18*, 1017–1024, doi:10.1016/j.cub.2008.06.034.
77. Green, C.B.; Zhao, X.; Hoyer, L.L. Use of Green Fluorescent Protein and Reverse Transcription-PCR To Monitor *Candida albicans* Agglutinin-Like Sequence Gene Expression in a Murine Model of Disseminated Candidiasis. *Infect Immun* 2005, *73*, 1852–1855, doi:10.1128/IAI.73.3.1852-1855.2005.
78. Bois, M.; Singh, S.; Samlalsingh, A.; Lipke, P.N.; Garcia, M.C. Does *Candida albicans* Als5p Amyloid Play a Role in Commensalism in *Caenorhabditis elegans*? *Eukaryot Cell* 2013, *12*, 703–711, doi:10.1128/EC.00020-13.
79. Behrens, N.E.; Lipke, P.N.; Pilling, D.; Gomer, R.H.; Klotz, S.A. Serum Amyloid P Component Binds Fungal Surface Amyloid and Decreases Human Macrophage Phagocytosis and Secretion of Inflammatory Cytokines. *mBio* 2019, *10*, e00218-19, doi:10.1128/mBio.00218-19.
80. Mayer, F.L.; Wilson, D.; Hube, B. *Candida albicans* Pathogenicity Mechanisms. *Virulence* 2013, *4*, 119–128, doi:10.4161/viru.22913.
81. Deorukhkar, S.C.; Saini, S.; Mathew, S. Virulence Factors Contributing to Pathogenicity of *Candida tropicalis* and Its Antifungal Susceptibility Profile. *Int J Microbiol* 2014, *2014*, 1–6, doi:10.1155/2014/456878.
82. Ghannoum, M.A. Potential Role of Phospholipases in Virulence and Fungal Pathogenesis. *Clin Microbiol Rev* 2000, *13*, 122–43, doi: 10.1128/CMR.13.1.122.
83. Mogavero, S.; Höfs, S.; Lauer, A.N.; Müller, R.; Brunke, S.; Allert, S.; Gerwien, F.; Groth, S.; Dolk, E.; Wilson, D.; et al. Candidalysin Is the Hemolytic Factor of *Candida albicans*. *Toxins* 2022, *14*, 874, doi:10.3390/toxins14120874.
84. Mohammed, B.L.; Jafar, N.B.; Mahammad, S.H. Estimation of Esterase Activity, Adhesion Ability, in Various *Candida* Species.; Athens, Greece, 2019; p. 020063, doi:10.1063/1.5138549.

85. Gácser, A.; Trofa, D.; Schäfer, W.; Nosanchuk, J.D. Targeted Gene Deletion in *Candida parapsilosis* Demonstrates the Role of Secreted Lipase in Virulence. *J Clin Invest* 2007, *117*, 3049–3058, doi:10.1172/JCI32294.
86. Ghannoum, M.A.; Hajjeh, R.A.; Scher, R.; Konnikov, N.; Gupta, A.K.; Summerbell, R.; Sullivan, S.; Daniel, R.; Krusinski, P.; Fleckman, P.; et al. A Large-Scale North American Study of Fungal Isolates from Nails: The Frequency of Onychomycosis, Fungal Distribution, and Antifungal Susceptibility Patterns. *J Am Acad Dermatol* 2000, *43*, 641–648, doi:10.1067/mjd.2000.107754.
87. Tietz, H.J.; Czaika, V.; Sterry, W. Case Report. Osteomyelitis Caused by High Resistant *Candida guilliermondii*. *Mycoses* 1999, *42*, 577–580, doi:10.1046/j.1439-0507.1999.00497.x.
88. Jung, D.S.; Farmakiotis, D.; Jiang, Y.; Tarrand, J.J.; Kontoyiannis, D.P. Uncommon *Candida* Species Fungemia among Cancer Patients, Houston, Texas, USA. *Emerg Infect Dis* 2015, *21*, doi:10.3201/eid2111.150404.
89. Xiao, Z.; Wang, Q.; Zhu, F.; An, Y. Epidemiology, Species Distribution, Antifungal Susceptibility and Mortality Risk Factors of Candidemia among Critically Ill Patients: A Retrospective Study from 2011 to 2017 in a Teaching Hospital in China. *Antimicrob Resist Infect Control* 2019, *8*, 89, doi:10.1186/s13756-019-0534-2.
90. Tseng, T.Y.; Chen, T.C.; Ho, C.M.; Lin, P.C.; Chou, C.H.; Tsai, C.T.; Wang, J.H.; Chi, C.Y.; Ho, M.W. Clinical Features, Antifungal Susceptibility, and Outcome of *Candida guilliermondii* Fungemia: An Experience in a Tertiary Hospital in Mid-Taiwan. *J Microbiol Immunol Infect* 2018, *51*, 552–558, doi:10.1016/j.jmii.2016.08.015.
91. Pfaller, M.A.; Diekema, D.J.; Mendez, M.; Kibbler, C.; Erzsebet, P.; Chang, S.C.; Gibbs, D.L.; Newell, V.A.; the Global Antifungal Surveillance Group *Candida guilliermondii*, an Opportunistic Fungal Pathogen with Decreased Susceptibility to Fluconazole: Geographic and Temporal Trends from the ARTEMIS DISK Antifungal Surveillance Program. *J Clin Microbiol* 2006, *44*, 3551–3556, doi:10.1128/JCM.00865-06.
92. Savini, V.; Catavitello, C.; Onofrillo, D.; Masciarelli, G.; Astolfi, D.; Balbinot, A.; Febbo, F.; D'Amario, C.; D'Antonio, D. What Do We Know about *Candida guilliermondii*? A Voyage throughout Past and Current Literature about This Emerging Yeast. *Mycoses* 2011, *54*, 434–441, doi:10.1111/j.1439-0507.2010.01960.x.
93. Van Der Waaij, D.; Berghuis-de Vries, J.M.; Lekkerkerk-van Der Wees, J.E.C. Colonization Resistance of the Digestive Tract in Conventional and Antibiotic-Treated Mice. *J Hyg* 1971, *69*, 405–411, doi:10.1017/S0022172400021653.

94. Eiff, C.V.; Peters, G. Nasal Carriage as a Source of *Staphylococcus aureus* Bacteremia. *N Engl J Med* 2001, *344*, 11–6, doi: 10.1056/NEJM200101043440102.
95. David, M.Z.; Daum, R.S. Community-Associated Methicillin-Resistant *Staphylococcus aureus*: Epidemiology and Clinical Consequences of an Emerging Epidemic. *Clin Microbiol Rev* 2010, *23*, 616–687, doi:10.1128/CMR.00081-09.
96. Clegg, J.; Soldaini, E.; McLoughlin, R.M.; Rittenhouse, S.; Bagnoli, F.; Phogat, S. *Staphylococcus aureus* Vaccine Research and Development: The Past, Present and Future, Including Novel Therapeutic Strategies. *Front Immunol* 2021, *12*, 705360, doi:10.3389/fimmu.2021.705360.
97. Iwase, T.; Uehara, Y.; Shinji, H.; Tajima, A.; Seo, H.; Takada, K.; Agata, T.; Mizunoe, Y. Staphylococcus Epidermidis Esp Inhibits *Staphylococcus aureus* Biofilm Formation and Nasal Colonization. *Nature* 2010, *465*, 346–349, doi:10.1038/nature09074.
98. Sugimoto, S.; Iwamoto, T.; Takada, K.; Okuda, K.; Tajima, A.; Iwase, T.; Mizunoe, Y. *Staphylococcus epidermidis* Esp Degrades Specific Proteins Associated with *Staphylococcus aureus* Biofilm Formation and Host-Pathogen Interaction. *J Bacteriol* 2013, *195*, 1645–1655, doi:10.1128/JB.01672-12.
99. Lai, Y.; Cogen, A.L.; Radek, K.A.; Park, H.J.; MacLeod, D.T.; Leichtle, A.; Ryan, A.F.; Di Nardo, A.; Gallo, R.L. Activation of TLR2 by a Small Molecule Produced by *Staphylococcus epidermidis* Increases Antimicrobial Defense against Bacterial Skin Infections. *J Investig Dermatol* 2010, *130*, 2211–2221, doi:10.1038/jid.2010.123.
100. Zipperer, A.; Konnerth, M.C.; Laux, C.; Berscheid, A.; Janek, D.; Weidenmaier, C.; Burian, M.; Schilling, N.A.; Slavetinsky, C.; Marschal, M.; et al. Human Commensals Producing a Novel Antibiotic Impair Pathogen Colonization. *Nature* 2016, *535*, 511–516, doi:10.1038/nature18634.
101. Nakatsuji, T.; Chen, T.H.; Narala, S.; Chun, K.A.; Two, A.M.; Yun, T.; Shafiq, F.; Kotol, P.F.; Bouslimani, A.; Melnik, A.V.; et al. Antimicrobials from Human Skin Commensal Bacteria Protect against *Staphylococcus aureus* and Are Deficient in Atopic Dermatitis. *Sci Transl Med* 2017, *9*, eaah4680, doi:10.1126/scitranslmed.aah4680.
102. Cogen, A.L.; Yamasaki, K.; Sanchez, K.M.; Dorschner, R.A.; Lai, Y.; MacLeod, D.T.; Torpey, J.W.; Otto, M.; Nizet, V.; Kim, J.E.; et al. Selective Antimicrobial Action Is Provided by Phenol-Soluble Modulins Derived from Staphylococcus epidermidis, a Normal Resident of the Skin. *J Investig Dermatol* 2010, *130*, 192–200, doi:10.1038/jid.2009.243.
103. Wollenberg, M.S.; Claesen, J.; Escapa, I.F.; Aldridge, K.L.; Fischbach, M.A.; Lemon, K.P. *Propionibacterium* -Produced Coproporphyrin III

Induces *Staphylococcus aureus* Aggregation and Biofilm Formation. *mBio* 2014, *5*, e01286-14, doi:10.1128/mBio.01286-14.
104. Ramsey, M.M.; Freire, M.O.; Gabrilska, R.A.; Rumbaugh, K.P.; Lemon, K.P. Staphylococcus aureus Shifts toward Commensalism in Response to *Corynebacterium* Species. *Front Microbiol* 2016, *7*, doi:10.3389/fmicb.2016.01230.
105. Davies, J.; Davies, D. Origins and Evolution of Antibiotic Resistance. *Microbiol Mol Biol Rev* 2010, *74*, 417–433, doi:10.1128/MMBR.00016-10.
106. Varela, M.F.; Stephen, J.; Lekshmi, M.; Ojha, M.; Wenzel, N.; Sanford, L.M.; Hernandez, A.J.; Parvathi, A.; Kumar, S.H. Bacterial Resistance to Antimicrobial Agents. *Antibiotics* 2021, *10*, 593, doi:10.3390/antibiotics10050593.
107. Reygaert, W.C. An Overview of the Antimicrobial Resistance Mechanisms of Bacteria. *AIMS Microbiol* 2018, *4*, 482–501, doi:10.3934/microbiol.2018.3.482.
108. Chancey, S.T.; Zähner, D.; Stephens, D.S. Acquired Inducible Antimicrobial Resistance in Gram-Positive Bacteria. *Future Microbiol* 2012, *7*, 959–978, doi:10.2217/fmb.12.63.
109. Van Daele, R.; Spriet, I.; Wauters, J.; Maertens, J.; Mercier, T.; Van Hecke, S.; Brüggemann, R. Antifungal Drugs: What Brings the Future? *Med Mycol* 2019, *57*, S328–S343, doi:10.1093/mmy/myz012.
110. Taei, M.; Chadeganipour, M.; Mohammadi, R. An Alarming Rise of Non-*albicans Candida* Species and Uncommon Yeasts in the Clinical Samples; a Combination of Various Molecular Techniques for Identification of Etiologic Agents. *BMC Res Notes* 2019, *12*, 779, doi:10.1186/s13104-019-4811-1.
111. Girmenia, C.; Pizzarelli, G.; Cristini, F.; Barchiesi, F.; Spreghini, E.; Scalise, G.; Martino, P. *Candida guilliermondii* Fungemia in Patients with Hematologic Malignancies. *J Clin Microbiol* 2006, *44*, 2458–2464, doi:10.1128/JCM.00356-06.
112. Guinea, J.; Zaragoza, Ó.; Escribano, P.; Martín-Mazuelos, E.; Pemán, J.; Sánchez-Reus, F.; Cuenca-Estrella, M. Molecular Identification and Antifungal Susceptibility of Yeast Isolates Causing Fungemia Collected in a Population-Based Study in Spain in 2010 and 2011. *Antimicrob Agents Chemother* 2014, *58*, 1529–1537, doi:10.1128/AAC.02155-13.
113. Ju-Nam, Y.; Lead, J.R. Manufactured Nanoparticles: An Overview of Their Chemistry, Interactions and Potential Environmental Implications. *Sci Total Environ* 2008, *400*, 396–414, doi:10.1016/j.scitotenv.2008.06.042.
114. Wiley, B.; Sun, Y.; Mayers, B.; Xia, Y. Shape-Controlled Synthesis of Metal Nanostructures: The Case of Silver. *Chem Eur J* 2005, *11*, 454–463, doi:10.1002/chem.200400927.

115. Oliveira, M.M.; Ugarte, D.; Zanchet, D.; Zarbin, A.J.G. Influence of Synthetic Parameters on the Size, Structure, and Stability of Dodecanethiol-Stabilized Silver Nanoparticles. *J Colloid Interface Sci* 2005, *292*, 429–435, doi:10.1016/j.jcis.2005.05.068.
116. Kim, D.; Jeong, S.; Moon, J. Synthesis of Silver Nanoparticles Using the Polyol Process and the Influence of Precursor Injection. *Nanotechnology* 2006, *17*, 4019–4024, doi:10.1088/0957-4484/17/16/004.
117. Ku, B.K.; Maynard, A.D. Generation and Investigation of Airborne Silver Nanoparticles with Specific Size and Morphology by Homogeneous Nucleation, Coagulation and Sintering. *J Aerosol Sci* 2006, *37*, 452–470, doi:10.1016/j.jaerosci.2005.05.003.
118. Kruis, F.E.; Fissan, H.; Rellinghaus, B. Sintering and Evaporation Characteristics of Gas-Phase Synthesis of Size-Selected PbS Nanoparticles. *Mater Sci Eng B* 2000, *69–70*, 329–334, doi:10.1016/S0921-5107(99)00298-6.
119. Magnusson, M.H.; Deppert, K.; Malm, J.O.; Bovin, J.O.; Samuelson, L. Gold Nanoparticles: Production, Reshaping, and Thermal Charging. *J Nanoparticle Res* 1999, *1*, 243–251, doi: 10.1023/A:1010012802415.
120. Mafuné, F.; Kohno, J.; Takeda, Y.; Kondow, T.; Sawabe, H. Structure and Stability of Silver Nanoparticles in Aqueous Solution Produced by Laser Ablation. *J Phys Chem B* 2000, *104*, 8333–8337, doi:10.1021/jp001803b.
121. Kim, S.; Yoo, B.K.; Chun, K.; Kang, W.; Choo, J.; Gong, M.S.; Joo, S.W. Catalytic Effect of Laser Ablated Ni Nanoparticles in the Oxidative Addition Reaction for a Coupling Reagent of Benzylchloride and Bromoacetonitrile. *J Mol Catal A Chem* 2005, *226*, 231–234, doi:10.1016/j.molcata.2004.10.038.
122. Tsuji, T.; Iryo, K.; Watanabe, N.; Tsuji, M. Preparation of Silver Nanoparticles by Laser Ablation in Solution: Influence of Laser Wavelength on Particle Size. *Appl Surf Sci* 2002, *202*, 80–85, doi:10.1016/S0169-4332(02)00936-4.
123. Tsuji, T.; Kakita, T.; Tsuji, M. Preparation of Nano-Size Particles of Silver with Femtosecond Laser Ablation in Water. *Appl Surf Sci* 2003, *206*, 314–320, doi:10.1016/S0169-4332(02)01230-8.
124. Prasad Yadav, T.; Manohar Yadav, R.; Pratap Singh, D. Mechanical Milling: A Top Down Approach for the Synthesis of Nanomaterials and Nanocomposites. *NN* 2012, *2*, 22–48, doi:10.5923/j.nn.20120203.01.
125. Mohanpuria, P.; Rana, N.K.; Yadav, S.K. Biosynthesis of Nanoparticles: Technological Concepts and Future Applications. *J Nanopart Res* 2008, *10*, 507–517, doi:10.1007/s11051-007-9275-x.
126. Kalabegishvili, T.L.; Kirkesali, E.I.; Rcheulishvili, A.N.; Ginturi, E.N.; Murusidze, I.G.; Pataraya, D.T.; Gurielidze, M.A.; Tsertsvadze, G.I.; Gabunia, V.N.; Lomidze, L.G.; et al. Synthesis of Gold Nanoparticles

by Some Strains of *Arthrobacter* Genera. *Mater Sci Eng A* 2012, *2*, 164–173.
127. Ansari, A.; Pervez, S.; Javed, U.; Abro, M.I.; Nawaz, M.A.; Qader, S.A.U.; Aman, A. Characterization and Interplay of Bacteriocin and Exopolysaccharide-Mediated Silver Nanoparticles as an Antibacterial Agent. *Int J Biol Macromol* 2018, *115*, 643–650, doi:10.1016/j.ijbiomac.2018.04.104.
128. Khodashenas, B.; Ghorbani, H.R. Optimisation of Nitrate Reductase Enzyme Activity to Synthesise Silver Nanoparticles. *IET Nanobiotechnology* 2016, *10*, 158–161, doi:10.1049/iet-nbt.2015.0062.
129. Nasrolahi Shirazi, A.; Mandal, D.; Tiwari, R.K.; Guo, L.; Lu, W.; Parang, K. Cyclic Peptide-Capped Gold Nanoparticles as Drug Delivery Systems. *Mol Pharmaceutics* 2013, *10*, 500–511, doi:10.1021/mp300448k.
130. Prabhu, S.; Poulose, E.K. Silver Nanoparticles: Mechanism of Antimicrobial Action, Synthesis, Medical Applications, and Toxicity Effects. *Int Nano Lett* 2012, *2*, 32, doi:10.1186/2228-5326-2-32.
131. Vaidyanathan, R.; Gopalram, S.; Kalishwaralal, K.; Deepak, V.; Pandian, S.R.K.; Gurunathan, S. Enhanced Silver Nanoparticle Synthesis by Optimization of Nitrate Reductase Activity. *Colloids Surf B Biointerfaces* 2010, *75*, 335–341, doi:10.1016/j.colsurfb.2009.09.006.
132. Kumar, S.A.; Abyaneh, M.K.; Gosavi, S.W.; Kulkarni, S.K.; Pasricha, R.; Ahmad, A.; Khan, M.I. Nitrate Reductase-Mediated Synthesis of Silver Nanoparticles from AgNO3. *Biotechnol Lett* 2007, *29*, 439–445, doi:10.1007/s10529-006-9256-7.
133. Siddiqi, K.S.; Husen, A.; Rao, R.A.K. A Review on Biosynthesis of Silver Nanoparticles and Their Biocidal Properties. *J Nanobiotechnol* 2018, *16*, 14, doi:10.1186/s12951-018-0334-5.
134. Ghasemi, S.M.; Dormanesh, B.; Abari, A.H.; Aliasghari, A.; Farahnejad, Z. Comparative Characterization of Silver Nanoparticles Synthesized by Spore Extract of *Bacillus subtilis* and *Geobacillus stearothermophilus*. *Nanomed J* 2018, *5*, 46–51, doi:10.22038/nmj.2018.05.007.
135. Abishad, P.; Vergis, J.; Unni, V.; Ram, V.P.; Niveditha, P.; Yasur, J.; Juliet, S.; John, L.; Byrappa, K.; Nambiar, P.; et al. Green Synthesized Silver Nanoparticles Using *Lactobacillus acidophilus* as an Antioxidant, Antimicrobial, and Antibiofilm Agent Against Multi-Drug Resistant Enteroaggregative *Escherichia coli*. *Probiotics Antimicrob Proteins* 2022, *14*, 904–914, doi:10.1007/s12602-022-09961-1.
136. Huq, Md.A. Green Synthesis of Silver Nanoparticles Using *Pseudoduganella eburnea* MAHUQ-39 and Their Antimicrobial

Mechanisms Investigation against Drug Resistant Human Pathogens. *IJMS* 2020, *21*, 1510, doi:10.3390/ijms21041510.
137. Ahmad, A.; Mukherjee, P.; Senapati, S.; Mandal, D.; Khan, M.I.; Kumar, R.; Sastry, M. Extracellular Biosynthesis of Silver Nanoparticles Using the Fungus *Fusarium oxysporum*. *Colloids Surf B Biointerfaces* 2003, *28*, 313–318, doi:10.1016/S0927-7765(02)00174-1.
138. Yassin, M.A.; Elgorban, A.M.; El-Samawaty, A.E.R.M.A.; Almunqedhi, B.M.A. Biosynthesis of Silver Nanoparticles Using *Penicillium verrucosum* and Analysis of Their Antifungal Activity. *Saudi J Biol Sci* 2021, *28*, 2123–2127, doi:10.1016/j.sjbs.2021.01.063.
139. Mistry, H.; Thakor, R.; Patil, C.; Trivedi, J.; Bariya, H. Biogenically Proficient Synthesis and Characterization of Silver Nanoparticles Employing Marine Procured Fungi *Aspergillus brunneoviolaceus* along with Their Antibacterial and Antioxidative Potency. *Biotechnol Lett* 2021, *43*, 307–316, doi:10.1007/s10529-020-03008-7.
140. Iravani, S. Green Synthesis of Metal Nanoparticles Using Plants. *Green Chem* 2011, *13*, 2638, doi:10.1039/c1gc15386b.
141. Vilchis-Nestor, A.R.; Sánchez-Mendieta, V.; Camacho-López, M.A.; Gómez-Espinosa, R.M.; Camacho-López, M.A.; Arenas-Alatorre, J.A. Solventless Synthesis and Optical Properties of Au and Ag Nanoparticles Using *Camellia sinensis* Extract. *Materials Lett* 2008, *62*, 3103–3105, doi:10.1016/j.matlet.2008.01.138.
142. Begum, N.A.; Mondal, S.; Basu, S.; Laskar, R.A.; Mandal, D. Biogenic Synthesis of Au and Ag Nanoparticles Using Aqueous Solutions of Black Tea Leaf Extracts. *Colloids Surf B Biointerfaces* 2009, *71*, 113–118, doi:10.1016/j.colsurfb.2009.01.012.
143. Vinodhini, S.; Vithiya, B.S.M.; Prasad, T.A.A. Green Synthesis of Silver Nanoparticles by Employing the *Allium fistulosum*, *Tabernaemontana divaricate* and *Basella alba* Leaf Extracts for Antimicrobial Applications. *J King Saud Univ Sci* 2022, *34*, 101939, doi:10.1016/j.jksus.2022.101939.
144. Hawar, S.N.; Al-Shmgani, H.S.; Al-Kubaisi, Z.A.; Sulaiman, G.M.; Dewir, Y.H.; Rikisahedew, J.J. Green Synthesis of Silver Nanoparticles from *Alhagi graecorum* Leaf Extract and Evaluation of Their Cytotoxicity and Antifungal Activity. *J Nanomater* 2022, *2022*, 1–8, doi:10.1155/2022/1058119.
145. Lara, H.H.; Garza-Treviño, E.N.; Ixtepan-Turrent, L.; Singh, D.K. Silver Nanoparticles Are Broad-Spectrum Bactericidal and Virucidal Compounds. *J Nanobiotechnol* 2011, *9*, 30, doi:10.1186/1477-3155-9-30.
146. Yin, I.X.; Zhang, J.; Zhao, I.S.; Mei, M.L.; Li, Q.; Chu, C.H. The Antibacterial Mechanism of Silver Nanoparticles and Its Application in Dentistry. *IJN* 2020, *15*, 2555–2562, doi:10.2147/IJN.S246764.

147. Gupta, A.; Landis, R.F.; Rotello, V.M. Nanoparticle-Based Antimicrobials: Surface Functionality Is Critical. *F1000Res* 2016, *5*, 364, doi:10.12688/f1000research.7595.1.
148. Ansari, M.A.; Khan, H.M..; Khan, A.A.; Malik, A.; Sultan, A.; Shahid, M.; Shujatullah, F.; Azam, A. Evaluation of Antibacterial Activity of Silver Nanoparticles against MSSA and MRSA on Isolates from Skin Infections. *Biol Med* 2011, *3*, 141–146.
149. Chen, S.; Carroll, D.L. Synthesis and Characterization of Truncated Triangular Silver Nanoplates. *Nano Lett* 2002, *2*, 1003–1007, doi:10.1021/nl025674h.
150. Lok, C.N.; Ho, C.M.; Chen, R.; He, Q.Y.; Yu, W.Y.; Sun, H.; Tam, P.K.H.; Chiu, J.F.; Che, C.-M. Proteomic Analysis of the Mode of Antibacterial Action of Silver Nanoparticles. *J. Proteome Res* 2006, *5*, 916–924, doi:10.1021/pr0504079.
151. Rai, M.K.; Deshmukh, S.D.; Ingle, A.P.; Gade, A.K. Silver Nanoparticles: The Powerful Nanoweapon against Multidrug-Resistant Bacteria: Activity of Silver Nanoparticles against MDR Bacteria. *J Appl Microbiol* 2012, *112*, 841–852, doi:10.1111/j.1365-2672.2012.05253.x.
152. Klueh, U.; Wagner, V.; Kelly, S.; Johnson, A.; Bryers, J.D. Efficacy of Silver-Coated Fabric to Prevent Bacterial Colonization and Subsequent Device-Based Biofilm Formation. *J Biomed Mater Res* 2000, *53*, 621–631, doi:10.1002/1097-4636(2000)53:6<621::AID-JBM2>3.0.CO;2-Q.
153. Ma, J.; Zhang, J.; Xiong, Z.; Yong, Y.; Zhao, X.S. Preparation, Characterization and Antibacterial Properties of Silver-Modified Graphene Oxide. *J Mater Chem* 2011, *21*, 3350–3352, doi:10.1039/C0JM02806A.
154. El Badawy, A.M.; Silva, R.G.; Morris, B.; Scheckel, K.G.; Suidan, M.T.; Tolaymat, T.M. Surface Charge-Dependent Toxicity of Silver Nanoparticles. *Environ Sci Technol* 2011, *45*, 283–287, doi:10.1021/es1034188.
155. Holt, K.B.; Bard, A.J. Interaction of Silver(I) Ions with the Respiratory Chain of *Escherichia coli*: An Electrochemical and Scanning Electrochemical Microscopy Study of the Antimicrobial Mechanism of Micromolar Ag^+. *Biochemistry* 2005, *44*, 13214–13223, doi:10.1021/bi0508542.
156. Mammari, N.; Lamouroux, E.; Boudier, A.; Duval, R.E. Current Knowledge on the Oxidative-Stress-Mediated Antimicrobial Properties of Metal-Based Nanoparticles. *Microorganisms* 2022, *10*, 437, doi:10.3390/microorganisms10020437.
157. Gülçin, İ. Antioxidant Activity of Food Constituents: An Overview. *Arch Toxicol* 2012, *86*, 345–391, doi:10.1007/s00204-011-0774-2.
158. Malka, E.; Perelshtein, I.; Lipovsky, A.; Shalom, Y.; Naparstek, L.; Perkas, N.; Patick, T.; Lubart, R.; Nitzan, Y.; Banin, E.; et al.

Eradication of Multi-Drug Resistant Bacteria by a Novel Zn-Doped CuO Nanocomposite. *Small* 2013, *9*, 4069–4076, doi:10.1002/smll.201301081.
159. Li, Y.; Zhang, W.; Niu, J.; Chen, Y. Mechanism of Photogenerated Reactive Oxygen Species and Correlation with the Antibacterial Properties of Engineered Metal-Oxide Nanoparticles. *ACS Nano* 2012, *6*, 5164–5173, doi:10.1021/nn300934k.
160. Ayala, A.; Muñoz, M.F.; Argüelles, S. Lipid Peroxidation: Production, Metabolism, and Signaling Mechanisms of Malondialdehyde and 4-Hydroxy-2-Nonenal. *Oxid Med Cell Longev* 2014, *2014*, 1–31, doi:10.1155/2014/360438.
161. Singh, M. Elucidation of Biogenic Silver Nanoparticles Susceptibility towards *Escherichia coli*: An Investigation on the Antimicrobial Mechanism. *IET nanobiotechnol.* 2016, *10*, 276–280, doi:10.1049/iet-nbt.2015.0063.
162. De Silva, C.; Nawawi, N.M.; Abd Karim, M.M.; Abd Gani, S.; Masarudin, M.J.; Gunasekaran, B.; Ahmad, S.A. The Mechanistic Action of Biosynthesised Silver Nanoparticles and Its Application in Aquaculture and Livestock Industries. *Animals* 2021, *11*, 2097, doi:10.3390/ani11072097.
163. Königs, A.M.; Flemming, H.C.; Wingender, J. Nanosilver Induces a Non-Culturable but Metabolically Active State in *Pseudomonas aeruginosa*. *Front Microbiol* 2015, *06*, doi:10.3389/fmicb.2015.00395.
164. Xiu, Z.M.; Ma, J.; Alvarez, P.J.J. Differential Effect of Common Ligands and Molecular Oxygen on Antimicrobial Activity of Silver Nanoparticles versus Silver Ions. *Environ Sci Technol* 2011, *45*, 9003–9008, doi:10.1021/es201918f.
165. Koch, A.L. The pH in the Neighborhood of Membranes Generating a Protonmotive Force. *J Theor Biol* 1986, *120*, 73–84, doi:10.1016/S0022-5193(86)80018-2.
166. Xiu, Z.; Zhang, Q.; Puppala, H.L.; Colvin, V.L.; Alvarez, P.J.J. Negligible Particle-Specific Antibacterial Activity of Silver Nanoparticles. *Nano Lett* 2012, *12*, 4271–4275, doi:10.1021/nl301934w.
167. Navarro, E.; Piccapietra, F.; Wagner, B.; Marconi, F.; Kaegi, R.; Odzak, N.; Sigg, L.; Behra, R. Toxicity of Silver Nanoparticles to *Chlamydomonas reinhardtii*. *Environ Sci Technol* 2008, *42*, 8959–8964, doi:10.1021/es801785m.
168. Lowry, G.V.; Gregory, K.B.; Apte, S.C.; Lead, J.R. Transformations of Nanomaterials in the Environment. *Environ Sci Technol* 2012, *46*, 6893–6899, doi:10.1021/es300839e.
169. Liu, J.; Sonshine, D.A.; Shervani, S.; Hurt, R.H. Controlled Release of Biologically Active Silver from Nanosilver Surfaces. *ACS Nano* 2010, *4*, 6903–6913, doi:10.1021/nn102272n.

170. Bell, R.A.; Kramer, J.R. Structural Chemistry and Geochemistry of Silver-Sulfur Compounds: Critical Review. *Environ Toxicol Chem* 1999, *18*, 9–22, doi:10.1002/etc.5620180103.
171. Abbaszadegan, A.; Ghahramani, Y.; Gholami, A.; Hemmateenejad, B.; Dorostkar, S.; Nabavizadeh, M.; Sharghi, H. The Effect of Charge at the Surface of Silver Nanoparticles on Antimicrobial Activity against Gram-Positive and Gram-Negative Bacteria: A Preliminary Study. *J Nanomat* 2015, *2015*, 1–8, doi:10.1155/2015/720654.
172. Chamakura, K.; Perez-Ballestero, R.; Luo, Z.; Bashir, S.; Liu, J. Comparison of Bactericidal Activities of Silver Nanoparticles with Common Chemical Disinfectants. *Colloids Surf B Biointerfaces* 2011, *84*, 88–96, doi:10.1016/j.colsurfb.2010.12.020.
173. Kittler, S.; Greulich, C.; Diendorf, J.; Köller, M.; Epple, M. Toxicity of Silver Nanoparticles Increases during Storage Because of Slow Dissolution under Release of Silver Ions. *Chem Mater* 2010, *22*, 4548–4554, doi:10.1021/cm100023p.
174. Neethu, S.; Midhun, S.J.; Sunil, M.A.; Soumya, S.; Radhakrishnan, E.K.; Jyothis, M. Efficient Visible Light Induced Synthesis of Silver Nanoparticles by *Penicillium polonicum* ARA 10 Isolated from *Chetomorpha antennina* and Its Antibacterial Efficacy against *Salmonella enterica* Serovar Typhimurium. *J Photochem Photobiol B* 2018, *180*, 175–185, doi:10.1016/j.jphotobiol.2018.02.005.
175. Agnihotri, S.; Mukherji, S.; Mukherji, S. Size-Controlled Silver Nanoparticles Synthesized over the Range 5–100 Nm Using the Same Protocol and Their Antibacterial Efficacy. *RSC Adv* 2014, *4*, 3974–3983, doi:10.1039/C3RA44507K.
176. Ramadan, M.A.; Shawkey, A.E.; Rabeh, M.A.; Abdellatif, A.O. Promising Antimicrobial Activities of Oil and Silver Nanoparticles Obtained from *Melaleuca alternifolia* Leaves against Selected Skin-Infecting Pathogens. *J Herb Med* 2020, *20*, 100289, doi:10.1016/j.hermed.2019.100289.
177. Mirzajani, F.; Ghassempour, A.; Aliahmadi, A.; Esmaeili, M.A. Antibacterial Effect of Silver Nanoparticles on *Staphylococcus aureus*. *Res Microbiol* 2011, *162*, 542–549, doi:10.1016/j.resmic.2011.04.009.
178. Ansari, M.A.; Khan, H.M.; Khan, A.A.; Ahmad, M.K.; Mahdi, A.A.; Pal, R.; Cameotra, S.S. Interaction of Silver Nanoparticles with *Escherichia coli* and Their Cell Envelope Biomolecules: Interaction of Silver Nanoparticles with *E. coli*. *J. Basic Microbiol* 2014, *54*, 905–915, doi:10.1002/jobm.201300457.
179. Jucker, B.A.; Harms, H.; Hug, S.J.; Zehnder, A.J.B. Adsorption of Bacterial Surface Polysaccharides on Mineral Oxides Is Mediated by Hydrogen Bonds. *Colloids Surf B Biointerfaces* 1997, *9*, 331–343, doi:10.1016/S0927-7765(97)00038-6.

180. Jeong, S.H.; Lee, J.W.; Ge, D.; Sun, K.; Nakashima, T.; Yoo, S.I.; Agarwal, A.; Li, Y.; Kotov, N.A. Reversible Nanoparticle Gels with Colour Switching. *J Mater Chem* 2011, *21*, 11639, doi:10.1039/c1jm11139f.
181. Randall, L.L. Function of Protonmotive Force in Translocation of Protein across Membranes. In *Methods in Enzymology*; Elsevier, 1986, Vol. 125, pp. 129–138 ISBN 978-0-12-182025-1.
182. Beher, M.G.; Schnaitman, C.A. Regulation of the OmpA Outer Membrane Protein of *Escherichia coli*. *J Bacteriol* 1981, *147*, 972–985, doi:10.1128/jb.147.3.972-985.1981.
183. Driessen, A.J.; Wickner, W. Proton Transfer Is Rate-Limiting for Translocation of Precursor Proteins by the *Escherichia coli* Translocase. *Proc Natl Acad Sci USA* 1991, *88*, 2471–2475, doi:10.1073/pnas.88.6.2471.
184. Thombre, R.S.; Shinde, V.; Thaiparambil, E.; Zende, S.; Mehta, S. Antimicrobial Activity and Mechanism of Inhibition of Silver Nanoparticles against Extreme Halophilic Archaea. *Front Microbiol* 2016, *7*, doi:10.3389/fmicb.2016.01424.
185. Gutiérrez, J.A.; Caballero, S.; Díaz, L.A.; Guerrero, M.A.; Ruiz, J.; Ortiz, C.C. High Antifungal Activity against *Candida* Species of Monometallic and Bimetallic Nanoparticles Synthesized in Nanoreactors. *ACS Biomater Sci Eng* 2018, *4*, 647–653, doi:10.1021/acsbiomaterials.7b00511.
186. Kim, K.J.; Sung, W.S.; Suh, B.K.; Moon, S.K.; Choi, J.S.; Kim, J.G.; Lee, D.G. Antifungal Activity and Mode of Action of Silver Nano-Particles on *Candida albicans*. *Biometals* 2009, *22*, 235–242, doi:10.1007/s10534-008-9159-2.
187. Radhakrishnan, V.S.; Reddy Mudiam, M.K.; Kumar, M.; Dwivedi, S.P.; Singh, S.P.; Prasad, T. Silver Nanoparticles Induced Alterations in Multiple Cellular Targets, Which Are Critical for Drug Susceptibilities and Pathogenicity in Fungal Pathogen (*Candida albicans*). *IJN* 2018, *13*, 2647–2663, doi:10.2147/IJN.S150648.
188. Muthamil, S.; Devi, V.A.; Balasubramaniam, B.; Balamurugan, K.; Pandian, S.K. Green Synthesized Silver Nanoparticles Demonstrating Enhanced in Vitro and in Vivo Antibiofilm Activity against *Candida* spp. *J Basic Microbiol* 2018, *58*, 343–357, doi:10.1002/jobm.201700529.
189. Jalal, M.; Ansari, M.A.; Alzohairy, M.A.; Ali, S.G.; Khan, H.M.; Almatroudi, A.; Siddiqui, M.I. Anticandidal Activity of Biosynthesized Silver Nanoparticles: Effect on Growth, Cell Morphology, and Key Virulence Attributes of *Candida* Species. *IJN* 2019, *14*, 4667–4679, doi:10.2147/IJN.S210449.
190. Murphy, M.P. How Mitochondria Produce Reactive Oxygen Species. *Biochem J* 2009, *417*, 1–13, doi:10.1042/BJ20081386.

191. Tu, B.P.; Weissman, J.S. Oxidative Protein Folding in Eukaryotes. *J Cell Biol* 2004, *164*, 341–346, doi:10.1083/jcb.200311055.
192. Hiltunen, J.K.; Mursula, A.M.; Rottensteiner, H.; Wierenga, R.K.; Kastaniotis, A.J.; Gurvitz, A. The Biochemistry of Peroxisomal β-Oxidation in the Yeast *Saccharomyces cerevisiae*. *FEMS Microbiol Rev* 2003, *27*, 35–64, doi:10.1016/S0168-6445(03)00017-2.
193. Pollegioni, L.; Piubelli, L.; Sacchi, S.; Pilone, M.S.; Molla, G. Physiological Functions of D-Amino Acid Oxidases: From Yeast to Humans. *Cell Mol Life Sci* 2007, *64*, 1373–1394, doi:10.1007/s00018-007-6558-4.
194. Bhattacharyya, A.; Chattopadhyay, R.; Mitra, S.; Crowe, S.E. Oxidative Stress: An Essential Factor in the Pathogenesis of Gastrointestinal Mucosal Diseases. *Physiol Rev* 2014, *94*, 329–354, doi:10.1152/physrev.00040.2012.
195. Veal, E.A.; Day, A.M.; Morgan, B.A. Hydrogen Peroxide Sensing and Signaling. *Mol Cell* 2007, *26*, 1–14, doi:10.1016/j.molcel.2007.03.016.
196. Simic, M.G.; Bergtold, D.S.; Karam, L.R. Generation of Oxy Radicals in Biosystems. *Mut Res* 1989, *214*, 3–12, doi:10.1016/0027-5107(89)90192-9.
197. Evans, M.V.; Turton, H.E.; Grant, C.M.; Dawes, I.W. Toxicity of Linoleic Acid Hydroperoxide to *Saccharomyces cerevisiae*: Involvement of a Respiration-Related Process for Maximal Sensitivity and Adaptive Response. *J Bacteriol* 1998, *180*, 483–490, doi:10.1128/JB.180.3.483-490.1998.
198. Halliwell, B. Reactive Species and Antioxidants. Redox Biology Is a Fundamental Theme of Aerobic Life. *Plant Physiology* 2006, *141*, 312–322, doi:10.1104/pp.106.077073.
199. Yamashoji, S. Different Characteristics between Menadione and Menadione Sodium Bisulfite as Redox Mediator in Yeast Cell Suspension. *Biochem Biophys Rep* 2016, *6*, 88–93, doi:10.1016/j.bbrep.2016.03.007.
200. Perrone, G.G.; Tan, S.X.; Dawes, I.W. Reactive Oxygen Species and Yeast Apoptosis. *Biochim Biophys Acta* 2008, *1783*, 1354–1368, doi:10.1016/j.bbamcr.2008.01.023.
201. Sheehan, D.; Meade, G.; Foley, V.M.; Dowd, C.A. Structure, Function and Evolution of Glutathione Transferases: Implications for Classification of Non-Mammalian Members of an Ancient Enzyme Superfamily. *Biochem J*, 2001, *360*, 1–16, doi: 10.1042/0264-6021:3600001.
202. Wheeler, G.L.; Quinn, K.A.; Perrone, G.; Dawes, I.W.; Grant, C.M. Glutathione Regulates the Expression of γ-Glutamylcysteine Synthetase via the Met4 Transcription Factor: Regulation of GSH Biosynthesis. *Mol Microbiol* 2002, *46*, 545–556, doi:10.1046/j.1365-2958.2002.03174.x.

203. Kosower, N.S.; Kosower, E.M. Diamide: An Oxidant Probe for Thiols. In *Methods in Enzymology*; Elsevier, 1995; Vol. 251, pp. 123–133 ISBN 978-0-12-182152-4.
204. Muller, E.G. A Glutathione Reductase Mutant of Yeast Accumulates High Levels of Oxidized Glutathione and Requires Thioredoxin for Growth. *MBoC* 1996, *7*, 1805–1813, doi:10.1091/mbc.7.11.1805.
205. Liochev, S.; Fridovich, I. Superoxide and Iron: Partners in Crime. *TBMB* 1999, *48*, 157–161, doi:10.1080/713803492.
206. Freitas, J.D.; Wintz, H.; Kim, J.H.; Poynton, H.; Fox, T.; Vulpe, C. Yeast, a Model Organism for Iron and Copper Metabolism Studies. *Biometals*, 2003, *16*, 185–97, doi: 10.1023/a:1020771000746.
207. Brennan, R.J.; Schiestl, R.H. Cadmium Is an Inducer of Oxidative Stress in Yeast. *Mutat Res*, 1996, *356*, 171–8, doi: 10.1016/0027-5107(96)00051-6.
208. Wysocki, R.; Tamás, M.J. How *Saccharomyces cerevisiae* Copes with Toxic Metals and Metalloids. *FEMS Microbiol Rev* 2010, *34*, 925–951, doi:10.1111/j.1574-6976.2010.00217.x.
209. Rajakumar, S.; Abhishek, A.; Selvam, G.S.; Nachiappan, V. Effect of Cadmium on Essential Metals and Their Impact on Lipid Metabolism in *Saccharomyces cerevisiae*. *Cell Stress Chaperones* 2020, *25*, 19–33, doi:10.1007/s12192-019-01058-z.
210. Pradhan, A.; Pinheiro, J.P.; Seena, S.; Pascoal, C.; Cássio, F. Polyhydroxyfullerene Binds Cadmium Ions and Alleviates Metal-Induced Oxidative Stress in *Saccharomyces cerevisiae*. *Appl Environ Microbiol* 2014, *80*, 5874–5881, doi:10.1128/AEM.01329-14.
211. Rhee, S.G.; Kang, S.W.; Jeong, W.; Chang, T.S.; Yang, K.S.; Woo, H.A. Intracellular Messenger Function of Hydrogen Peroxide and Its Regulation by Peroxiredoxins. *Curr Opin Cell Biol* 2005, *17*, 183–189, doi:10.1016/j.ceb.2005.02.004.
212. Le Moan, N.; Clement, G.; Le Maout, S.; Tacnet, F.; Toledano, M.B. The *Saccharomyces cerevisiae* Proteome of Oxidized Protein Thiols. *J Biol Chem* 2006, *281*, 10420–10430, doi:10.1074/jbc.M513346200.
213. Holmgren, A. Thioredoxin and Glutaredoxin Systems. *J Biol Chem* 1989, *264*, 13963–13966, doi:10.1016/S0021-9258(18)71625-6.
214. Preiss, T.; Baron-Benhamou, J.; Ansorge, W.; Hentze, M.W. Homodirectional Changes in Transcriptome Composition and mRNA Translation Induced by Rapamycin and Heat Shock. *Nat Struct Mol Biol* 2003, *10*, 1039–1047, doi:10.1038/nsb1015.
215. Smirnova, J.B.; Selley, J.N.; Sanchez-Cabo, F.; Carroll, K.; Eddy, A.A.; McCarthy, J.E.G.; Hubbard, S.J.; Pavitt, G.D.; Grant, C.M.; Ashe, M.P. Global Gene Expression Profiling Reveals Widespread yet Distinctive Translational Responses to Different Eukaryotic Translation Initiation Factor 2B-Targeting Stress Pathways. *Mol Cell Biol* 2005, *25*, 9340–9349, doi:10.1128/MCB.25.21.9340-9349.2005.

216. Godon, C.; Lagniel, G.; Lee, J.; Buhler, J.-M.; Kieffer, S.; Perrot, M.; Boucherie, H.; Toledano, M.B.; Labarre, J. The H2O2 Stimulon in *Saccharomyces cerevisiae*. *J Biol Chem* 1998, *273*, 22480–22489, doi:10.1074/jbc.273.35.22480.
217. Shenton, D.; Grant, C.M. Protein S-Thiolation Targets Glycolysis and Protein Synthesis in Response to Oxidative Stress in the Yeast *Saccharomyces cerevisiae*. *Biochem J* 2003, *374*, 513–519, doi:10.1042/bj20030414.
218. Shenton, D.; Smirnova, J.B.; Selley, J.N.; Carroll, K.; Hubbard, S.J.; Pavitt, G.D.; Ashe, M.P.; Grant, C.M. Global Translational Responses to Oxidative Stress Impact upon Multiple Levels of Protein Synthesis. *J Biol Chem* 2006, *281*, 29011–29021, doi:10.1074/jbc.M601545200.
219. Mascarenhas, C.; Edwards-Ingram, L.C.; Zeef, L.; Shenton, D.; Ashe, M.P.; Grant, C.M. Gcn4 Is Required for the Response to Peroxide Stress in the Yeast *Saccharomyces cerevisiae*. *MBoC* 2008, *19*, 2995–3007, doi:10.1091/mbc.e07-11-1173.
220. Swaminathan, S.; Masek, T.; Molin, C.; Pospisek, M.; Sunnerhagen, P. Rck2 Is Required for Reprogramming of Ribosomes during Oxidative Stress. *Mole Biol Cell* 2006, *17*, 1472–82, doi: 10.1091/mbc.e05-07-0632.
221. Chechik, G.; Oh, E.; Rando, O.; Weissman, J.; Regev, A.; Koller, D. Activity Motifs Reveal Principles of Timing in Transcriptional Control of the Yeast Metabolic Network. *Nat Biotechnol* 2008, *26*, 1251–1259, doi:10.1038/nbt.1499.
222. Ralser, M.; Wamelink, M.M.C.; Latkolik, S.; Jansen, E.E.W.; Lehrach, H.; Jakobs, C. Metabolic Reconfiguration Precedes Transcriptional Regulation in the Antioxidant Response. *Nat Biotechnol* 2009, *27*, 604–605, doi:10.1038/nbt0709-604.
223. Ralser, M.; Wamelink, M.M.; Kowald, A.; Gerisch, B.; Heeren, G.; Struys, E.A.; Klipp, E.; Jakobs, C.; Breitenbach, M.; Lehrach, H.; et al. Dynamic Rerouting of the Carbohydrate Flux Is Key to Counteracting Oxidative Stress. *J Biol* 2007, *6*, 10, doi:10.1186/jbiol61.
224. Izawa, S.; Maeda, K.; Miki, T.; Mano, J.; Inoue, Y.; Kimura, A. Importance of Glucose-6-Phosphate Dehydrogenase in the Adaptive Response to Hydrogen Peroxide in *Saccharomyces cerevisiae*. *Biochem J* 1998, *330*, 811–817, doi:10.1042/bj3300811.
225. Oves, M.; Aslam, M.; Rauf, M.A.; Qayyum, S.; Qari, H.A.; Khan, M.S.; Alam, M.Z.; Tabrez, S.; Pugazhendhi, A.; Ismail, I.M.I. Antimicrobial and Anticancer Activities of Silver Nanoparticles Synthesized from the Root Hair Extract of Phoenix Dactylifera. *Mat Sci Eng C Mater Biol Appl* 2018, *89*, 429–443, doi:10.1016/j.msec.2018.03.035.
226. Mussin, J.E.; Roldán, M.V.; Rojas, F.; Sosa, M.D.L.Á.; Pellegri, N.; Giusiano, G. Antifungal Activity of Silver Nanoparticles in

Combination with Ketoconazole against *Malassezia furfur*. *AMB Expr* 2019, *9*, 131, doi:10.1186/s13568-019-0857-7.
227. Jia, D.; Sun, W. Silver Nanoparticles Offer a Synergistic Effect with Fluconazole against Fluconazole-Resistant *Candida albicans* by Abrogating Drug Efflux Pumps and Increasing Endogenous ROS. *Infect Genet Evol* 2021, *93*, 104937, doi:10.1016/j.meegid.2021.104937.
228. Yusupov, M.; Van Der Paal, J.; Neyts, E.C.; Bogaerts, A. Synergistic Effect of Electric Field and Lipid Oxidation on the Permeability of Cell Membranes. *Biochim Biophys Acta Gen Subj* 2017, *1861*, 839–847, doi:10.1016/j.bbagen.2017.01.030.
229. Wang, G.; Feng, H.; Hu, L.; Jin, W.; Hao, Q.; Gao, A.; Peng, X.; Li, W.; Wong, K.-Y.; Wang, H.; et al. An Antibacterial Platform Based on Capacitive Carbon-Doped TiO2 Nanotubes after Direct or Alternating Current Charging. *Nat Commun* 2018, *9*, 2055, doi:10.1038/s41467-018-04317-2.
230. Wang, C.; Yue, L.; Wang, S.; Pu, Y.; Zhang, X.; Hao, X.; Wang, W.; Chen, S. Role of Electric Field and Reactive Oxygen Species in Enhancing Antibacterial Activity: A Case Study of 3D Cu Foam Electrode with Branched CuO–ZnO NWs. *J Phys Chem C* 2018, *122*, 26454–26463, doi:10.1021/acs.jpcc.8b08232.
231. Shekhova, E.; Kniemeyer, O.; Brakhage, A.A. Induction of Mitochondrial Reactive Oxygen Species Production by Itraconazole, Terbinafine, and Amphotericin B as a Mode of Action against *Aspergillus fumigatus*. *Antimicrob Agents Chemother* 2017, *61*, e00978-17, doi:10.1128/AAC.00978-17.
232. Lakshmeesha, T.R.; Kalagatur, N.K.; Mudili, V.; Mohan, C.D.; Rangappa, S.; Prasad, B.D.; Ashwini, B.S.; Hashem, A.; Alqarawi, A.A.; Malik, J.A.; et al. Biofabrication of Zinc Oxide Nanoparticles With *Syzygium aromaticum* Flower Buds Extract and Finding Its Novel Application in Controlling the Growth and Mycotoxins of *Fusarium graminearum*. *Front Microbiol* 2019, *10*, 1244, doi:10.3389/fmicb.2019.01244.
233. Kotnik, T.; Rems, L.; Tarek, M.; Miklavčič, D. Membrane Electroporation and Electropermeabilization: Mechanisms and Models. *Annu Rev Biophys* 2019, *48*, 63–91, doi:10.1146/annurev-biophys-052118-115451.
234. Gabriel, B.; Teissié, J. Control by Electrical Parameters of Short- and Long-Term Cell Death Resulting from Electropermeabilization of Chinese Hamster Ovary Cells. *Biochim Biophys Acta Mol Cell Res* 1995, *1266*, 171–178, doi:10.1016/0167-4889(95)00021-J.
235. Simioni, A.; Valpione, S.; Granziera, E.; Rossi, C.R.; Cavallin, F.; Spina, R.; Sieni, E.; Aliberti, C.; Stramare, R.; Campana, L.G. Ablation of Soft Tissue Tumours by Long Needle Variable Electrode-Geometry Electrochemotherapy: Final Report from a Single-Arm, Single-Centre

Phase-2 Study. *Sci Rep* 2020, *10*, 2291, doi:10.1038/s41598-020-59230-w.
236. Batista Napotnik, T.; Polajžer, T.; Miklavčič, D. Cell Death Due to Electroporation – A Review. *Bioelectrochemistry* 2021, *141*, 107871, doi:10.1016/j.bioelechem.2021.107871.
237. Neumann, E.; Schaefer-Ridder, M.; Wang, Y.; Hofschneider, P.H. Gene Transfer into Mouse Lyoma Cells by Electroporation in High Electric Fields. *EMBO J* 1982, *1*, 841–845, doi:10.1002/j.1460-2075.1982.tb01257.x.
238. Golberg, A. Emerging Electroporation-Based Technologies for Wound Care. In *Innovations and Emerging Technologies in Wound Care*; Elsevier, 2020; pp. 155–170 ISBN 978-0-12-815028-3.
239. Kravez, E.; Villiger, M.; Bouma, B.; Yarmush, M.; Yakhini, Z.; Golberg, A. Prediction of Scar Size in Rats Six Months after Burns Based on Early Post-Injury Polarization-Sensitive Optical Frequency Domain Imaging. *Front Physiol* 2017, *8*, 967, doi:10.3389/fphys.2017.00967.
240. Delemotte, L.; Tarek, M. Molecular Dynamics Simulations of Lipid Membrane Electroporation. *J Membrane Biol* 2012, *245*, 531–543, doi:10.1007/s00232-012-9434-6.
241. Kotnik, T.; Kramar, P.; Pucihar, G.; Miklavcic, D.; Tarek, M. Cell Membrane Electroporation- Part 1: The Phenomenon. *IEEE Electr Insul Mag* 2012, *28*, 14–23, doi:10.1109/MEI.2012.6268438.
242. Levine, Z.A.; Vernier, P.T. Calcium and Phosphatidylserine Inhibit Lipid Electropore Formation and Reduce Pore Lifetime. *J Membrane Biol* 2012, *245*, 599–610, doi:10.1007/s00232-012-9471-1.
243. Gibot, L.; Montigny, A.; Baaziz, H.; Fourquaux, I.; Audebert, M.; Rols, M.-P. Calcium Delivery by Electroporation Induces In vitro Cell Death through Mitochondrial Dysfunction without DNA Damages. *Cancers* 2020, *12*, 425, doi:10.3390/cancers12020425.
244. Muratori, C.; Pakhomov, A.G.; Gianulis, E.C.; Jensen, S.D.; Pakhomova, O.N. The Cytotoxic Synergy of Nanosecond Electric Pulses and Low Temperature Leads to Apoptosis. *Sci Rep* 2016, *6*, 36835, doi:10.1038/srep36835.
245. Pakhomova, O.N.; Gregory, B.; Semenov, I.; Pakhomov, A.G. Calcium-Mediated Pore Expansion and Cell Death Following Nanoelectroporation. *Biochim Biophys Acta* 2014, *1838*, 2547–2554, doi:10.1016/j.bbamem.2014.06.015.
246. Fink, B.D.; Bai, F.; Yu, L.; Sivitz, W.I. Regulation of ATP Production: Dependence on Calcium Concentration and Respiratory State. *Am J Physiol Cell Physiol* 2017, *313*, C146–C153, doi:10.1152/ajpcell.00086.2017.
247. Wiczew, D.; Szulc, N.; Tarek, M. Molecular Dynamics Simulations of the Effects of Lipid Oxidation on the Permeability of Cell Membranes.

Bioelectrochemistry, 2021, *141*, doi: 10.1016/j.bioelechem.2021.107869.
248. Michel, O.; Pakhomov, A.G.; Casciola, M.; Saczko, J.; Kulbacka, J.; Pakhomova, O.N. Electropermeabilization Does Not Correlate with Plasma Membrane Lipid Oxidation. *Bioelectrochemistry* 2020, *132*, 107433, doi:10.1016/j.bioelechem.2019.107433.
249. Napotnik, T.B.; Wu, Y.H.; Gundersen, M.A.; Miklavčič, D.; Vernier, P.T. Nanosecond Electric Pulses Cause Mitochondrial Membrane Permeabilization in Jurkat Cells. *Bioelectromagnetics* 2012, *33*, 257–264, doi:10.1002/bem.20707.
250. Pakhomova, O.N.; Khorokhorina, V.A.; Bowman, A.M.; Rodaitė-Riševičienė, R.; Saulis, G.; Xiao, S.; Pakhomov, A.G. Oxidative Effects of Nanosecond Pulsed Electric Field Exposure in Cells and Cell-Free Media. *Arc Biochem Biophys* 2012, *527*, 55–64, doi:10.1016/j.abb.2012.08.004.
251. Galluzzi, L.; Vitale, I.; Aaronson, S.A.; Abrams, J.M.; Adam, D.; Agostinis, P.; Alnemri, E.S.; Altucci, L.; Amelio, I.; Andrews, D.W.; et al. Molecular Mechanisms of Cell Death: Recommendations of the Nomenclature Committee on Cell Death 2018. *Cell Death Differ* 2018, *25*, 486–541, doi:10.1038/s41418-017-0012-4.
252. Schweichel, J.U.; Merker, H.J. The Morphology of Various Types of Cell Death in Prenatal Tissues. *Teratology* 1973, *7*, 253–266, doi:10.1002/tera.1420070306.
253. Galluzzi, L.; Maiuri, M.C.; Vitale, I.; Zischka, H.; Castedo, M.; Zitvogel, L.; Kroemer, G. Cell Death Modalities: Classification and Pathophysiological Implications. *Cell Death Differ* 2007, *14*, 1237–1243, doi:10.1038/sj.cdd.4402148.
254. Carmona-Gutierrez, D.; Bauer, M.A.; Zimmermann, A.; Aguilera, A.; Austriaco, N.; Ayscough, K.; Balzan, R.; Bar-Nun, S.; Barrientos, A.; Belenky, P.; et al. Guidelines and Recommendations on Yeast Cell Death Nomenclature. *Microb Cell* 2018, *5*, 4–31, doi:10.15698/mic2018.01.607.
255. Falcone, C.; Mazzoni, C. External and Internal Triggers of Cell Death in Yeast. *Cell Mol Life Sci* 2016, *73*, 2237–2250, doi:10.1007/s00018-016-2197-y.
256. Madeo, F.; Fröhlich, E.; Fröhlich, K.-U. A Yeast Mutant Showing Diagnostic Markers of Early and Late Apoptosis. *J Cell Biol* 1997, *139*, 729–734, doi:10.1083/jcb.139.3.729.
257. Fröhlich, K.-U.; Madeo, F. Apoptosis in Yeast - a Monocellular Organism Exhibits Altruistic Behaviour. *FEBS Lett* 2000, *473*, 6–9, doi:10.1016/S0014-5793(00)01474-5.
258. Chaves, S.R.; Rego, A.; Martins, V.M.; Santos-Pereira, C.; Sousa, M.J.; Côrte-Real, M. Regulation of Cell Death Induced by Acetic Acid in Yeasts. *Front Cell Dev Biol* 2021, *9*, 642375, doi:10.3389/fcell.2021.642375.

259. Ludovico, P.; Sousa, M.J.; Silva, M.T.; Leão, C.; Côrte-Real, M. *Saccharomyces cerevisiae* Commits to a Programmed Cell Death Process in Response to Acetic Acid. *Microbiology* 2001, *147*, 2409–2415, doi:10.1099/00221287-147-9-2409.
260. Madeo, F.; Fröhlich, E.; Ligr, M.; Grey, M.; Sigrist, S.J.; Wolf, D.H.; Fröhlich, K.U. Oxygen Stress: A Regulator of Apoptosis in Yeast. *The J Cell Biol* 1997, *145*, 757–767, doi:10.1083/jcb.145.4.757.
261. Carmona-Gutierrez, D.; Eisenberg, T.; Büttner, S.; Meisinger, C.; Kroemer, G.; Madeo, F. Apoptosis in Yeast: Triggers, Pathways, Subroutines. *Cell Death Differ* 2010, *17*, 763–773, doi:10.1038/cdd.2009.219.
262. Galluzzi, L.; Vitale, I.; Abrams, J.M.; Alnemri, E.S.; Baehrecke, E.H.; Blagosklonny, M.V.; Dawson, T.M.; Dawson, V.L.; El-Deiry, W.S.; Fulda, S.; et al. Molecular Definitions of Cell Death Subroutines: Recommendations of the Nomenclature Committee on Cell Death 2012. *Cell Death Differ* 2012, *19*, 107–120, doi:10.1038/cdd.2011.96.
263. Grosfeld, E.V.; Bidiuk, V.A.; Mitkevich, O.V.; Ghazy, E.S.M.O.; Kushnirov, V.V.; Alexandrov, A.I. A Systematic Survey of Characteristic Features of Yeast Cell Death Triggered by External Factors. *JoF* 2021, *7*, 886, doi:10.3390/jof7110886.
264. Liu, Y.; Levine, B. Autosis and Autophagic Cell Death: The Dark Side of Autophagy. *Cell Death Differ* 2015, *22*, 367–376, doi:10.1038/cdd.2014.143.
265. Camougrand, N.; Kissova, I.; Velours, G.; Manon, S. Uth1p: A Yeast Mitochondrial Protein at the Crossroads of Stress, Degradation and Cell Death. *FEMS Yeast Res* 2004, *5*, 133–140, doi:10.1016/j.femsyr.2004.05.001.
266. Eisenberg, T.; Carmona-Gutierrez, D.; Büttner, S.; Tavernarakis, N.; Madeo, F. Necrosis in Yeast. *Apoptosis* 2010, *15*, 257–268, doi:10.1007/s10495-009-0453-4.
267. Liang, Q.; Zhou, B. Copper and Manganese Induce Yeast Apoptosis via Different Pathways. *MBoC* 2007, *18*, 4741–4749, doi:10.1091/mbc.e07-05-0431.
268. Carmona-Gutiérrez, D.; Bauer, M.A.; Ring, J.; Knauer, H.; Eisenberg, T.; Büttner, S.; Ruckenstuhl, C.; Reisenbichler, A.; Magnes, C.; Rechberger, G.N.; et al. The Propeptide of Yeast Cathepsin D Inhibits Programmed Necrosis. *Cell Death Dis* 2011, *2*, e161–e161, doi:10.1038/cddis.2011.43.
269. Sheibani, S.; Richard, V.; Beach, A.; Leonov, A.; Feldman, R.; Mattie, S.; Khelghatybana, L.; Piano, A.; Greenwood, M.; Vali, H.; et al. Macromitophagy, Neutral Lipids Synthesis, and Peroxisomal Fatty Acid Oxidation Protect Yeast from "Liponecrosis", a Previously Unknown Form of Programmed Cell Death. *Cell Cycle* 2014, *13*, 138–147, doi:10.4161/cc.26885.

270. Stuknytė, M.; Guglielmetti, S.; Ricci, G.; Kuisienė, N.; Mora, D.; Parini, C.; Čitavičius, D. Identification Andin Silico Characterisation of Putative Conjugative Transfer Genes on *Geobacillus stearothermophilus* Plasmids. *Ann Microbiol* 2007, *57*, 407–414, doi:10.1007/BF03175081.
271. Malunavicius, V.; Druteika, G.; Sadauskas, M.; Veteikyte, A.; Matijosyte, I.; Lastauskiene, E.; Gegeckas, A.; Gudiukaite, R. Usage of GD-95 and GD-66 Lipases as Fusion Partners Leading to Improved Chimeric Enzyme LipGD95-GD66. *Int J Biol Macromol* 2018,*118*, 1594–1603, doi:10.1016/j.ijbiomac.2018.07.002.
272. Lastauskienė, E.; Zinkevičienė, A.; Girkontaitė, I.; Kaunietis, A.; Kvedarienė, V. Formic Acid and Acetic Acid Induce a Programmed Cell Death in Pathogenic *Candida* Species. *Curr Microbiol* 2014, *69*, 303–310, doi:10.1007/s00284-014-0585-9.
273. Kasemets, K.; Suppi, S.; Künnis-Beres, K.; Kahru, A. Toxicity of CuO Nanoparticles to Yeast *Saccharomyces cerevisiae* BY4741 Wild-Type and Its Nine Isogenic Single-Gene Deletion Mutants. *Chem Res Toxicol* 2013, *26*, 356–367, doi:10.1021/tx300467d.
274. Suarez-Arnedo, A.; Torres Figueroa, F.; Clavijo, C.; Arbeláez, P.; Cruz, J.C.; Muñoz-Camargo, C. An Image J Plugin for the High Throughput Image Analysis of in vitro Scratch Wound Healing Assays. *PLoS ONE* 2020, *15*, e0232565, doi:10.1371/journal.pone.0232565.
275. Vallar, S.; Houivet, D.; El Fallah, J.; Kervadec, D.; Haussonne, J.M. Oxide Slurries Stability and Powders Dispersion: Optimization with Zeta Potential and Rheological Measurements. *J Eur Ceram Soc* 1999, *19*, 1017–1021, doi:10.1016/S0955-2219(98)00365-3.
276. LeBel, C.P.; Ischiropoulos, H.; Bondy, S.C. Evaluation of the Probe 2‘,7‘-Dichiorofluorescin as an Indicator of Reactive Oxygen Species Formation and Oxidative Stress. *Chem Res Toxicol*, 1992, *5*, 227–31, doi: 10.1021/tx00026a012.
277. Elbahnasawy, M.A.; Shehabeldine, A.M.; Khattab, A.M.; Amin, B.H.; Hashem, A.H. Green Biosynthesis of Silver Nanoparticles Using Novel Endophytic *Rothia endophytica*: Characterization and Anticandidal Activity. *J Drug Deliv Sci Technol* 2021, *62*, 102401, doi:10.1016/j.jddst.2021.102401.
278. Bayır, H.; Anthonymuthu, T.S.; Tyurina, Y.Y.; Patel, S.J.; Amoscato, A.A.; Lamade, A.M.; Yang, Q.; Vladimirov, G.K.; Philpott, C.C.; Kagan, V.E. Achieving Life through Death: Redox Biology of Lipid Peroxidation in Ferroptosis. *Cell Chem Biol* 2020, *27*, 387–408, doi:10.1016/j.chembiol.2020.03.014.
279. Theodossiou, T.A.; Wälchli, S.; Olsen, C.E.; Skarpen, E.; Berg, K. Deciphering the Nongenomic, Mitochondrial Toxicity of Tamoxifens As Determined by Cell Metabolism and Redox Activity. *ACS Chem Biol* 2016, *11*, 251–262, doi:10.1021/acschembio.5b00734.

280. Henglein, A. Physicochemical Properties of Small Metal Particles in Solution: "Microelectrode" Reactions, Chemisorption, Composite Metal Particles, and the Atom-to-Metal Transition. *J Phys Chem* 1993, *97*, 5457–5471, doi:10.1021/j100123a004.
281. Sastry, M.; Mayya, K.S.; Bandyopadhyay, K. pH Dependent Changes in the Optical Properties of Carboxylic Acid Derivatized Silver Colloidal Particles. *Colloids Surf A: Physicochem Eng Asp* 1997, *127*, 221–228, doi:10.1016/S0927-7757(97)00087-3.
282. Patil, V.; Sastry, M. Electrostatically Controlled Diffusion of Carboxylic Acid Derivatized Q-State CdS Nanoparticles in Thermally Evaporated Fatty Amine Films. *J Chem Soc Faraday Trans* 1997, *93*, 4347–4353, doi:10.1039/a704355d.
283. Austin, L.A.; MacKey, M.A.; Dreaden, E.C.; El-Sayed, M.A. The Optical, Photothermal, and Facile Surface Chemical Properties of Gold and Silver Nanoparticles in Biodiagnostics, Therapy, and Drug Delivery. *Arch Toxicol* 2014, *88*, 1391–1417, doi:10.1007/s00204-014-1245-3.
284. Bhainsa, K.C.; D'Souza, S.F. Extracellular Biosynthesis of Silver Nanoparticles Using the Fungus *Aspergillus fumigatus*. *Colloids Surf B Biointerfaces* 2006, *47*, 160–164, doi:10.1016/J.COLSURFB.2005.11.026.
285. Elbeshehy, E.K.F.; Elazzazy, A.M.; Aggelis, G. Silver Nanoparticles Synthesis Mediated by New Isolates of Bacillus spp., Nanoparticle Characterization and Their Activity against Bean Yellow Mosaic Virus and Human Pathogens. *Front Microbiol* 2015, *6*, doi:10.3389/fmicb.2015.00453.
286. John, M.S.; Nagoth, J.A.; Ramasamy, K.P.; Mancini, A.; Giuli, G.; Miceli, C.; Pucciarelli, S. Synthesis of Bioactive Silver Nanoparticles Using New Bacterial Strains from an Antarctic Consortium. *Marine Drugs* 2022, *20*, doi:10.3390/md20090558.
287. Elamawi, R.M.; Al-Harbi, R.E.; Hendi, A.A. Biosynthesis and Characterization of Silver Nanoparticles Using *Trichoderma longibrachiatum* and Their Effect on Phytopathogenic Fungi. *Egypt J Biol Pest Co* 2018, *28*, doi:10.1186/s41938-018-0028-1.
288. Alsamhary, K.I. Eco-Friendly Synthesis of Silver Nanoparticles by *Bacillus subtilis* and Their Antibacterial Activity. *Saudi J Biol Sci* 2020, *27*, 2185–2191, doi:10.1016/j.sjbs.2020.04.026.
289. Singh, H.; Du, J.; Singh, P.; Yi, T.H. Extracellular Synthesis of Silver Nanoparticles by *Pseudomonas* sp. THG-LS1.4 and Their Antimicrobial Application. *J Pharm Anal* 2018, *8*, 258–264, doi:10.1016/j.jpha.2018.04.004.
290. Shankar, A.; Kumar, V.; Kaushik, N.K.; Kumar, A.; Malik, V.; Singh, D.; Singh, B. Sporotrichum Thermophile Culture Extract-Mediated Greener Synthesis of Silver Nanoparticles: Eco-Friendly Functional

Group Transformation and Anti-Bacterial Study. *Curr Res Green Sustain Chem* 2020, *3*, 100029, doi:10.1016/j.crgsc.2020.100029.
291. Romano, I.; Vitiello, G.; Gallucci, N.; Di Girolamo, R.; Cattaneo, A.; Poli, A.; Di Donato, P. Extremophilic Microorganisms for the Green Synthesis of Antibacterial Nanoparticles. *Microorganisms* 2022, *10*, 1885, doi:10.3390/microorganisms10101885.
292. Deljou, A.; Goudarzi, S. Green Extracellular Synthesis of the Silver Nanoparticles Using Thermophilic *Bacillus* sp. AZ1 and Its Antimicrobial Activity Against Several Human Pathogenetic Bacteria. *Iran J Biotechnol* 2016, *14*, 25–32, doi:10.15171/ijb.1259.
293. Parvekar, P.; Palaskar, J.; Metgud, S.; Maria, R.; Dutta, S. The Minimum Inhibitory Concentration (MIC) and Minimum Bactericidal Concentration (MBC) of Silver Nanoparticles against *Staphylococcus aureus*. *Biomater Investig Dent* 2020, *7*, 105–109, doi:10.1080/26415275.2020.1796674.
294. Tyavambiza, C.; Elbagory, A.M.; Madiehe, A.M.; Meyer, M.; Meyer, S. The Antimicrobial and Anti-Inflammatory Effects of Silver Nanoparticles Synthesised from *Cotyledon orbiculata* Aqueous Extract. *Nanomaterials* 2021, *11*, 1343, doi:10.3390/nano11051343.
295. Ahmed, F.; Qayyum, S.; Husain, Q. Benign Nano-Assemblages of Silver Induced by β Galactosidase with Augmented Antimicrobial and Industrial Dye Degeneration Potential. *Mater Sci Eng C Mater Biol Appl* 2018, *91*, 570–578, doi:10.1016/j.msec.2018.05.077.
296. Khan, S.; Rukayadi, Y.; Jaafar, A.H.; Ahmad, N.H. Antibacterial Potential of Silver Nanoparticles (SP-AgNPs) Synthesized from *Syzygium polyanthum* (Wight) Walp. against Selected Foodborne Pathogens. *Heliyon* 2023, *9*, e22771, doi:10.1016/j.heliyon.2023.e22771.
297. Lara, H.H.; Ayala-Núñez, N.V.; Ixtepan Turrent, L.D.C.; Rodríguez Padilla, C. Bactericidal Effect of Silver Nanoparticles against Multidrug-Resistant Bacteria. *World J Microbiol Biotechnol* 2010, *26*, 615–621, doi:10.1007/s11274-009-0211-3.
298. Mare, A.D.; Ciurea, C.N.; Man, A.; Mareș, M.; Toma, F.; Berța, L.; Tanase, C. In vitro Antifungal Activity of Silver Nanoparticles Biosynthesized with Beech Bark Extract. *Plants* 2021, *10*, 2153, doi:10.3390/plants10102153.
299. Mare, A.D.; Man, A.; Ciurea, C.N.; Toma, F.; Cighir, A.; Mareș, M.; Berța, L.; Tanase, C. Silver Nanoparticles Biosynthesized with Spruce Bark Extract—A Molecular Aggregate with Antifungal Activity against *Candida* Species. *Antibiotics* 2021, *10*, 1261, doi:10.3390/antibiotics10101261.
300. Novickij, V.; Švedienė, J.; Paškevičius, A.; Markovskaja, S.; Girkontaitė, I.; Zinkevičienė, A.; Lastauskienė, E.; Novickij, J. Pulsed Electric Field-Assisted Sensitization of Multidrug-Resistant *Candida*

albicans to Antifungal Drugs. *Future Microbiol* 2018, *13*, 535–546, doi:10.2217/fmb-2017-0245.
301. Novickij, V.; Švedienė, J.; Paškevičius, A.; Markovskaja, S.; Lastauskienė, E.; Zinkevičienė, A.; Girkontaitė, I.; Novickij, J. Induction of Different Sensitization Patterns of MRSA to Antibiotics Using Electroporation. *Molecules* 2018, *23*, 1799, doi:10.3390/molecules23071799.
302. Muñoz, N.M.; Minhaj, A.A.; Dupuis, C.J.; Ensor, J.E.; Golardi, N.; Jaso, J.M.; Dixon, K.A.; Figueira, T.A.; Galloway-Peña, J.R.; Hill, L.; et al. What Are the Effects of Irreversible Electroporation on a *Staphylococcus aureus* Rabbit Model of Osteomyelitis? *Clin Orthop Relat Res* 2019, *477*, 2367–2377, doi:10.1097/CORR.0000000000000882.
303. Novickij, V.; Zinkevičienė, A.; Perminaitė, E.; Čėsna, R.; Lastauskienė, E.; Paškevičius, A.; Švedienė, J.; Markovskaja, S.; Novickij, J.; Girkontaitė, I. Non-Invasive Nanosecond Electroporation for Biocontrol of Surface Infections: An in vivo Study. *Sci Rep* 2018, *8*, 14516, doi:10.1038/s41598-018-32783-7.
304. Dolat, E.; Rajabi, O.; Salarabadi, S.S.; Yadegari-Dehkordi, S.; Sazgarnia, A. Silver Nanoparticles and Electroporation: Their Combinational Effect on *Leishmania major*. *Bioelectromagnetics* 2015, *36*, 586–596, doi:10.1002/bem.21945.
305. Vazquez-Muñoz, R.; Meza-Villezcas, A.; Fournier, P.G.J.; Soria-Castro, E.; Juarez-Moreno, K.; Gallego-Hernández, A.L.; Bogdanchikova, N.; Vazquez-Duhalt, R.; Huerta-Saquero, A. Enhancement of Antibiotics Antimicrobial Activity Due to the Silver Nanoparticles Impact on the Cell Membrane. *PLoS ONE* 2019, *14*, e0224904, doi:10.1371/journal.pone.0224904.
306. Lee, B.; Lee, M.J.; Yun, S.J.; Kim, K.; Choi, I.H.; Park, S. Silver Nanoparticles Induce Reactive Oxygen Species-Mediated Cell Cycle Delay and Synergistic Cytotoxicity with 3-Bromopyruvate in Candida albicans, but Not in *Saccharomyces cerevisiae*. *IJN* 2019, *14*, 4801–4816, doi:10.2147/IJN.S205736.
307. Zhou, L.; Zhao, X.; Li, M.; Lu, Y.; Ai, C.; Jiang, C.; Liu, Y.; Pan, Z.; Shi, J. Antifungal Activity of Silver Nanoparticles Synthesized by Iturin against *Candida albicans* in vitro and in vivo. *Appl Microbiol Biotechnol* 2021, *105*, 3759–3770, doi:10.1007/s00253-021-11296-w.
308. Hwang, I.; Lee, J.; Hwang, J.H.; Kim, K.; Lee, D.G. Silver Nanoparticles Induce Apoptotic Cell Death in *Candida albicans* through the Increase of Hydroxyl Radicals. *FEBS J* 2012, *279*, 1327–1338, doi:10.1111/j.1742-4658.2012.08527.x.
309. Prateeksha; Singh, B.; Gupta, V.; Deeba, F.; Bajpai, R.; Pandey, V.; Naqvi, A.; Upreti, D.; Gathergood, N.; Jiang, Y.; et al. Non-Toxic and Ultra-Small Biosilver Nanoclusters Trigger Apoptotic Cell Death in

Fluconazole-Resistant *Candida albicans* via Ras Signaling. *Biomolecules* 2019, *9*, 47, doi:10.3390/biom9020047.
310. Babele, P.K.; Singh, A.K.; Srivastava, A. Bio-Inspired Silver Nanoparticles Impose Metabolic and Epigenetic Toxicity to *Saccharomyces cerevisiae*. *Front Pharmacol* 2019, *10*, 1016, doi:10.3389/fphar.2019.01016.
311. Galandáková, A.; Franková, J.; Ambrožová, N.; Habartová, K.; Pivodová, V.; Zálešák, B.; Šafářová, K.; Smékalová, M.; Ulrichová, J. Effects of Silver Nanoparticles on Human Dermal Fibroblasts and Epidermal Keratinocytes. *Hum Exp Toxicol* 2016, *35*, 946–957, doi:10.1177/0960327115611969.
312. Salesa, B.; Assis, M.; Andrés, J.; Serrano-Aroca, Á. Carbon Nanofibers versus Silver Nanoparticles: Time-Dependent Cytotoxicity, Proliferation, and Gene Expression. *Biomedicines* 2021, *9*, 1155, doi:10.3390/biomedicines9091155.

SANTRAUKA

Įvadas

Nuolat didėjantis bakterijų ir mieliagrybių atsparumas priešmikrobinei terapijai verčia ieškoti naujų priemonių kovojant su bakterinėmis ir grybelinėmis infekcijomis. Dėl visuomenės senėjimo ir daugėjant žmonių, kenčiančių nuo su imunitetu susijusių sutrikimų, bei kitų priežasčių, didėja sergančiųjų odos ligomis skaičius. Dauguma ant odos esančių mikroorganizmų yra komensalai ir nors manoma, kad daugelis šių odą kolonizuojančių komensalų yra nekenksmingi, žmonėms su susilpnėjusia imunine sistema jie gali sukelti rimtų odos ligų [1]. Disbiozė arba odos mikrobiotos disbalansas dažnai yra daugelio odos ligų priežastis [2].

Dėl disbiozės *Candida* infekcijos tampa vis dažnesnės ir sukelia rimtų padarinių žmonėms, turintiems autoimuninių ar su imunitetu susijusių sutrikimų [3]. Be to, ši jautri žmonių grupė dažnai ilgą laiką praleidžia ligoninėse, o *Candida* mielės ant medicininės įrangos, reikalingos pacientams gydyti, gali suformuoti bioplėveles, kurios gali sutrikdyti gydymą [5]. Nors *Candida albicans* yra daugelio tyrimų objektas, susirūpinimą kelia vis didėjantis ne-*albicans* sukeliamų ligų skaičius. Neatidėliotina problema yra šių rūšių atsparumas flukanazolui ir amfotericinui B [6].

Odos ligos, kurias sukelia mieliagrybiai, nėra vienintelė problema. Dažnas ir netinkamas antibiotikų vartojimas leido bakterijoms išvystyti atsparumo mechanizmus [8]. Infekcijas, sukeltas bakterijų pasižyminčių daugybiniu atsparumu antibiotikams, sunku gydyti taikant šiuolaikinę antibiotikų terapiją, todėl tokioms infekcijoms būdingas didelis sergamumas ir mirštamumas [9]. Visos šios priežastys skatina ieškoti alternatyvų šiuo metu vartojamiems vaistams.

Išskirtinės fizikinės ir cheminės sidabro nanodalelių (AgND) savybės yra plačiai pripažintos ir gali būti naudojamos įvairiais tikslais. AgND tampa vis svarbesnės antimikrobinėje terapijoje dėl didėjančio mikroorganizmų atsparumo šiuo metu naudojamoms priešmikrobinėms medžiagoms. AgND gamybai gali būti naudojami fizikiniai ir cheminiai metodai, tačiau jie yra kenksmingi aplinkai ir sukuria šalutinius produktus. Taigi, AgND gavimui dabar yra pritaikomi ir biologiniai metodai, kurie yra draugiškesni aplinkai [10]. Pakankamai žinoma apie AgND, gaunamas naudojant augalus, grybelius ir mezofilines bakterijas, tačiau vis dar mažai žinoma apie AgND, gaunamas naudojant termofilines bakterijas. Taigi, šioje disertacijoje aprašoma

termofilinių *Geobacillus* spp. bakterijų indukuojama AgND sintezė, šių AgND savybės ir priešmikrobinis potencialas.

Vienas pagrindinių AgND privalumų, palyginus su šiuo metu vartojamais vaistais, yra kompleksinis priešmikrobinis poveikis. Jos veikia įvairias ląstelės dalis, tokias kaip ląstelės sienelė, membranos, baltymai, DNR ir fermentai, taip sutrikdydamos įvairias ląstelės funkcijas. Be to, jos sukelia oksidacinį stresą, kuris dar labiau sustiprina AgND priešmikrobinį poveikį [11]. Skirtingais metodais gautų AgND priešmikrobinis mechanizmas gali skirtis, todėl svarbu nustatyti, kaip ši priešmikrobinė medžiaga veikia ląsteles [12]. Šiuo tikslu, disertacijoje yra nustatomas AgND poveikis membranoms, ROS generacijai ir lipidų peroksidacijai bei ar sustiprėja kaspazių aktyvacija po poveikio AgND (t.y., ar vyksta programuota ląstelių žūtis).

Tačiau, nors AgND plačiai naudojamos kosmetikoje, AgND naudojimas ligoms gydyti kelia susirūpinimų. Kadangi jos neturi vieno konkretaus taikinio ląstelėje, AgND gali pakenkti ir žmogaus ląstelėms, daugiausiai sukeldamos oksidacinį stresą. Todėl nerimaujama, kad AgND gali pažeisti žmogaus organus. Atlikti tyrimai rodo, kad ši savybė gali priklausyti nuo AgND gavimo būdo, jų dydžio, formos bei kitų savybių [13–15]. Šiuo tikslu šioje disertacijoje taip pat nustatomas toksinis poveikis žmogaus keratinocitų ląstelėms ir šių ląstelių migracijai po poveikio AgND.

Tikslas

Pritaikyti sidabro nanodaleles, gautas taikant termofilinių *Geobacillus* spp. bakterijų indukuotą sintezę, su žmogaus odos ligomis susijusių mikroorganizmų biokontrolei.

Uždaviniai:

1. Optimizuoti AgND sintezę naudojant termofilines *Geobacillus* spp. bakterijas;
2. Nustatyti, ar gautos AgND turi priešmikrobinių savybių prieš odos patogeninius mikroorganizmus (*Staphylococcus aureus*, *Streptococcus pyogenes*, *Pseudomonas aeruginosa*, *Candida guilliermondii*);
3. Įvertinti, ar elektroporacija sustiprina šių AgND priešmikrobinį poveikį;
4. Nustatyti AgND sukeltos ląstelių žūties mikroorganizmuose mechanizmą;

5. Nustatyti, ar gautų AgND koncentracija, kuri veikia mikroorganizmus, turi citotoksinį poveikį žmogaus keratinocitų ląstelėms.

Darbo svarba ir mokslinis naujumas

Nors *Geobacillus* spp. bakterijos jau buvo panaudotos sidabro nanodalelių sintezei [16], vis dar yra mažai žinoma apie jų antimikrobines savybes ir pritaikymą realybėje. Šioje disertacijoje pateikiama išsami AgND, gautų *Geobacillus* spp. bakterijų indukuotos sintezės būdu, analizė ir jų priešmikrobinis potencialas.

Taip pat yra mažai informacijos apie AgND poveikį odos patogenams, ypač *S. pyogenes* ir *C. guilliermondii*, kuri yra pateikiama šiame darbe. Literatūroje yra daug duomenų apie AgND, gautų naudojant cheminius, fizikinius ir biologinius metodus, priešmikrobinio poveikio mechanizmą, tačiau vis dar nėra informacijos apie AgND, gautų naudojant termofilinius mirkoorganizmus, poveikio mechanizmą. Šioje disertacijoje aprašomi galimi antimikrobinio poveikio mechanizmai prieš odos patogenines bakterijas ir mieles. Taigi, šis darbas praplečia žinias apie AgND, gautų naudojant termofilinius mikroorganizmus, priešmikrobines savybes.

Kadangi AgND naudojimas, dėl veikliųjų koncentracijų ir galimo citotoksinio poveikio, ligų gydymui kelia susirūpinimų, šioje disertacijoje pirmą kartą buvo pritaikytas AgND ir elektroporacijos derinys, sustiprinantis šios nanomedžiagos antimikrobinį poveikį.

Šiame darbe taip pat pirmą kartą įvertintas AgND, gautų naudojant termofilines *Geobacillus* spp. bakterijas, citotoksinis poveikis žmogaus keratinocitų ląstelėms. Tai leidžia įvertinti, ar šias AgND yra saugu naudoti patogeninės odos mikrobiotos biokontrolei realiame gyvenime.

Ginamieji teiginiai:

1. Termofilinės *Geobacillus* spp. bakterijos yra tinkamos sidabro nanodalelių sintezei;
2. AgND, gautos naudojant *Geobacillus* spp. bakterijas, turi priešmikrobinių savybių prieš patogeninius mikroorganizmus;
3. Elektroporacija sustiprina priešmikrobinį AgND poveikį;
4. AgND, gautos naudojant *Geobacillus* spp. bakterijas, veikia mikroorganizmų ląstelių membranas, sustiprina ROS generaciją ir sukelia programuotą mielių ląstelių mirtį;

5. 5 μg/mL koncentracijos AgND, gautos naudojant *Geobacillus* spp. bakterijas, neturi citotoksinio poveikio žmogaus keratinocitų ląstelėms.

Metodai

Ekstraląstelinė sidabro nanodalelių sintezė

Geobacillus spp. kamienai auginami aerobinėmis sąlygimis 100 mL skystoje *Geobacillus* sp. kultivavimo terpėje 250 mL Erlenmejerio kolbose. Kultūros auginamos orbitinėje purtyklėje (Esco, Singapūras) 55 °C temperatūroje, aeruojant 180 aps./min. Po 48 val. inkubacijos ląstelės atskiriamos 10 min. centrifuguojant 16 000× *g*. Supernatantai be ląstelių naudojami kaip medžiaga AgND sintezei. Į surinktus *Geobacillus* spp. supernatantus pridedama galutinės koncentracijos 2 mM $AgNO_3$. Visi mišiniai inkubuojami orbitinėje purtyklėje 48 val. 55 °C temperatūroje ir 200 aps./min. Supernatantai be $AgNO_3$ ir bakterijų kultivavimo terpė, papildyta 2 mM $AgNO_3$, naudojami kaip kontrolės. Po 48 val. inkubacijos mišiniai centrifuguojami 3000× *g* 10 min., kad būtų pašalinti terpės komponentai. AgND surinkimui, mišiniai centrifuguojami 16 000× *g* greičiu 15 min. Nekonvertuotų sidabro jonų ir kitų priemaišų pašalinimui, gautos AgND tris kartus plaunamos 70 % etanoliu ir tris kartus dejonizuotu vandeniu, centrifuguojant 16 000× *g* 15 min.

„Lašelių testas“, skirtas nustatyti mažiausią AgND inhibicinę koncentraciją (MIK) prieš odos patogenines bakterijas ir mieles

„Lašelių testas“, siekiant nustatyti AgND MIK, buvo atliktas pagal Kasemets et al. [273]. Mikroorganizmų kultūra auginama aerobiniu būdu 5 mL skystoje LB (*S. aureus*, *S. pyogenes*, *P. aeruginosa*) arba YPD (*C. guilliermondii*) terpėje, kol ji pasiekia OD_{600}=1 esant 37 °C arba 30 °C temperatūrai. 1 mL užaugintų mikroorganizmų kultūros tris kartus plaunamas centrifuguojant ir pakartotinai resuspenduojant 1 M sorbitolio tirpale. 100 μL paruoštos mikroorganizmų kultūros suspensijos išpilstoma į 96 šulinėlių plokštelę. Toliau pridedama po 100 μL skirtingų koncentracijų *Geobacillus* spp. 18, 25, 95 ir 612 kamienų AgND. Kaip kontrolė naudojama 100 μL paruoštos mikroorganizmų suspensijos ir 100 μL 1 M sorbitolio. Plokštelė 24 val. inkubuojama 35 °C (bakterijoms) arba 30 °C (mielėms) temperatūros termostate. Po inkubacijos 5 μL iš kiekvieno šulinėlio perkeliama ant agarizuotos LB (bakterijoms) arba YPD (mielėms) terpės ir inkubuojama

esant tomis pačiomis temperatūromis. Rezultatai vertinami po 24 val. (bakterijoms) arba po 48 val. (mielėms).

Odos patogenų elektroporacija

Tiriamos bakterijos ir mielės auginamos 5 mL skystoje LB arba YPD terpėje 25 mL mėgintuvėliuose. Kultūros auginamos orbitinėje purtyklėje atitinkamai 37 °C arba 30 °C temperatūroje, kol pasiekia eksponentinę fazę. Tada kultūros paruošiamos elektroporacijai: tris kartus plaunamos dejonizuotu vandeniu ir tris kartus 1 M sorbitolio tirpalu. Ląstelės praskiedžiamos 1 M sorbitolio tirpalu, kad galutinė ląstelių koncentracija suspensijoje būtų $1,5 \times 10^4$ KFV/mL. Tada 80 µL ląstelių suspensijos perkeliama į elektroporacijai skirtą kiuvetę. Ląstelės veikiamos vienu 100 µs elektrinio lauko impulsu, kurio PEF amplitudė yra nuo 2,5 iki 15 kV/cm (2,5 kV/cm žingsnis). Kaip kontrolė naudojamos elektroporacija nepaveiktos ląstelės. Po elektroporacijos ląstelių suspensija perkeliama ant agarizuotos LB arba YPD (pagal mikroorganizmo tipą) terpės ir inkubuojama 24 val. 35 °C (bakterijoms) arba 48 val. 30 °C (mielėms) termostate. Rezultatai vertinami skaičiuojant KFV.

ROS generacijos mikroorganizmų ląstelėse nustatymas po poveikio sidabro nanodalelėmis

Mikroorganizmų kultūros auginamos aerobinėmis sąlygomis skystoje YPD terpėje 30 °C (mielėms) arba skystoje LB terpėje 37 °C (bakterijoms) iki mikroorganizmų kultūra pasiekia eksponentinę fazę. Toliau ląstelės du kartus centrifuguojant ir resuspenduojant plaunamos 1 M sorbitolio tirpalu. Tada ląstelės paruošiamos ROS generacijos analizei naudojant modifikuotą DCFDA/H_2DCDFA-Cellular ROS Assay Kit (ab113851) protokolą. Mėginiai praskiedžiami iki 1×10^4 KFV/mL. Ląstelės plaunamos ir suspenduojamos 1 × Buffer prieš dažymą, o pridėjus 20 µM DCFDA dažo inkubuojamos 2 val. 30 °C temperatūroje. Po to ląstelės paveikiamos AgND ir inkubuojamos 30 °C temperatūroje 15 min. (*C. guilliermondii*) arba 1 val. (bakterijoms ir *S. cerevisiae*). AgND nepaveiktos ląstelės naudojamos kaip neigiama kontrolė. Po to ląstelės du kartus plaunamos 1 × Buffer. Toliau mėginiai analizuojami VU GMC Biochemijos institute „FACSort“ (*C. guilliermondii*) arba su VU GMC Biotechnologijos institute „BD FACSymphony™ A1“ tėkmės citometru (bakterijoms ir *S. cerevisiae*) (sužadinimo bangos ilgis 488 nm, emisijos bangos ilgis 535 nm). Analizuojamas 20 000 ląstelių mėginys. Analizei naudota „Flowing Software 2.5.1“ programa.

Ląstelių membranų pralaidumo pokyčių įvertinimas

Mikroorganizmų ląstelių membranų pralaidumo pokyčiai nustatyti ląsteles dažant propidžio jodidu (PI). Po 30 min. poveikio *Geobacillus* spp. 25 ir 612 AgND, ląstelės plaunamos centrifuguojant ir resuspenduojant 1 × PBS buferyje. Toliau ląstelės dažomos pridedant 1 µL PI (1 mg/mL). Ląstelės su dažu inkubuojamos 10 min. kambario temperatūroje. Po inkubacijos ląstelės plaunamos 1 × PBS buferiu ir fiksuojamos 10 % buferiniu formaldehidu 30 min. *C. guilliermondii*, *S. aureus* ir *S. pyogenes* atveju fluorescencija matuojama „BD FACSymphony™ A1“ tėkmės citometru (sužadinimo bangos ilgis 488 nm, emisijos bangos ilgis 535 nm). Analizuojamas 20 000 ląstelių mėginys. Analizei naudota „Flowing Software 2.5.1“ programa. *S. cerevisiae* ir *P. aeruginosa* atveju mėginio lašas perkeliamas ant poli-L-lizinu padengto stikliuko, uždengto dengiamuoju stikleliu. Mėginiai analizuojami naudojant VU GMC Biomokslų instituto „Olympus IX83“ inversinės šviesos mikroskopą.

Aktyvių kaspazių identifikavimas

Aktyvios kaspazės mielių ląstelėse identifikuojamos naudojant CaspACE™ FITC-VAD-FMK In Situ Marker rinkinį. Po apoptozės indukcijos ląstelės tris kartus plaunamos centrifuguojant ir resuspenduojant 1 × PBS buferiu. Po plovimo mielių ląstelės suspenduojamos 1 mL 1 × PBS buferyje ir 300 µL ląstelių suspensijos perkeliamos į naują mėgintuvėlį. Po to pridedama 1 µL FITC-VAD-FMK dažo ir inkubuojama 30 min. (*S. cerevisiae*) arba 1 val. (*C. guilliermondii*) 30 °C temperatūroje. Po inkubacijos ląstelės tris kartus plaunamos centrifuguojant ir resuspenduojant 1 × PBS buferiu. Toliau ląstelės fiksuojamos 10 % buferiniu formaldehidu 30 min. kambario temperatūroje. Po fiksacijos ląstelės tris kartus plaunamos centrifuguojant ir resuspenduojant 1 × PBS buferiu. Lašas mėginio perkeliamas ant stikliuko, padengto poli-L-lizinu, uždengto dengiamuoju stikleliu. Mėginiai analizuojami VU GMC Biomokslų institute „Nikon eclipse 80*i*“ fluorescenciniu mikroskopu. Tėkmės citometrijos matavimams buvo naudojamas BD FACSymphony™ A1 tėkmės citometras (sužadinimo bangos ilgis 488 nm, emisijos bangos ilgis 535 nm). Analizei naudojama „Flowing Software 2.5.1“.

Sidabro nanodalelių citotoksiškumo įvertinimas MTT metodu

Keratinocitų (Ker-CT) ląstelės nuplaunamos ir prilipusios ląstelės atskiriamos nuo paviršiaus, kaip aprašyta 2.5.16 skyrelyje. Po to kai ląstelės centrifuguojamos ir nupilamas supernatantas, ląstelių skaičius 1 mL suspensijos yra suskaičiuojamas naudojant šviesinį mikroskopą ir Neubauerio skaičiavimo kamerą. Suskaičiuotos ląstelės praskiedžiamos iki 1,4–1,7 × 10^5 ląstelių/mL koncentracijos. Gauta ląstelių suspensija po 200 µL supilstoma į 96 šulinėlių plokštelę. Plokštelė 24 val. inkubuojama termostate (37 °C, 5 % CO_2, 95 % drėgmė).

Po inkubacijos, įvertinus ląstelių sukibimą šulinėliuose (monosluoksnio susiformavimą) naudojant inversinį mikroskopą (konfluencija turi siekti 70–80 %), šulinėliai papildomi skirtingomis *Geobacillus* sp. 612 kamieno AgND koncentracijomis (5, 10, 15, 20 ir 25 µg/mL) ir po 200 µL Ker-CT mitybinės terpės. Kiekvienai koncentracijai naudojama po tris šulinėlius. Plokštelė 24 val. inkubuojama termostate (37 °C, 5 % CO_2, 95 % drėgmė).

Po inkubacijos *Geobacillus* sp. 612 AgND citotoksinis poveikis vertinamas naudojant 3-(4,5-dimetiltiazol-2-il)-2,5-difeniltetrazolio bromido (MTT) metodą. Naudojamas 5 mg/mL MTT dažas (MTT dažas sumaišomas su PBS buferiu), kuris prieš naudojimą pašildomas 37 °C vandens vonelėje. Labai atsargiai, nuo šulinėlio kraštų *Geobacillus* sp. AgND ir terpės mišiniai surenkami ir palunami PBS. 200 µL PBS supilamas į šulinėlius su ląstelėmis ir nedelsiant surenkamas. Šis procesas kartojamas du kartus. Prideda 50 µL MTT tirpalo ir inkubuojama 1 val. 37 °C termostate (5 % CO_2, 95 % drėgmė). Po inkubacijos MTT tirpalas surenkamas iš šulinėlių. Gautas mėlynas junginys iš ląstelių eliuuojamas 50 µL 96 % etilo alkoholiu. Į keletą šulinėlių supilama po 50 µL etilo alkoholio (rezultatų analizės fonas). Rezultatai plokštelėje vertinami spektrofotometriškai (OT_{570}).

Sidabro nanodalelių įtakos keratinocitų proliferaciniam aktyvumui tyrimas

Kai Ker-CT ląstelės pasiekia 70–80 % konfluenciją, ląstelės paveikiamos *Geobacillus* sp. 612 kamieno AgND 24, 48 ir 72 val. Ląstelių skaičius 1 mL įvertinamas ir apskaičiuojamas naudojantis šviesiniu mikroskopu ir Neubauerio skaičiavimo kamera. Suskaičiuotos ląstelės praskiedžiamos iki 7×10^4–$1{,}1 \times 10^5$ ląstelių/mL koncentracijos. Gauta ląstelių suspensija po 200 µL supilstoma į 96 šulinėlių plokštelę. Plokštelė 24 val. inkubuojama termostate (37 °C, 5 % CO_2, 95 % drėgmė). Kai ląstelės pasiekia 70 % konfluenciją, pradinė terpė pakeičiama šviežia Ker-CT mitybine terpe,

papildyta skirtingomis *Geobacillus* sp. 612 kamieno AgND koncentracijomis ir plokštelė inkubuojama 24, 48 ir 72 val. Pasibaigus inkubacijai atliekamas MTT metodas.

Rezultatai

Ekstraląstelinė sidabro nanodalelių biosintezė ir jų charakterizavimas

Šiame darbe keturi *Geobacillus* spp. kamienai (18, 25, 95 ir 612) buvo atrinkti tolimesnei AgND gamybai. Tyrimai parodė, kad šie *Geobacillus* spp. kamienai sėkmingai indukavo AgND sintezę. Bakterijų supernarantų spalva pasikeitė iš šviesiai rudos į tamsiai rudą po 48 val. inkubacijos su vandeniniu 2 mM koncentracijos $AgNO_3$ tirpalu 55 °C temperatūroje. Šis spalvos pokytis rodo Ag^+ jonų redukciją ir AgND susidarymą. Vienas iš labiausiai paplitusių AgND struktūrinių charakteristikų nustatymo metodų yra UV–Vis spektroskopija, kuri buvo naudojama patvirtinti AgND susidarymą [134]. AgND būdingas pikas buvo matomas 410–425 nm diapozone visuose keturiuose tirtuose mėginiuose (**Fig. 3.1.**). Bakterijų auginimo terpėje (kontrolinis mėginys), paveiktoje 2 mM $AgNO_3$, buvo pastebėtas spalvos pasikeitimas nuo šviesiai rudos iki žalsvai rudos, tačiau po centrifugavimo nebuvo pastebėta susidariusių agregatų. Taip pat buvo atlikta ir gautų AgND SEM analizė, kuri parodė, kad pagamintos dalelės yra sferinės (**Fig. 3.2.**).

Siekiant nustatyti gautų AgND dydį ir dydžio pasiskirstymą, buvo atlikta DLS analizė. Kiekvieno *Geobacillus* spp. kamieno AgND mėginiui buvo atlikta po 100 atskirų matavimų. Rezultatai parodė, kad didžiosios dalies gautų AgND skersmuo yra mažesnis nei 100 nm. Tačiau buvo nustatyta ir agregatų, o dalelių dydžio pasiskirstymas yra gana platus (**Fig. 3.3a**). Kadangi tiriant *Geobacillus* spp. AgND priešmikrobinį poveikį jos yra dedamos į mikroorganizmų mitybines terpes ar sorbitolio tirpalą, šių AgND dydžiai taip pat buvo pamatuoti ir painkubavus jas šiose terpėse. Rezultatai rodo, kad po AgND inkubacijos mitybinėse terpėse arba sorbitolio tirpale susidaro daugiau agregatų, nei vandenyje (**Fig. 3.3b**, **Fig. 3.3c** ir **Fig. 3.3d**). Šiuos skirtumus galima paaiškinti tuo, kad terpėse gausu maistinių medžiagų (cukrų, peptidų, druskų ir kt.), galinčių sukelti atskirų dalelių agregaciją.

Siekiant paaiškinti dalelių agregaciją dispersijose, buvo atlikti papildomi zeta potencialo matavimai esant 25 °C temperatūrai, naudojant Smoluchowski modelį. Rezultatai parodė, kad visų naudotų *Geobacillus* spp. kamienų AgND zeta potencialai yra neigiami ir svyruoja tarp −25 ir −31 mV vandeninėje aplinkoje (**Table 3.1.**). Laikoma, kad jei absoliuti ND zeta potencialo vertė yra didesnė nei 30 mV, jos yra stabilios [275]. Kadangi *Geobacillus* sp. 25

kamieno AgND zeta potencialo vertė yra −31,28 ± 0,47 mV ir turi mažiausiai agregatų (apie 1 %), duomenys sutampa su šia teorija.

Zeta potencialo vertės taip pat buvo įvertintos ir po AgND inkubacijos (12 val.) 1 M sorbitolio tirpale ir LB bei YPD mitybinėse terpėse (**Table 3.1.**). Visais atvejais galima pastebėti, kad *Geobacillus* spp. AgND zeta potencialo vertės pasikeitė, tačiau jos rodo, kad dalelės yra stabilios. Šių verčių pokyčiai galimi dėl to, kad tirpaluose, ypač mitybinėse terpėse, yra cukrų, druskų, peptidų ir kitų priemaišų, kurios keičia šių AgND biologinį prieinamumą ir aktyvumą.

MIK nustatymas prieš odos patogenus naudojant „lašelių testą“

Kasemets et al. pasiūlė „lašelių testą“, kad būtų galima nustatyti AgND MIK prieš mikroorganizmus [273]. Šis metodas buvo pritaikytas nustatyti MIK prieš odos patogenus (bakterijas *S. aureus*, *S. pyogenes* ir *P. aeruginosa* ir mieles *C. guilliermondii*). MIK nustatomos vizualiai, kai po inkubacijos su AgND nėra matomos tiriamo mikroorganizmo kolonijos ant agarizuotos terpės. Eksperimentas kiekvienam mikroorganizmui su kiekvieno *Geobacillus* spp. kamieno AgND buvo pakartotas mažiausiai tris kartus.

Gauti rezultatai rodo, kad prieš patogeninius mikroorganizmus geriausiai veikė *Geobacillus* sp. 612 kamieno AgND. Taip pat buvo gauta, kad prieš prokariotinius mikroorganizmus reikia mažesnių AgND koncentracijų, nei prieš eukariotinius (**Table 3.2.** ir **Fig. 3.4.**). Tačiau remiantis literatūros duomenimis, AgND turėtų efektyviau veikti prieš gramneigiamas bakterijas, nei prieš gramteigiamas, o šio tyrimo metu buvo nustatyta, kad MIK vertės prieš gramteigiamas *S. aureus* ir *S. pyogenes* bakterijas yra mažesnės, nei prieš gramneigiamą *P. aeruginosa* bakteriją. Tai galima paaiškinti tuo, kad *P. aeruginosa* eksperimentų metu suformavo bioplėvelę, todėl su šios bakterijos bioplėvelėmis buvo atliktas atskiras tyrimas.

Sidabro nanodalelių priešmikrobinio poveikio stiprinimas naudojant elektroporaciją

C. guilliermondii ląstelės statistiškai reikšmingai eliminuotos po elektroporacijos taikant įvairius elektrinio lauko stiprumus (10, 12,5 ir 15 kV/cm) be AgND. Esant 15 kV/cm elektrinio lauko stiprumui buvo pašalinta 35,63 ± 2,26 % *C. guilliermondii* ląstelių (lyginant su elektroporacija nepaveiktomis ląstelėmis) (**Fig. 3.5.**).

Tiriant elektroporacijos ir AgND kombinuotą poveikį *C. guilliermondii* ląstelėms, pradžioje buvo naudotos MIK vertės (10 μg/mL koncentracija

Geobacillus spp. 18, 25 ir 95 ir 5 μg/mL koncentracija *Geobacillus* sp. 612), tačiau poveikis buvo toks stiprus, kad agarizuotoje terpėje nebuvo matomos augančios kolonijos. Dėl to, norint įvertinti gyvybingų ląstelių skaičiaus pokyčio rezultatus procentais, AgND koncentracija buvo sumažinta 10 kartų. Statistiškai patikimas gyvybingų ląstelių skaičiaus sumažėjimas buvo pastebimas su visomis tirtomis *Geobacillus* spp. AgND ir su įvairiais elektrinio lauko stiprumais (**Fig. 3.5.**). Didžiausias poveikis buvo nustatytas naudojant 15 kV/cm elektrinio lauko stiprumą. Lyginant su nepaveiktomis ląstelėmis, labiausiai *C. guilliermondii* gyvybingų ląstelių skaičius sumažėjo naudojant *Geobacillus* sp. 612 AgND (iki 2,67 ± 1,82 %).

Be to, buvo nustatyta, kad padidėjęs negyvų ląstelių skaičius, atsiradęs naudojant visų keturių *Geobacillus* spp. AgND ir elektroporaciją, statistiškai reikšmingai skiriasi, lyginant tik su elektroporacija ar tik su AgND paveiktomis *C. guilliermondii* ląstelėmis. Remiantis šiais rezultatais galima daryti prielaidą, kad negyvų ląstelių padidėjimą lemia tiek elektroporacija, tiek AgND (veikiant kartu), todėl elektroporacija sustiprina AgND priešgrybelines savybes.

ROS generacijos mikroorganizmų ląstelėse nustatymas po poveikio sidabro nanodalelėmis

DCFDA/H_2DCDFA-Cellular ROS Assay Kit (ab113851) buvo naudojamas siekiant nustatyti ROS generaciją mikroorganizmų ląstelėse po poveikio AgND. Ląstelių ROS generacijai matuoti yra naudojamas fluorescencinis dažas DCFDA (2',7'-dichlorfluoresceino diacetatas). Dažui patekus į ląsteles, esterazės paverčia dažą į nefluorescencinę medžiagą. Ši medžiaga, kai paveikiama ROS, virsta fluorescencine molekule DCF (2',7'-dichlorfluoresceinas) [276].

C. guilliermondii atveju ROS generacija buvo tirta po poveikio visų keturių *Geobacillus* spp. AgND. Statistiškai patikimi pokyčiai buvo nustatyti po poveikio su visomis tirtomis AgND (**Fig. 3.7.** ir **Fig. 3.8.**). Didžiausias ROS generacijos pokytis, lyginant su AgND nepaveikta kontrole, buvo šias mielių ląsteles paveikus *Geobacillus* sp. 25 kamieno AgND (fluorescencijos intensyvumas padidėjo 7,73 ± 0,64 karto. *S. cerevisiae* atveju ROS generacijos pokyčiai buvo vertinami po poveikio *Geobacillus* spp. 25 ir 612 kamienų AgND, tačiau statistiškai patikimo pokyčio, lyginant su AgND nepaveikta kontrole, nustatyta nebuvo.

Bakterijų atveju, ROS generacijos pokyčiai buvo įvertinti po poveikio *Geobacillus* spp. 25 ir 612 kamienų AgND (**Fig. 3.25.**). Didžiausias pokytis buvo nustatytas *S. aureus* ląsteles paveikus *Geobacillus* sp. 612 kamieno

AgND (80,65 ± 6,71 % ląstelių turėjo padidėjusį ROS kiekį). *S. pyogenes* atveju *Geobacillus* sp. 25 AgND sukėlė didesnę ROS generaciją (56,54 ± 18,21 %). *P. aeruginosa* bakterijose po poveikio *Geoabcillus* sp. 612 AgND 49,03 ± 3,34 % ląstelių turėjo padidėjusį ROS kiekį.

Ląstelių membranų pralaidumo pokyčių įvertinimas

Ląstelių membranų pralaidumas po poveikio AgND buvo tirtas naudojant *Geobacillus* spp. 25 ir 612 kamienų AgND. Membranos pralaidumo pokyčiai šiame darbe buvo įvertinti dažant ląsteles propidžio jodidu (PI), kuris pro pralaidžias membranas patekęs į ląstelių vidų, prisijungia prie DNR ir raudonai nudažo ląsteles.

Statistiškai patikimi ląstelių membranų pralaidumo pokyčiai buvo nustatyti po 30 min. poveikio 10 μg/mL koncentracijos *Geobacillus* sp. 25 ir 5 μg/mL *Geobacillus* sp. 612 AgND su abejomis tirtomis mielėmis (*C. guilliermondii* ir *S. cerevisiae*) (**Fig. 3.17.**). *C. guilliermondii* atveju po poveikio *Geobacillus* sp. 25 AgND 65,29 ± 0,51 % ląstelių turėjo pralaidžias membranas, o *Geobacillus* sp. 612 AgND atveju – 61,00 ± 5,72 %. *S. cerevisiae* atveju atitinkamai 58,98 ± 4,69 % ir 72,93 ± 4,80 % ląstelių turėjo PI pralaidžias membranas po poveikio AgND.

Bakterijų atveju, statistiškai patikimi membranos pralaidumo pokyčiai buvo taip pat nustatyti po poveikio *Geobacillus* spp. 25 ir 612 kamienų AgND su visomis tirtomis bakterijomis (*S. aureus*, *S. pyogenes* ir *P. aeruginosa*) (**Fig. 3.26.**). *S. aureus* atveju 34,65 ± 10,60 % ląstelių su pralaidžiomis membranomis buvo nustatyta po poveikio 2,6 μg/mL *Geobacillus* sp. 25 AgND ir 33,37 ± 6,66 % po poveikio 2,6 μg/mL *Geobacillus* sp. 612 AgND. *S. pyogenes* atveju 39,55 ± 1,96 % ir 23,68 ± 6,75 % atitinkamai po poveikio *Geobacillus* sp. 25 AgND (4,17 μg/mL) ir *Geobacillus* sp. 612 AgND (1,04 μg/mL), o *P. aeruginosa* atveju 82,81 ± 0,86 % ir 57,59 ± 2,79 % atitinkamai po poveikio *Geobacillus* sp. 25 AgND (5,21 μg/mL) ir *Geobacillus* sp. 612 AgND (2,09 μg/mL).

Pagal gautus rezultatus galima daryti prielaidą, kad gramneigiamų bakterijų membranos yra pralaidesnės *Geobacillus* spp. AgND, nei gramteigiamų bakterijų. Be to, atliekant ROS generacijos pokyčių tyrimus, atliekant tėkmės citometrijos matavimus, buvo analizuojamas mažesnis *P. aeruginosa* ląstelių skaičius (lyginant su nepaveiktais mėginiais), kas leidžia daryti prielaidą, jog gramneigiamų bakterijų atveju, AgND padaro tiesioginę žalą ląstelių membranoms, taip sukeldamos ląstelių lizę.

Aktyvių kaspazių identifikavimas

Aktyvioms kaspazėms mielių ląstelėse identifikuoti buvo naudojamas FITC-VAD-FMK In situ markeris (FITC), kuris yra konjuguotas su kaspazės inhibitoriumi VAD-FMK. Kai šis markeris patenka į ląstelę ir prisijungia prie aktyvuotų kaspazių, stebima fluorescencija, kuri tarnauja kaip apoptozės žymuo. Ląstelės su aktyvuotomis kaspazėmis nusidažo žaliai, o ląstelės be aktyvių kaspazių nenusidažo.

C. guilliermondii mielių ląsteles 1 val. paveikus *Geobacillus* spp. 25 ir 612 kamienų AgND (atitinkamai 10 ir 5 μg/mL koncentracija), buvo nustatyta, kad atitinkamai 44,69 ± 5,22 % ir 32,71 ± 4,87 % mielių ląstelių turėjo aktyvuotas kaspazes (**Fig. 3.19.**). *S. cerevisiae* atveju ląsteles paveikus tomis pačiomis *Geobacillus* spp. 25 ir 612 kamienų AgND koncentracijomis nustatyta atitinkamai 72,35 ± 8,95 % ir 66,64 ± 10,52 % ląstelių su aktyviomis kaspazėmis (**Fig. 3.19.**). Visais atvejais mielių ląstelių su aktyviomis kaspazėmis pokytis buvo statistiškai reikšmingas ($p < 0,05$). Rezultatai rodo, kad mielių ląsteles paveikus *Geobacillus* spp. AgND yra sukeliama programuota ląstelių žūtis.

Sidabro nanodalelių citotoksiškumo keratinocitams įvertinimas

Siekiant nustatyti *Geobacillus* sp. 612 kamieno AgND poveikį ląstelių kultūroms, atliktas jų citotoksiškumo Ker-CT ląstelių kultūrai tyrimas. Mažiausia naudota *Geobacillus* sp. 612 kamieno AgND koncentracija sutampa su didžiausia nustatyta MIK reikšme (prieš *C. guilliermondii*). Rezultatai rodo, kad ši koncentracija nėra citotoksiška tirtoms Ker-CT ląstelėms (**Fig. 3.27.**). Tačiau didesnės AgND koncentracijos sukelia citotoksinį poveikį Ker-CT ląstelėms.

Sidabro nanodalelių įtakos keratinocitų ląstelių proliferaciniam aktyvumui tyrimas

Nustačius citotoksinį *Geobacillus* sp. 612 kamieno AgND poveikį Ker-CT ląstelėms, ištirtas Ker-CT proliferacinis aktyvumas esant skirtingoms AgND koncentracijoms (**Fig. 3.29.**). Šie rezultatai leidžia įvertinti, ar aplinkoje esant AgND bėgant laikui ląstelės dauginasi ar miršta. Gauti rezultatai rodo, kad esant 5 μ g/mL AgND koncentracijai, Ker-CT ląstelės nei dauginasi, nei miršta per 72 val., tačiau naudojant didesnes koncentracijas jų proliferacinis aktyvumas mažėja.

Išvados

1. Termofilinės *Geobacillus* spp. bakterijos yra tinkamos stabilių AgND, pasižyminčių priešmikrobiniu aktyvumu, gavimui. Didžioji dalis gautų AgND yra mažesnės nei 100 nm skersmens ir jų zeta potencialas svyruoja nuo −25 iki −31 mV;
2. Sidabro nanodalelės, gautos naudojant *Geobacillus* spp. bakterijas turi priešmikrobinių savybių prieš odos patogenines bakterijas ir mieles. Jos pažeidžia ląstelių membranas, padidina ROS generaciją, sukelia lipidų peroksidaciją ir aktyvina kaspazes;
3. Elektroporacija sustiprina priešmikrobinį AgND poveikį odos patogeniniams mikroorganizmams. Taikant elektroporaciją ir AgND kartu sutrumpinamas poveikio laikas;
4. AgND, gautų naudojant *Geobacillus* spp. bakterijas, žūties mechanizmas skiriasi tarp skirtingų mikroorganizmų. Pagrindinis poveikio gramteigiamoms bakterijoms mechanizmas yra padidėjusi ROS generacija, gramneigiamoms bakterijoms – tiesioginis ląstelių membranų pažeidimas. Mielių ląstelėse šios AgND sukelia su kaspazėmis susijusią programuotą ląstelių žūtį;
5. *Geobacillus* sp. 612 kamieno AgND 5 μg/mL koncentracija, kuri yra veiksminga prieš patogenines mieles, neturi citotoksinio poveikio žmogaus keratinocitų ląstelėms ir nepaveikia keratinocitų migracijos.

AKNOWLEDGEMENTS

First and foremost, I would like to thank my supervisor Dr. Eglė Lastauskienė for this journey which started in my first year of Masters' studies. While I was Eglė student, I really learned a lot that will help me in my future. Thank you Eglė for your great trust and belief in me.

This dissertation would also not exist without several other people who contributed to this work in one way or another. I would like to thank Dr. Vaidas Klimkevičius, with whom I was able to carry out detailed research on the physical properties of AgNP. Also, I would like to thank Dr. Virginija Bukelskienė, Dr. Ieva Rinkūnaitė, and Giedrė Didzinskaitė for performing and helping to plan experiments with human keratinocyte cells. I must also mention and thank Indrė Dalgėdienė, who performed most of the flow cytometry measurements, and Eimina Dirvelytė, who performed part of the microscopy. Thank you all for your help and the work you have done.

I cannot forget the great helpers, my students - Povilas, Estera, Diana, Kotryna, Dainius. Also Pavel, Viktorija, Ieva, Lukas, Gabija. Thank you all for your time in the lab, and your patience, understanding, and your support then I needed that the most.

And last but not least I would like to thank my family, colleagues, and friends, especially Gintarė, Rolandas, Vilius, Mindaugas, and *Mikrobai*, for keeping me sane, their support and encouragement, for believing in me than I didn't even believe in myself.

LIST OF PUBLICATIONS

Publications of the dissertation topic:

Cekuolyte K, Gudiukaite R, Klimkevicius V, Mazrimaite V, Maneikis A, Lastauskiene E. Biosynthesis of Silver Nanoparticles Produced Using *Geobacillus* spp. Bacteria. *Nanomaterials.* 2023; 13(4):702. https://doi.org/10.3390/nano13040702

Kotryna Čekuolytė, Diana Šapaitė, Estera Žemgulytė, Renata Gudiukaitė, and Eglė Lastauskienė. Induction of Apoptosis with Silver Nanoparticles Obtained Using Thermophilic Bacteria. *Journal of Functional Biomaterials.* https://doi.org/10.3390/jfb15060142

Other publications:

Petras Venckus, Ieva Endriukaitytė, Kotryna Čekuolytė, Renata Gudiukaitė, Andrius Pakalniškis, Eglė Lastauskienė. Effect of biosynthesized silver nanoparticles on the growth of the green microalga *Haematococcus pluvialis* and astaxanthin synthesis. *Nanomaterials*. 2023; *13*(10), 1618; https://doi.org/10.3390/nano13101618

K. Čekuolytė, E. Žemgulytė, R. Gudiukaitė, V. Novickij, A. Maneikis, R. Galinis, G. Galinis, E. Lastauskienė. Sidabro nanodalelių ir elektroporacijos poveikis *Candida* genties mielėms. Mikrobiologija 2022, Lietuvos mikrobiologų draugijos konferencija, balandžio 28-29, Birštonas, Lietuva.

K. Cekuolyte, E. Zemgulyte, R. Gudiukaite, E. Lastauskiene. Silver nanoparticles tool for biocontrol of pathogenic skin microbiota? Arqus Research Focus Forum "Healthy Aging from a Multidisciplinary Perspective". June 27-29, 2022. Life Sciences Center, Vilnius, Lithuania.

Kotryna Čekuolytė, Salomėja Šapranauskaitė, Renata Gudiukaitė, Vitalij Novickij, Eglė Lastauskienė. Combined Effect of Silver Nanopartciles and Electroporation Provides New Antibacterial Tool in Destruction of Biofilms. FEMS Conference on Microbiology 2022. 30 June – 2 July, Belgrade, Serbia

Kotryna Čekuolytė, Renata Gudiukaitė, Vaidas Klimkevičius, Veronika Mažrimaitė, Andrius Maneikis, Eglė Lastauskienė. *Geobacillus* spp. bacteria induced biosynthesis of silver nanoparticles. COINS 2023 international conference of life sciences, April 24-27, 2023 Vilnius, Lithuania (**Top 3 Oral presentation**)

Kotryna Čekuolytė, Diana Šapaitė, Estera Žemgulytė, Eglė Lastauskienė. Potential mechanisms of antimicrobial action of silver nanoparticles obtained using *Geobacillus* spp. bacteria. 5th Congress of Baltic Microbiologists, October 11-13 2023, Vilnius, Lithuania

CURRICULUM VITAE

Education

2013 – 2017	Vilnius University, BSc Microbiology and Biotechnology
2017 – 2019	Vilnius University, MSc Microbiology and Biotechnology

Work experience

2020 – now	Vilnius University, junior assistant
2021 – 2022	Vilnius University, junior research fellow
2022 – 2023	Vilnius University, project expert („Aukštųjų mokyklų tinkle optimizavimas ir studijų kokybės gerinimas Šiaulių universitetą prijungiant prie Vilniaus universiteto" Nr. 09.3.1-ESFA-V-738-030001)

Teaching experience

2022 – 2023	Medical Microbiology (Seminars)
2021 – now	Environmental Microbiology
2020 - now	Microbiology (Lab works)
2019 – now	Supervisor of Bachelor and Masters students

Participation in biomedical research

2021 – 2022	01.2.2-MITA-K-702 "Promotion of commercialization and internationalization of R&D results project: "Nanosilver and graphene oxide inks" („Nanosidabro ir grafeno oksido rašalai") Nr. 01.2.2-MITA-K-702-12-0002 Supervisor BMI: Prof. Dr. Eglė Lastauskienė
2019 – 2023	Research council of Lithuania, PhD project "Analysis of the *Geobacillus* sp. Synthetized Silver Nanoparticles Mechanisms of Action on the Biocontrol of Pathogenic Skin Microbiota." No. KD-19142. Supervisor: Prof. Dr. Eglė Lastauskienė

NOTES

NOTES

Vilniaus universiteto leidykla
Saulėtekio al. 9, III rūmai, LT-10222 Vilnius
El. p. info@leidykla.vu.lt, www.leidykla.vu.lt
bookshop.vu.lt, journals.vu.lt
Tiražas 15 egz.